Electronic Supplementary Material (ESI) for Materials Chemistry Frontiers.
This journal is © the Partner Organisations 2020

Morphology, Structure and Cytotoxicity of Dye-loaded Lipid Nanoparticles Based on Monoamine Pillar[5]arenes

L. S. Yakimova,[a] E. G. Guralnik,[a] D. N. Shurpik,[a] V. G. Evtugyn,[b] Y. N. Osin,[b] E. V. Subakaeva,[c] E. A. Sokolova,[c] P. V. Zelenikhin,[c] and I. I. Stoikov[a*]

[a.] *A.M.Butlerov Chemical Institute, Kazan Federal University, 420008 Kremlevskaya, 18, Kazan, Russian Federation.* Tel.: +7-843-2337462; fax: +7-843-2752253; e-mail: Ivan.Stoikov@mail.ru

[b.] *Interdisciplinary Centre for Analytical Microscopy, Kazan Federal University, 420008, Kremlevskaya Street, 18, Kazan, Russian Federation*

[c.] *Institute of Fundamental Medicine and Biology, Kazan Federal University, 420008, Kremlevskaya Street, 18, Kazan, Russian Federation*

Electronic Supplementary Information (58 pages)

1. NMR, MALDI-TOF MS, IR spectra of the compounds 4-6

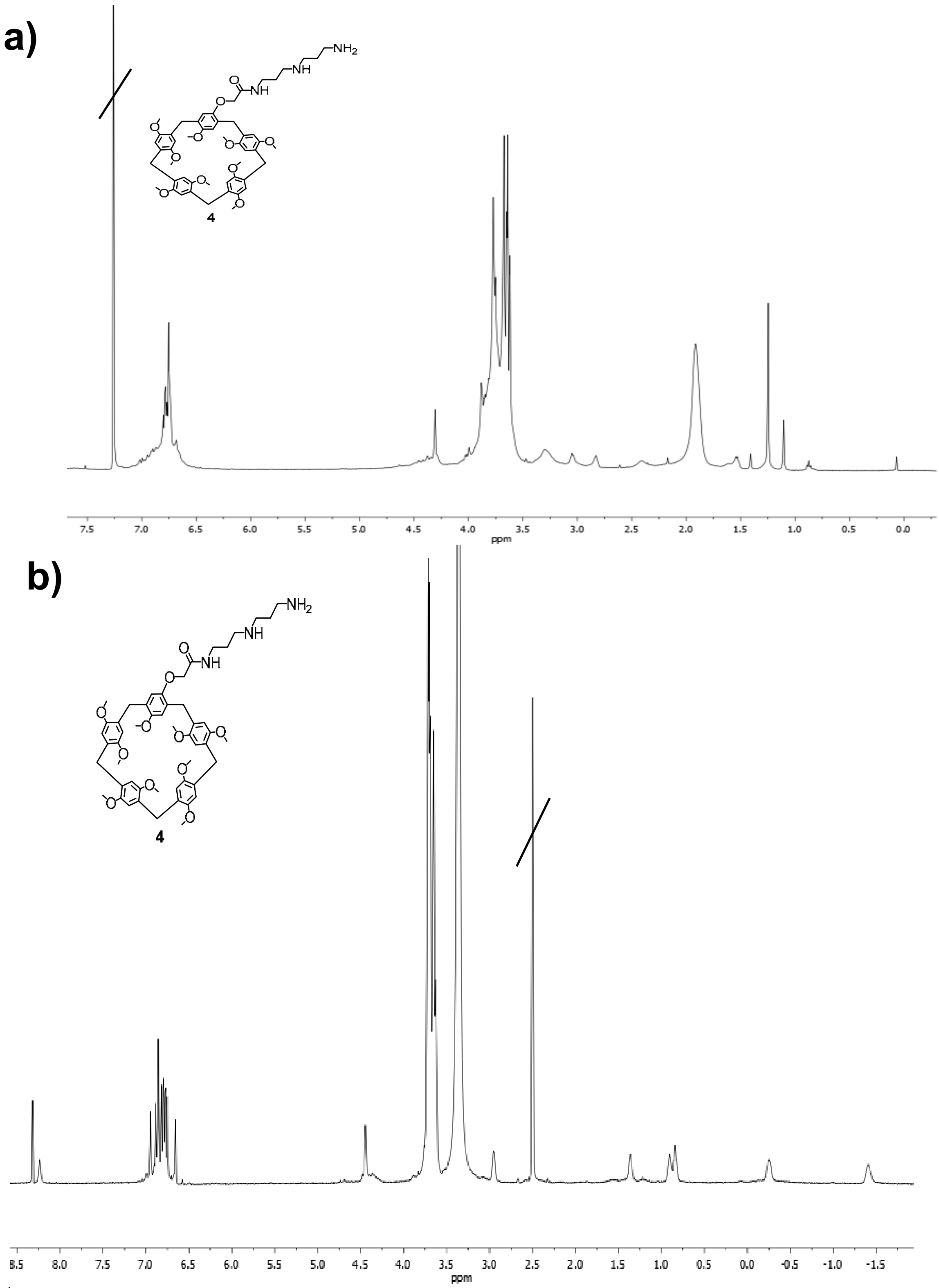

Fig. S1. [1]H NMR spectrum of 4-N-[2-(2-aminopropylamino)propyl]acetamidoxy-8,14,18,23,26,28,31,32,35-nonamethoxypillar[5]arene **(4):** a). $CDCl_3$, 298 K, 400 MHz; b). DMSO-d_6, 298 K, 400 MHz.

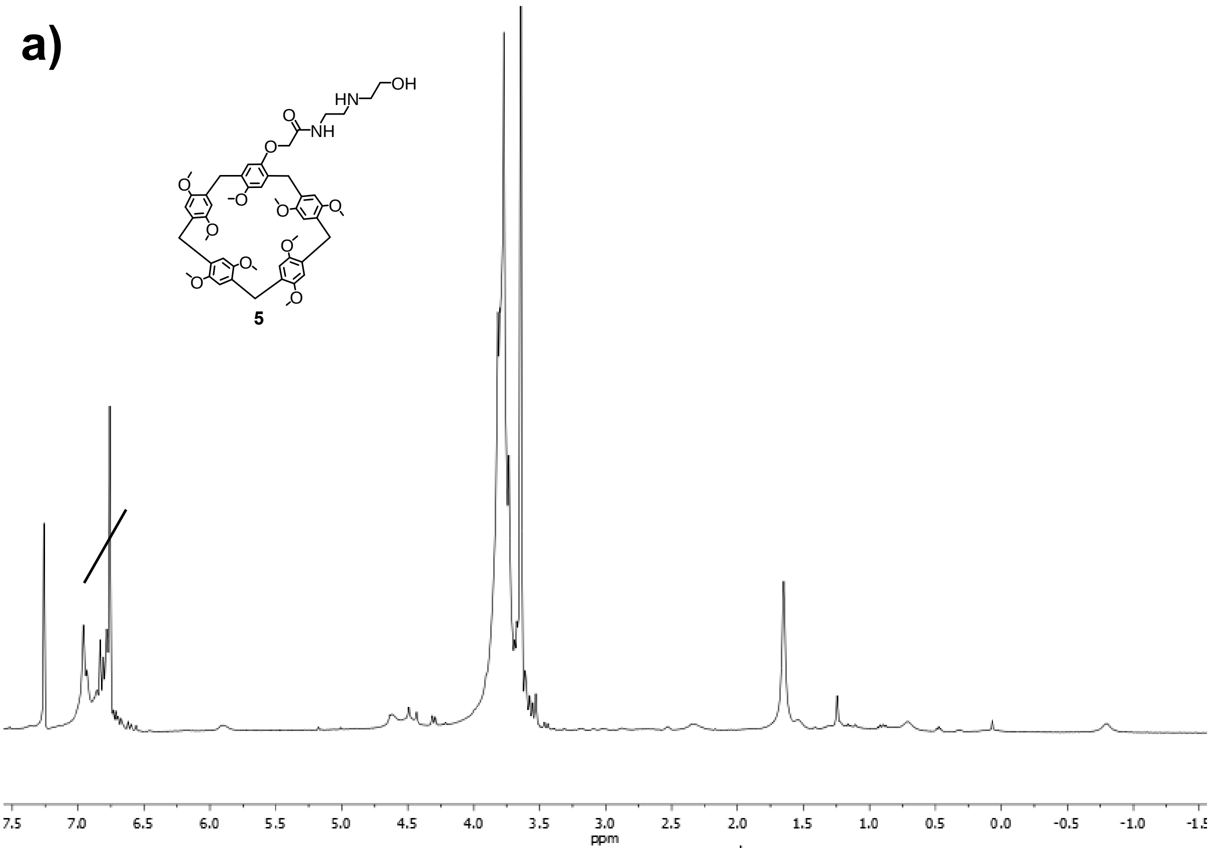

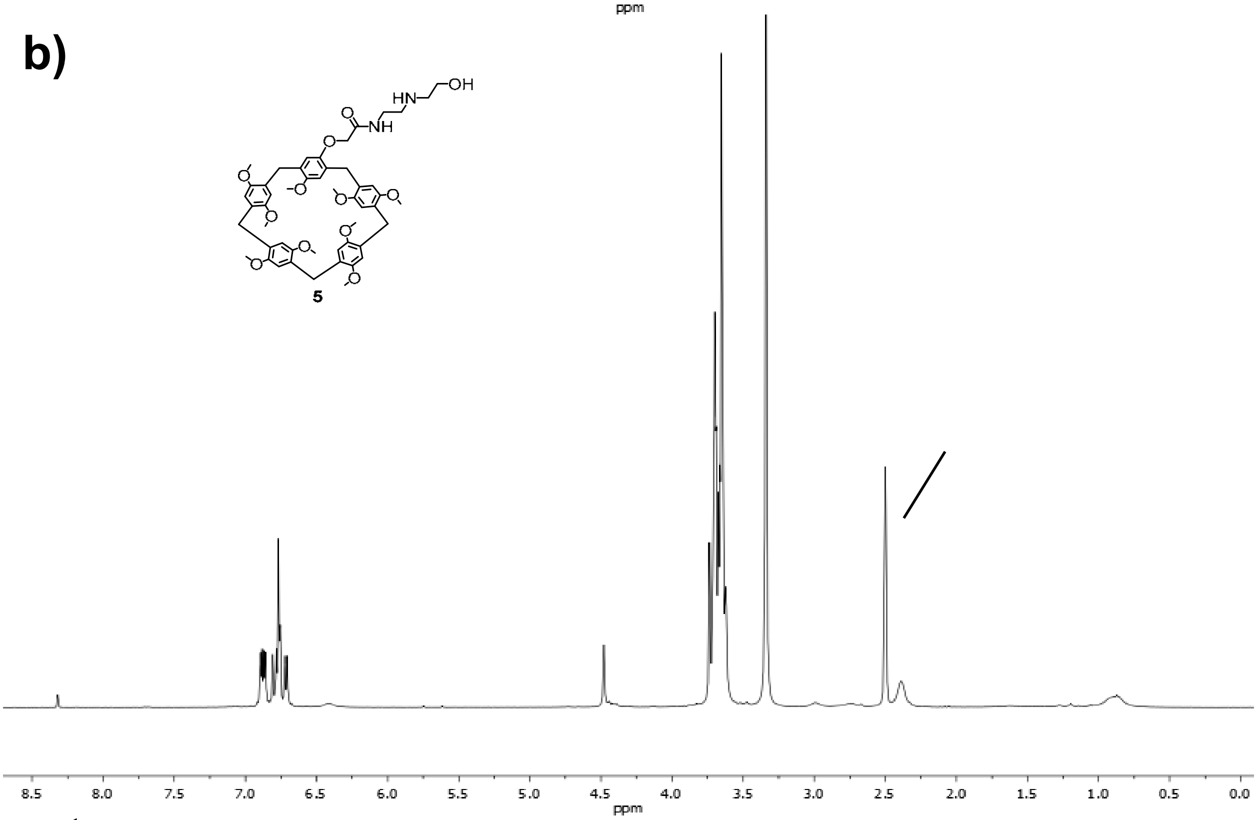

Fig. S2. ^{1}H NMR spectrum of 4-N-[2-(2-aminoethylhydroxy)ethyl]acetamidoxy-8,14,18,23,26,28,31,32,35-nonamethoxypillar[5]arene **(5):** a). $CDCl_3$, 298 K, 400 MHz; b). DMSO-d_6, 298 K, 400 MHz.

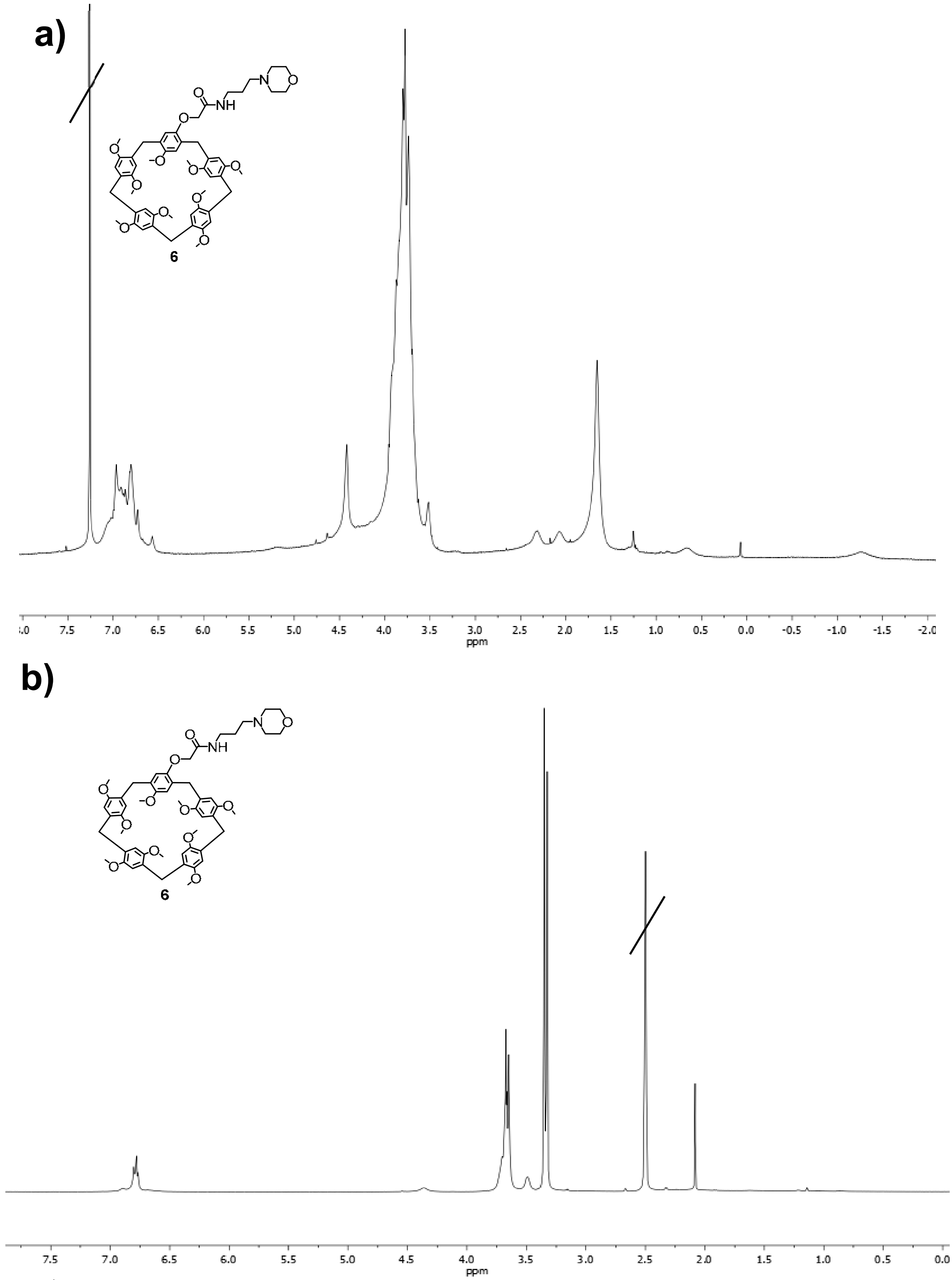

Fig. S3. ^{1}H NMR spectrum of 4-N-[2-(2-aminomorpholine)propyl]acetamidoxy-8,14,18,23,26,28,31,32,35-nonamethoxypillar[5]arene **(6):** a). $CDCl_3$, 298 K, 400 MHz; b). DMSO-*d*$_6$, 298 K, 400 MHz.

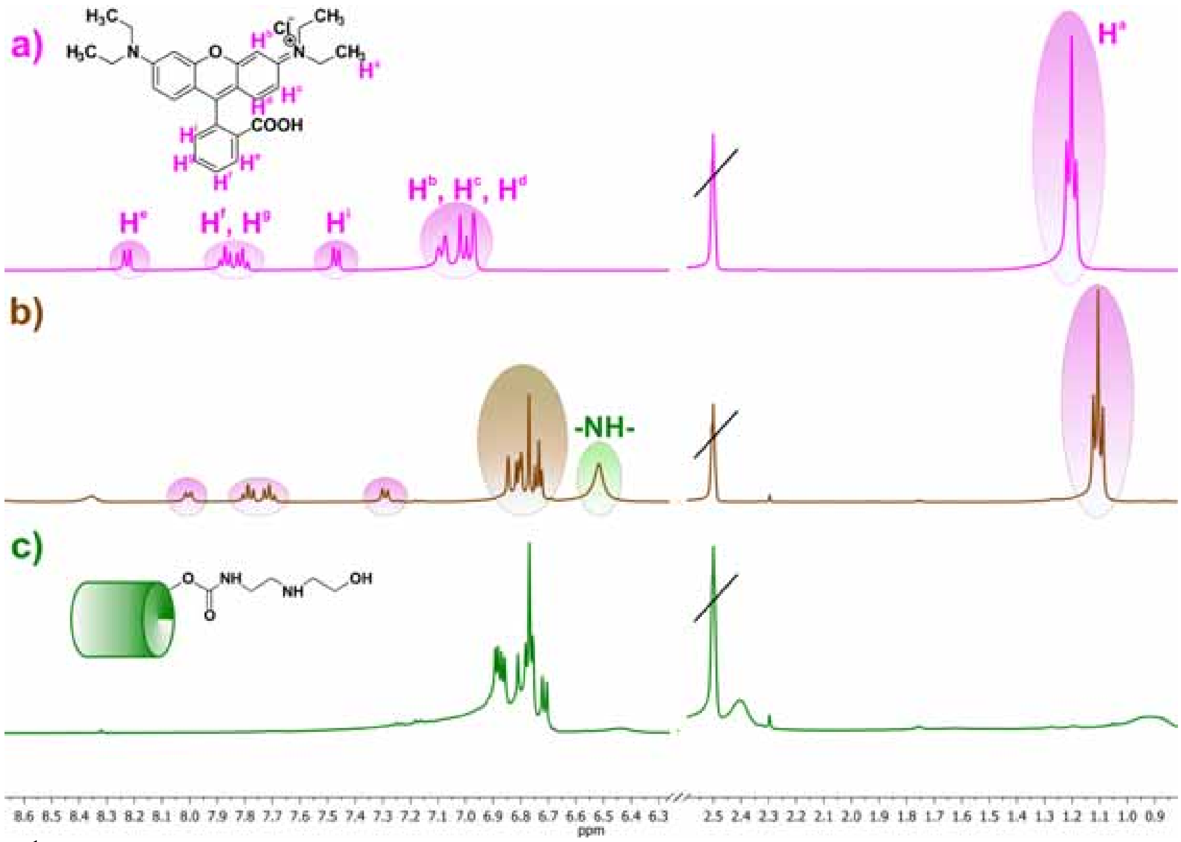

Fig. S4. ^{1}H NMR spectra of initial pillar[5]arene **5** and host/guest system for **5** and RhB (1:1) (DMSO-d_6, 298 K, 400 MHz).

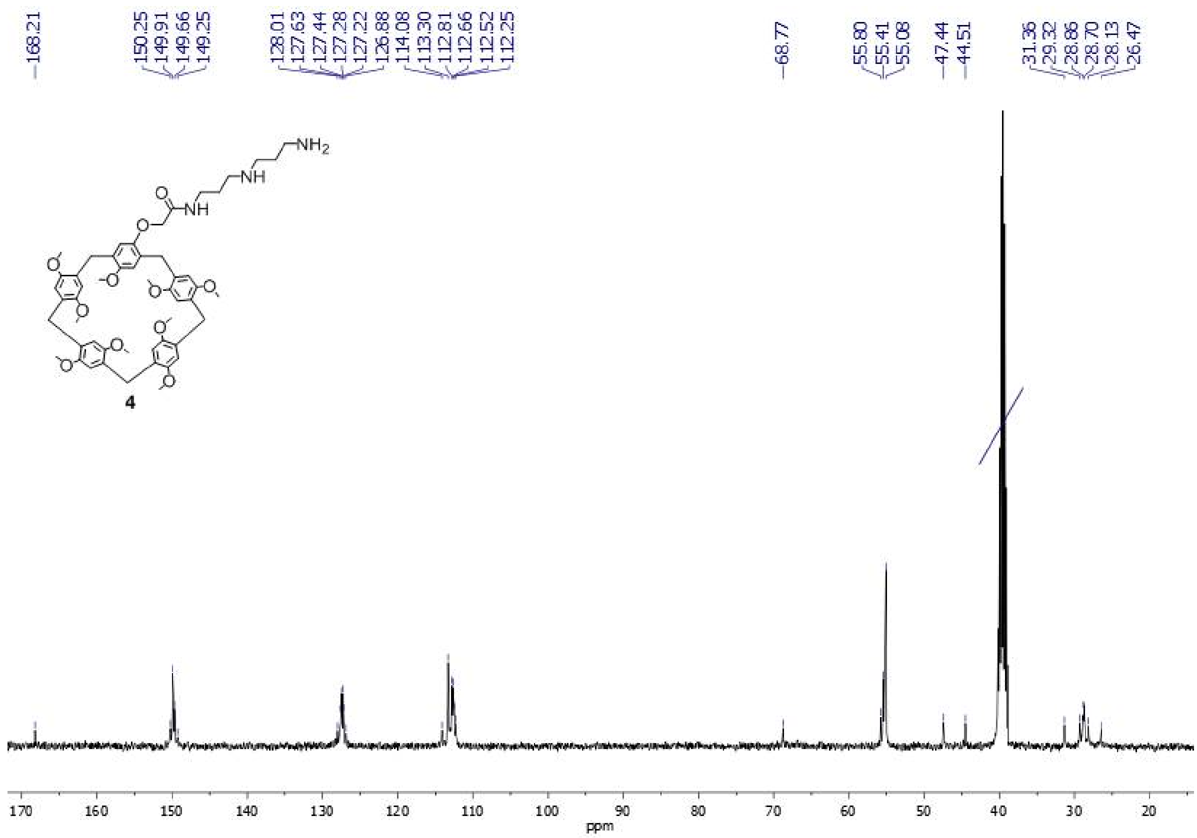

Fig. S5. ^{13}C NMR spectrum of 4-N-[2-(2-aminopropylamino)propyl]acetamidoxy-8,14,18,23,26,28,31,32,35-nonamethoxypillar[5]arene **(4)**, DMSO-d_6, 298 K, 100 MHz.

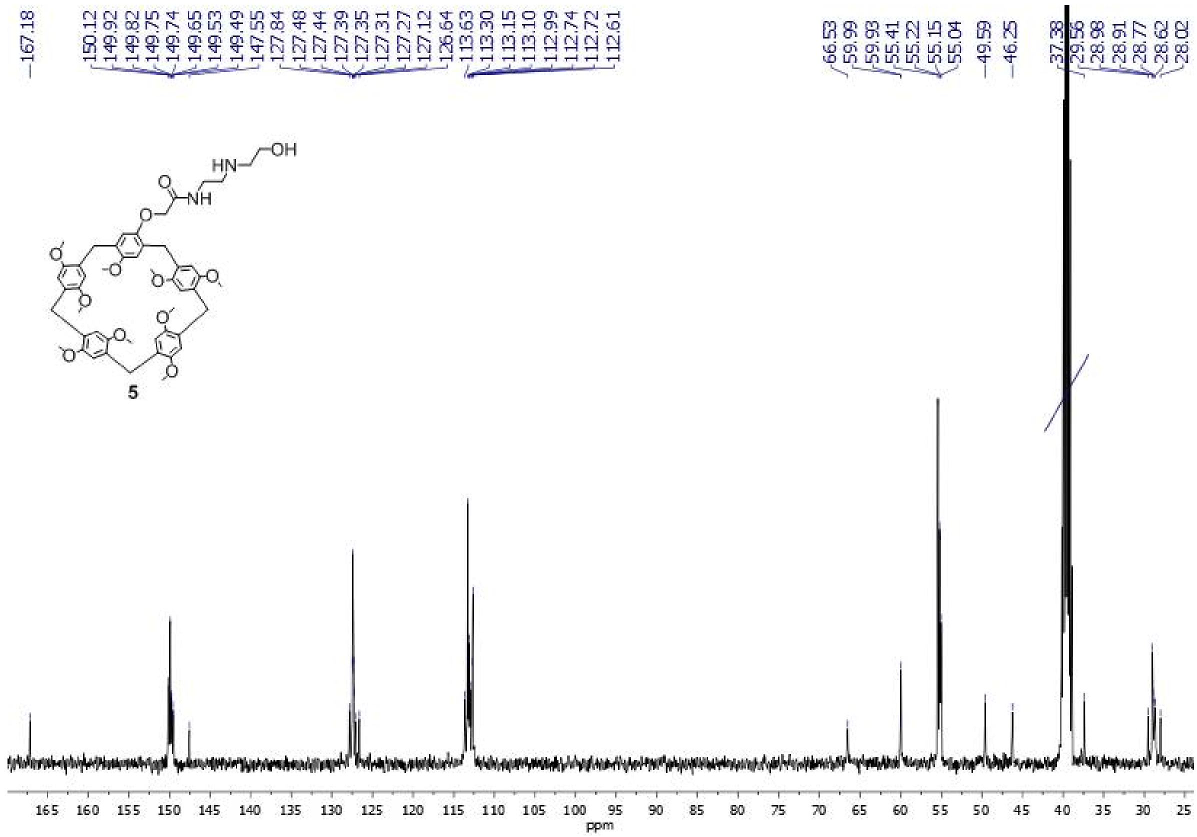

Fig. S6. ^{13}C NMR spectrum of 4-N-[2-(2-aminoethylhydroxy)ethyl]acetamidoxy-8,14,18,23,26,28,31,32,35-nonamethoxypillar[5]arene **(5)**, DMSO-d_6, 298 K, 100 MHz.

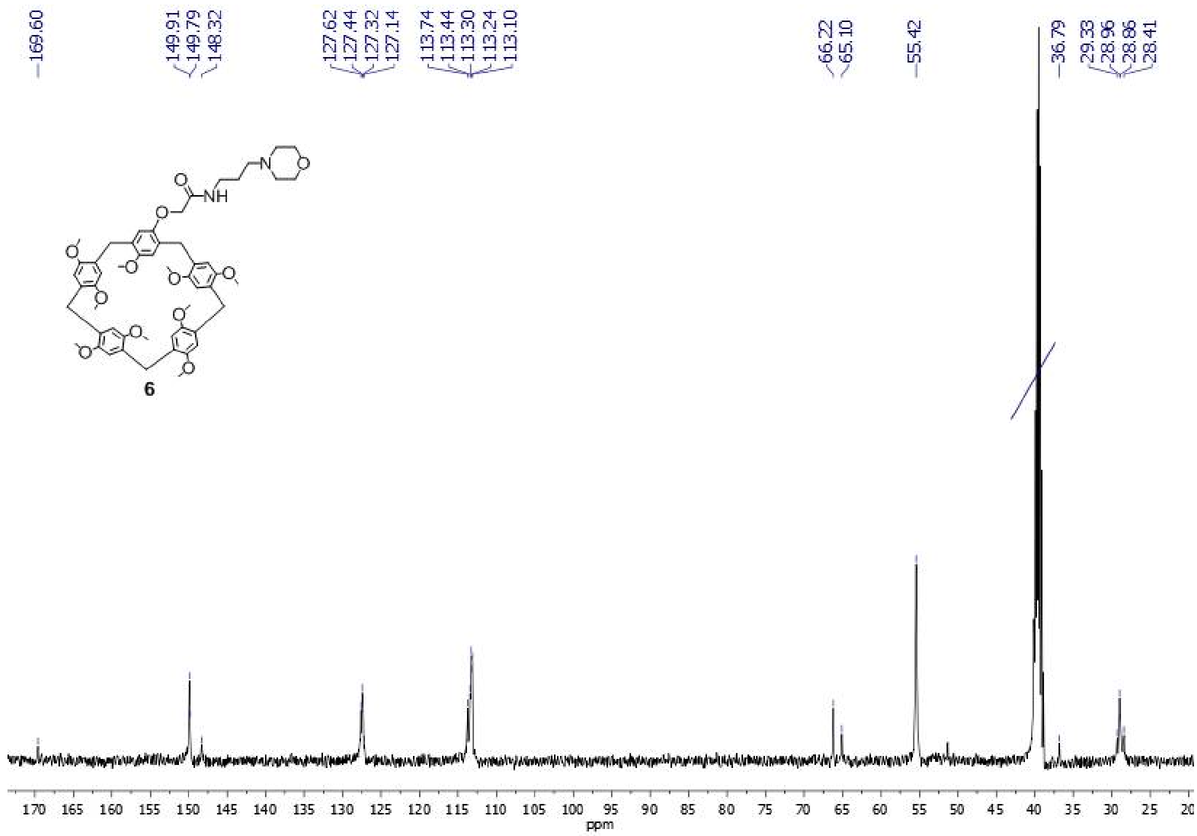

Fig. S7. ^{13}C NMR spectrum of 4-N-[2-(2-aminomorpholine)propyl]acetamidoxy-8,14,18,23,26,28,31,32,35-nonamethoxypillar[5]arene **(6)**, DMSO-d_6, 298 K, 100 MHz.

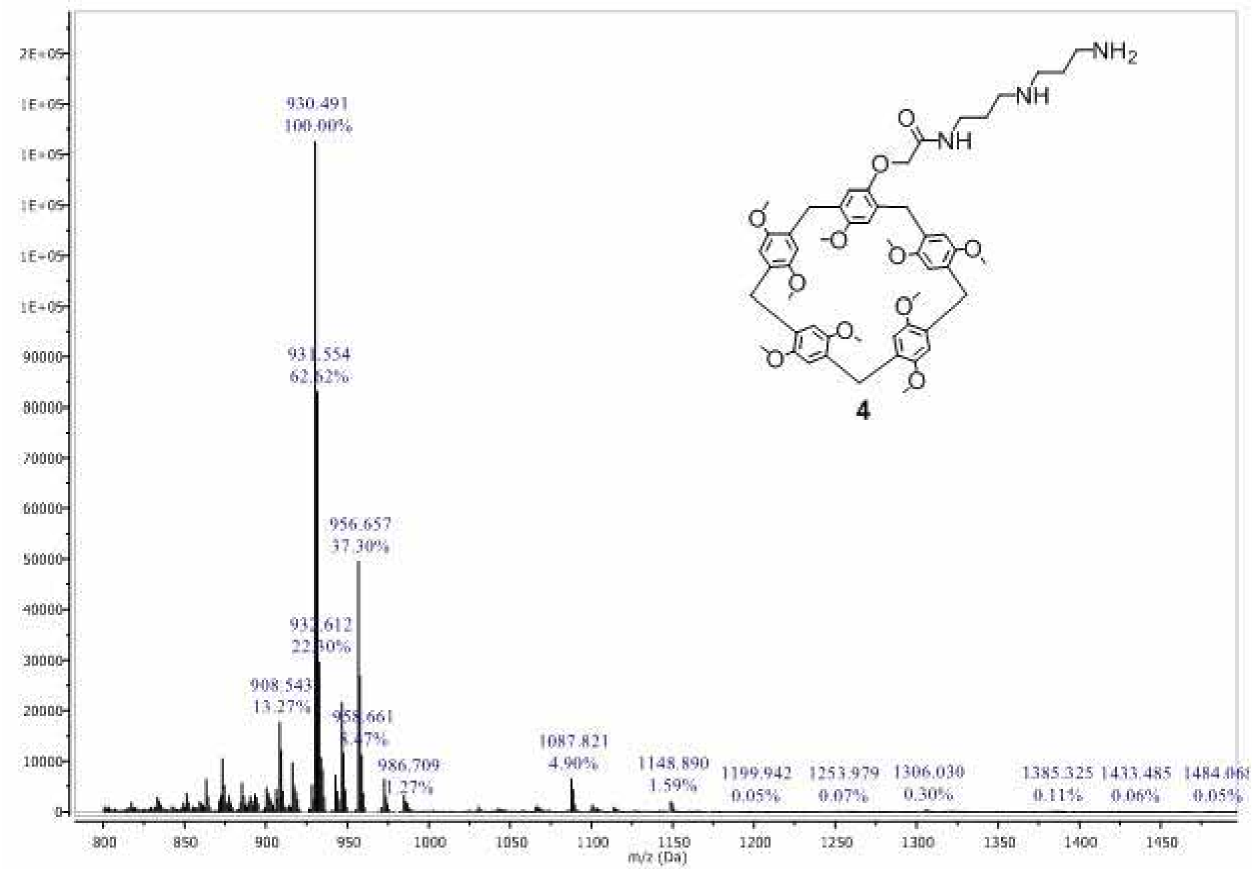

Fig. S8. Mass spectrum (MALDI-TOF, 4-nitroaniline matrix) of 4-N-[2-(2-aminopropylamino)propyl]acetamidoxy-8,14,18,23,26,28,31,32,35-nonamethoxypillar[5]arene **(4)**.

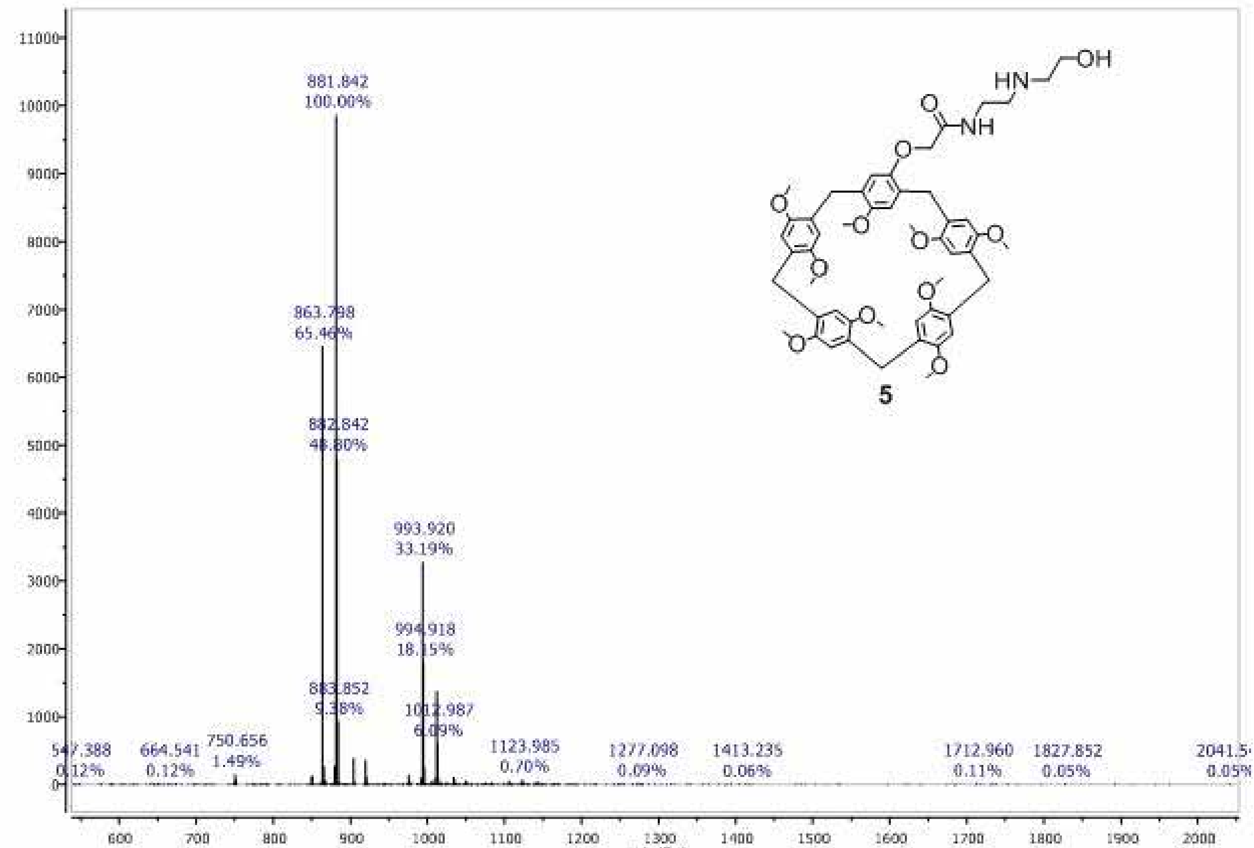

Fig. S9. Mass spectrum (MALDI-TOF, 4-nitroaniline matrix) of 4-N-[2-(2-aminoethylhydroxy)ethyl]acetamidoxy-8,14,18,23,26,28,31,32,35-nonamethoxypillar[5]arene **(5)**.

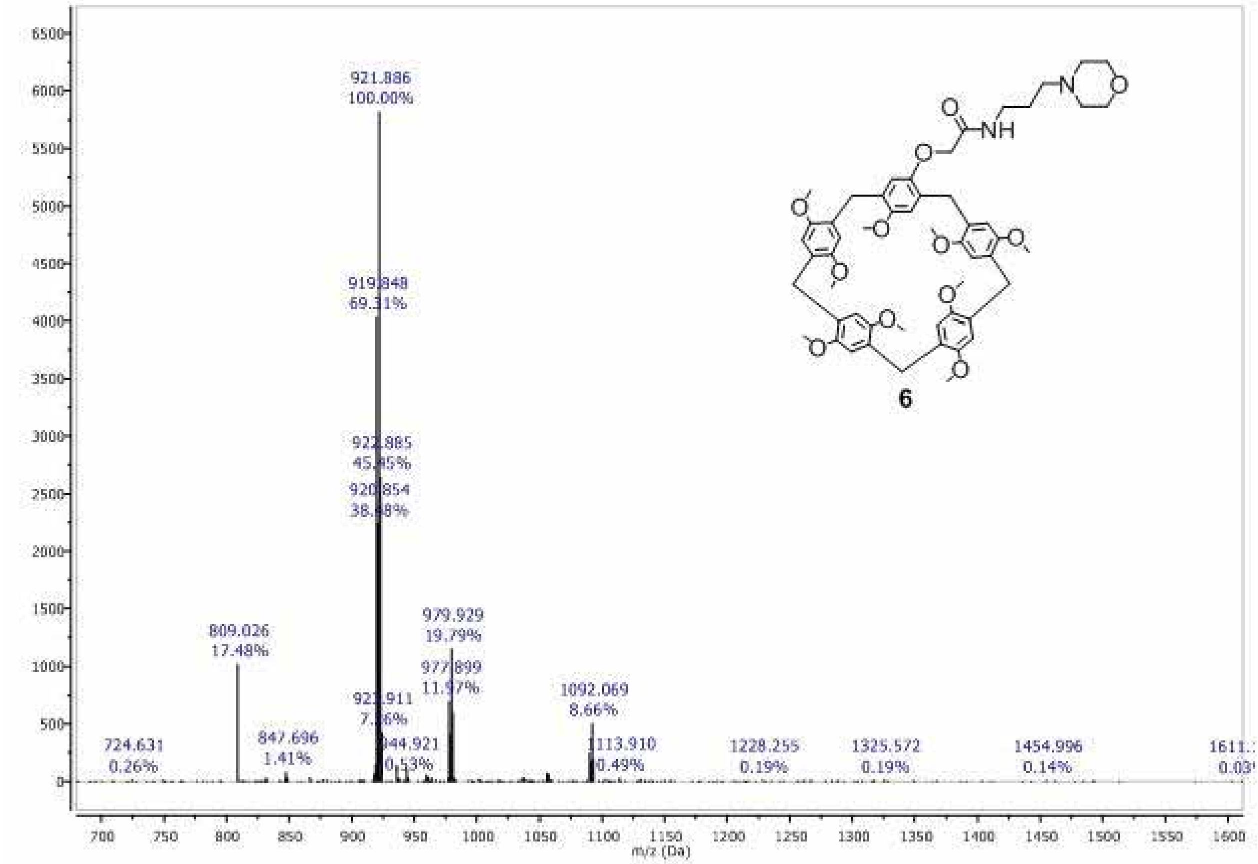

Fig. S10. Mass spectrum (MALDI-TOF, 4-nitroaniline matrix) of 4-N-[2-(2-aminomorpholine)propyl]acetamidoxy-8,14,18,23,26,28,31,32,35-nonamethoxypillar[5]arene **(6)**.

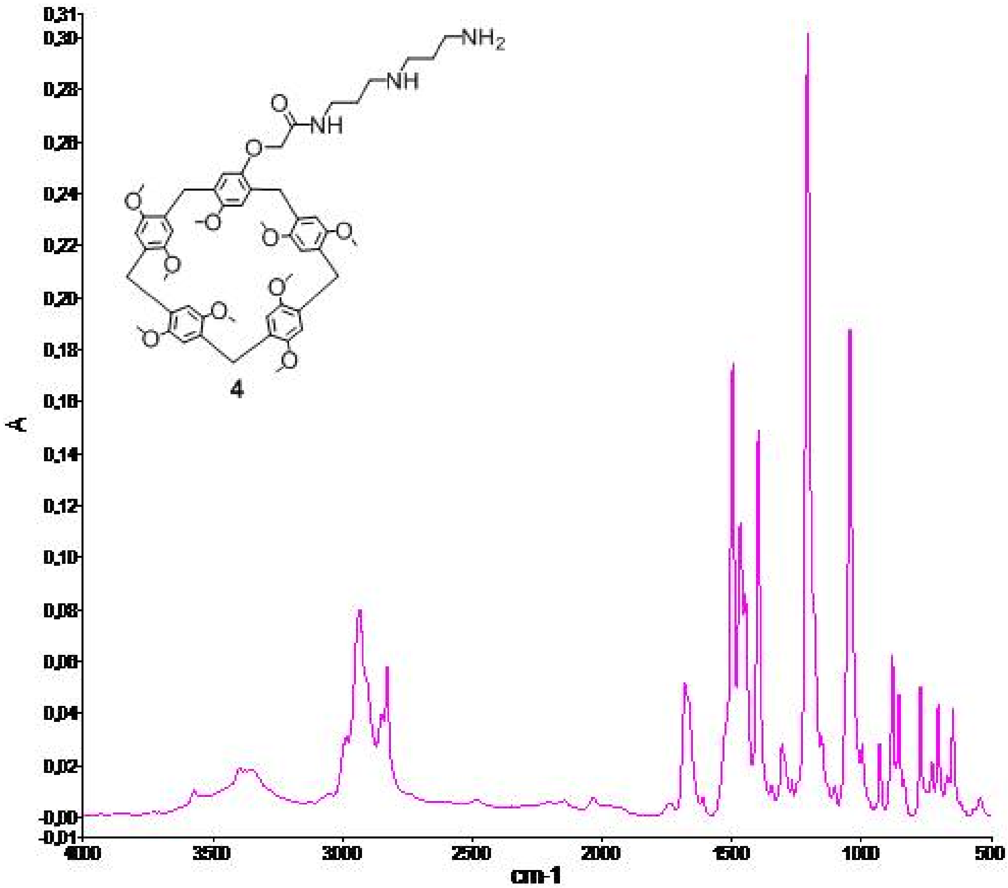

Fig. S11. IR spectrum of 4-N-[2-(2-aminopropylamino)propyl]acetamidoxy-8,14,18,23,26,28,31,32,35-nonamethoxypillar[5]arene **(4)**.

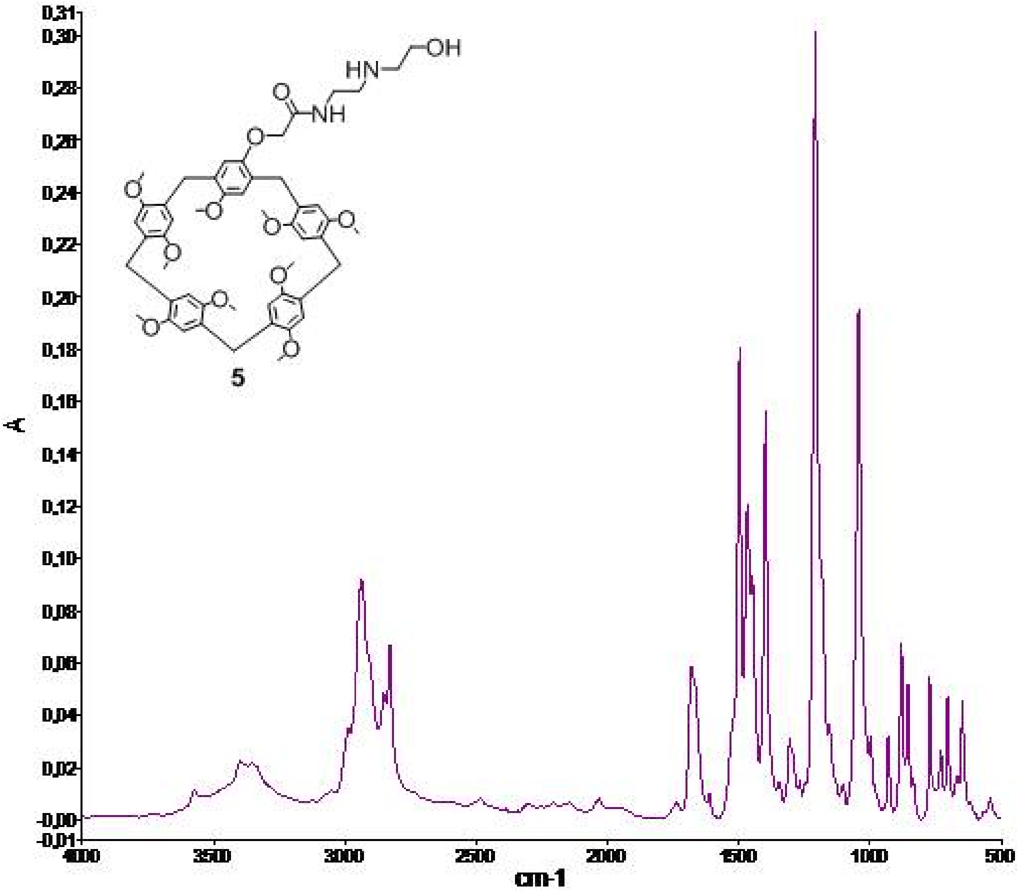

Fig. S12. IR spectrum of 4-N-[2-(2-aminoethylhydroxy)ethyl]acetamidoxy-8,14,18,23,26,28,31,32,35-nonamethoxypillar[5]arene **(5)**.

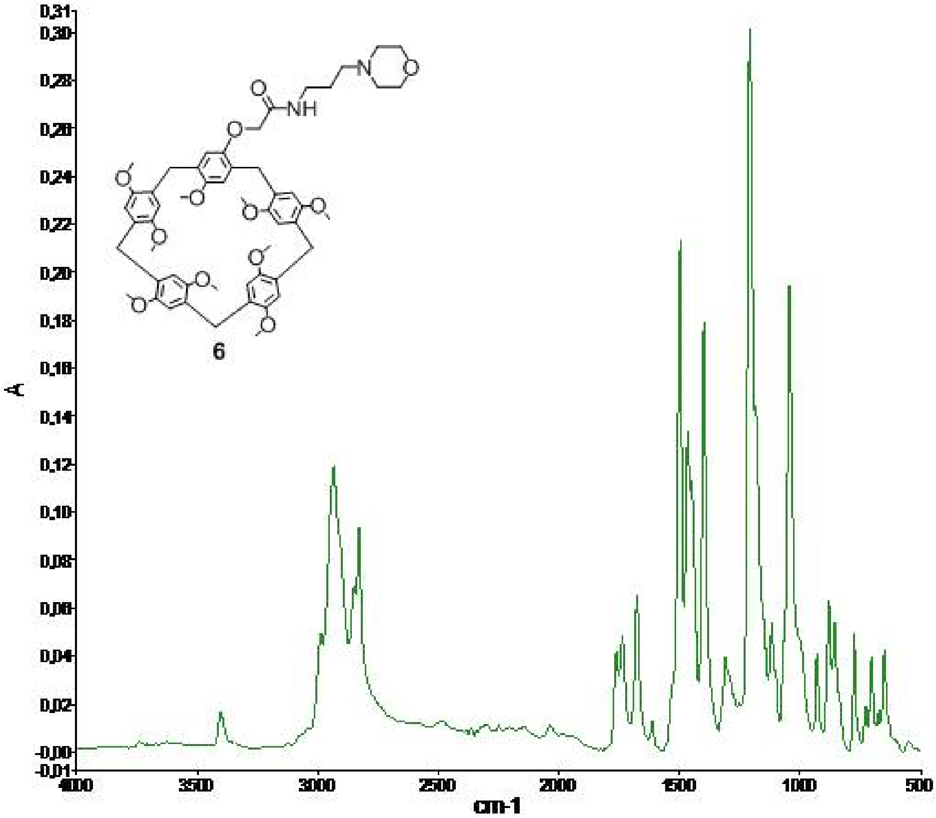

Fig. S13. IR spectrum of 4-N-[2-(2-aminomorpholine)propyl]acetamidoxy-8,14,18,23,26,28,31,32,35-nonamethoxypillar[5]arene **(6)**.

2. Transmission electron microscopy (TEM) analysis of SLNs

TEM analysis of SLN-[4-6]

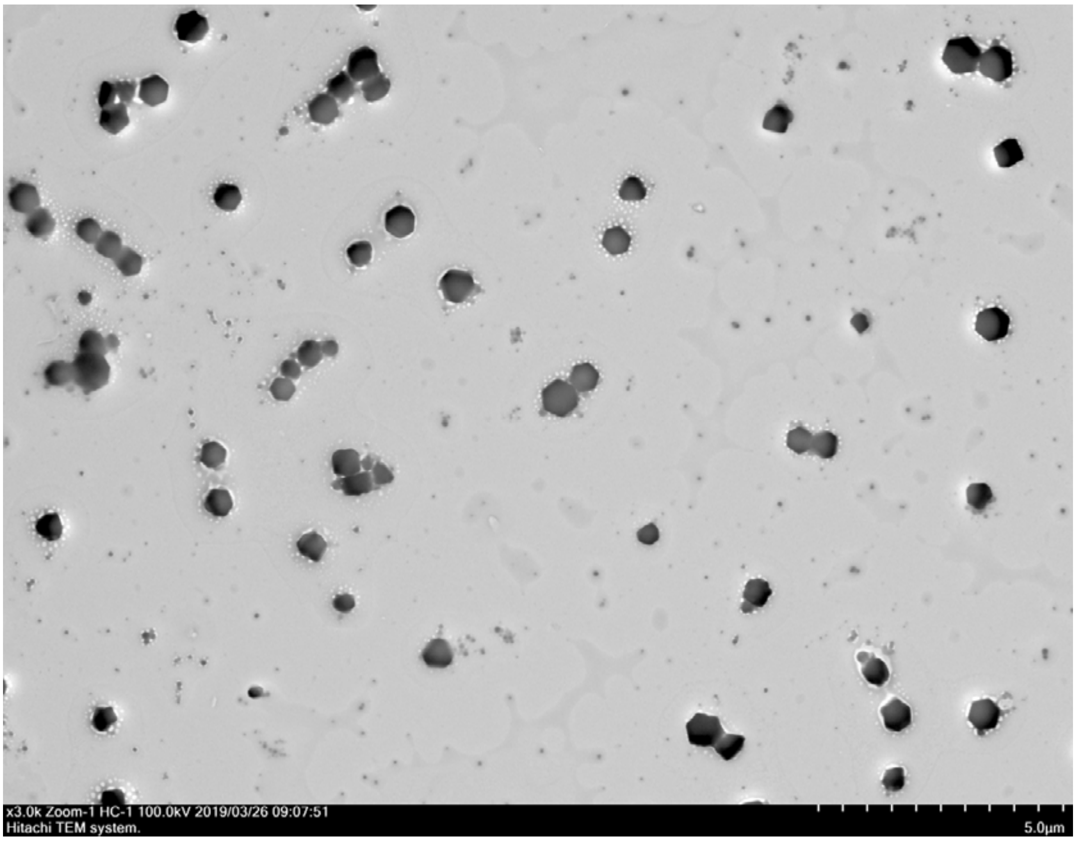

Fig. S14. TEM image of SLN-**4** after the solvent evaporation.

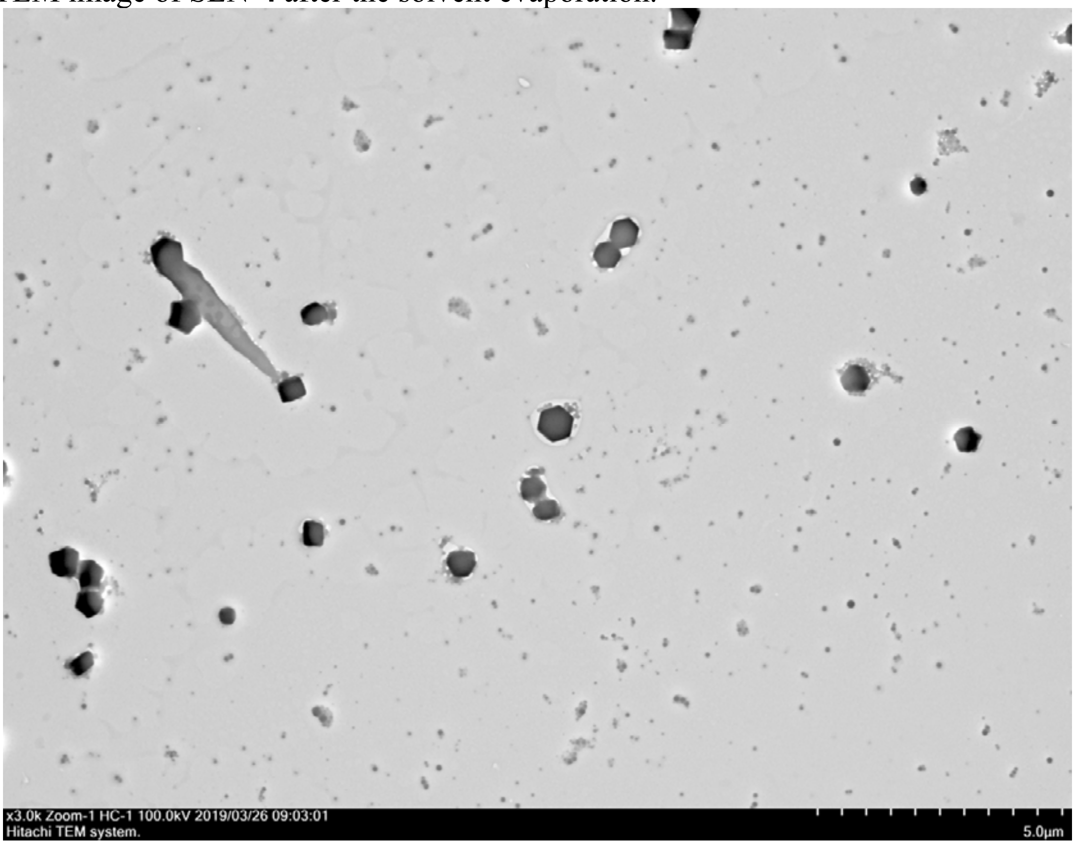

Fig. S15. TEM image of SLN-**4** after the solvent evaporation.

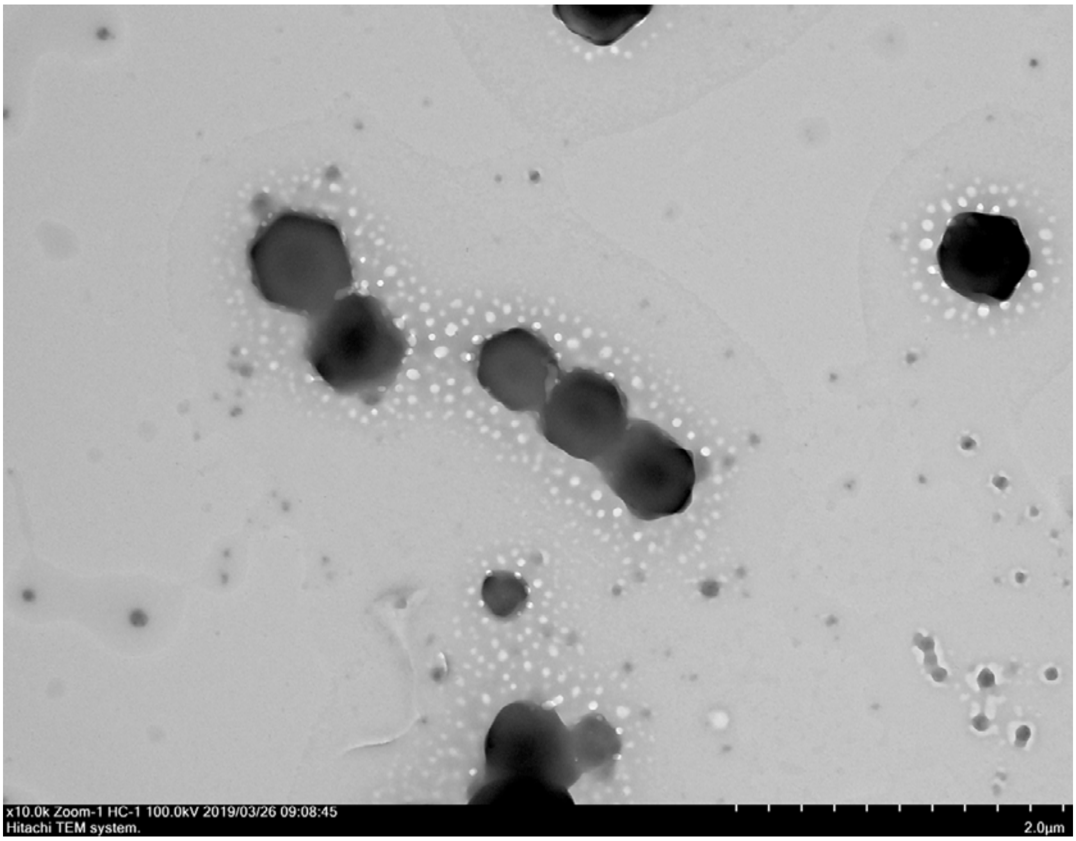

Fig. S16. TEM image of SLN-**4** after the solvent evaporation.

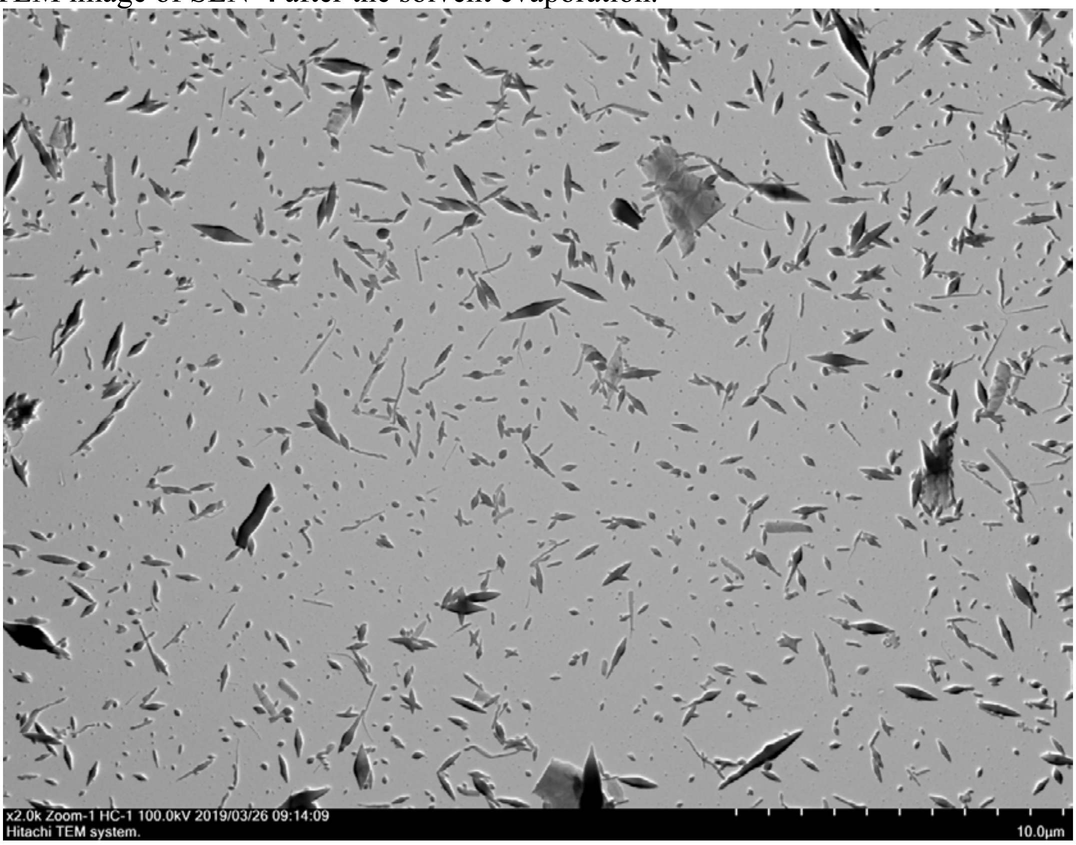

Fig. S17. TEM image of SLN-**5** after the solvent evaporation.

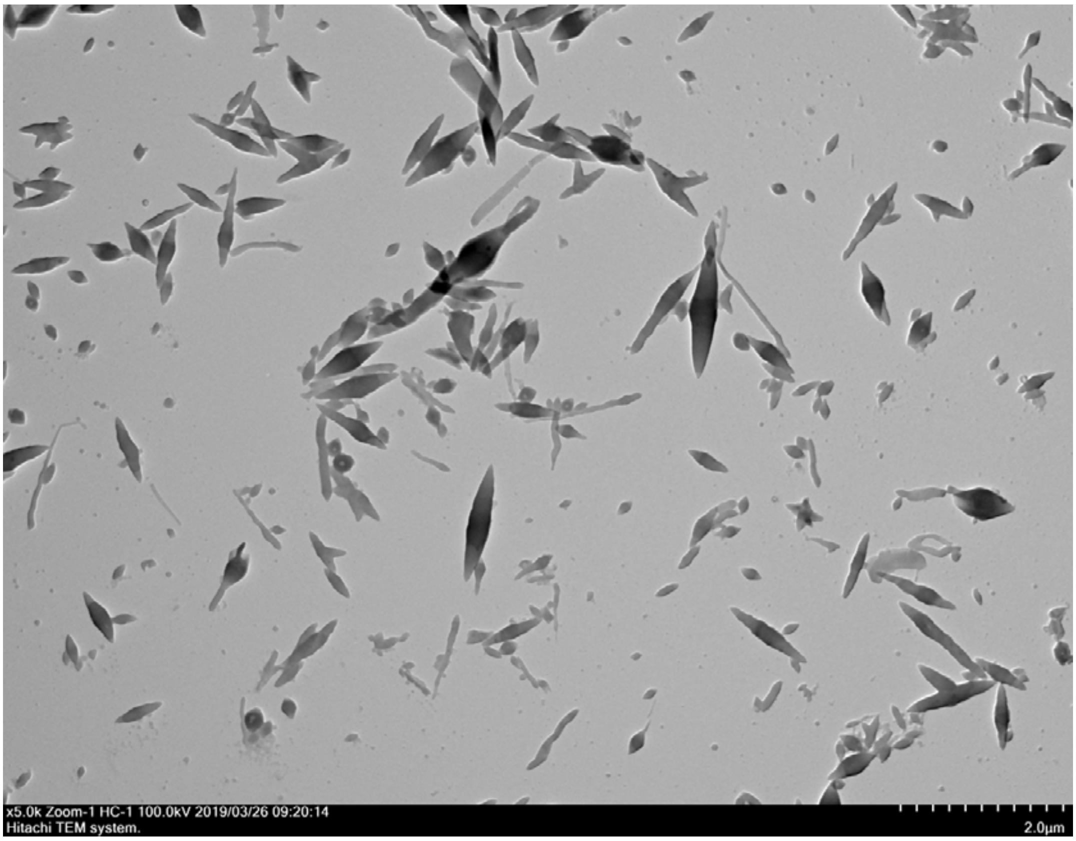

Fig. S18. TEM image of SLN-**5** after the solvent evaporation.

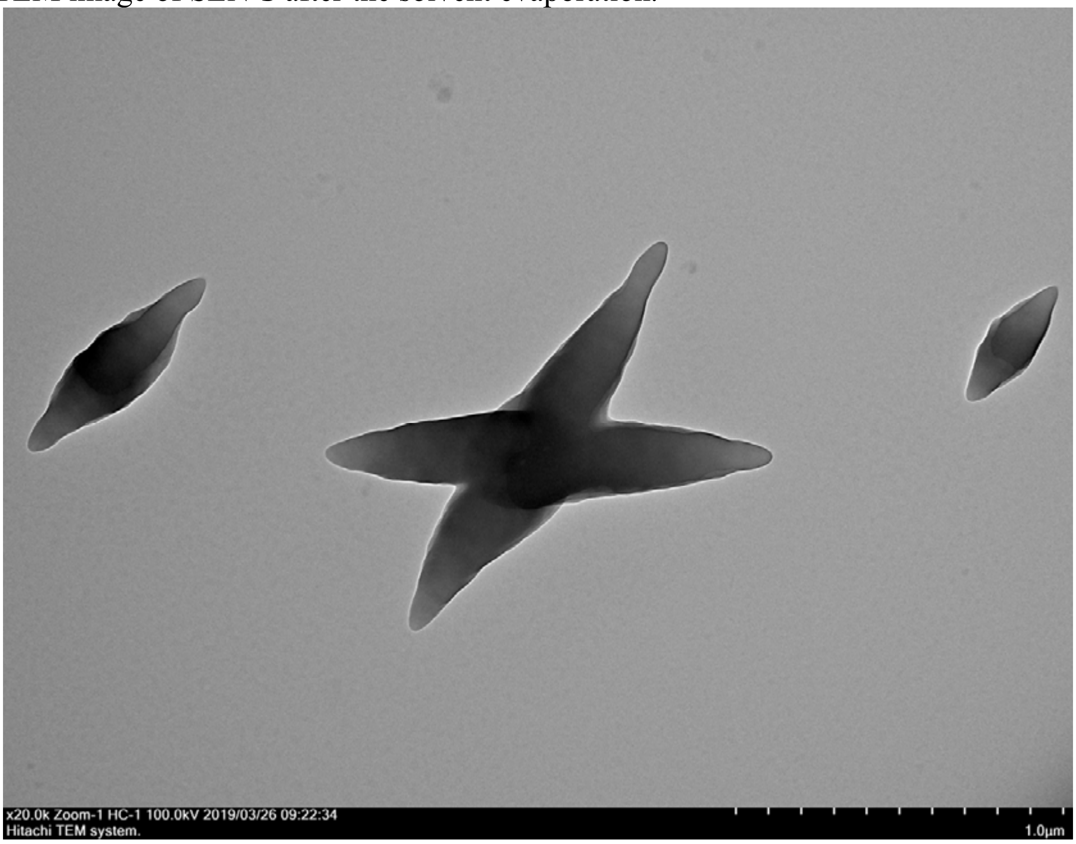

Fig. S19. TEM image of SLN-**5** after the solvent evaporation.

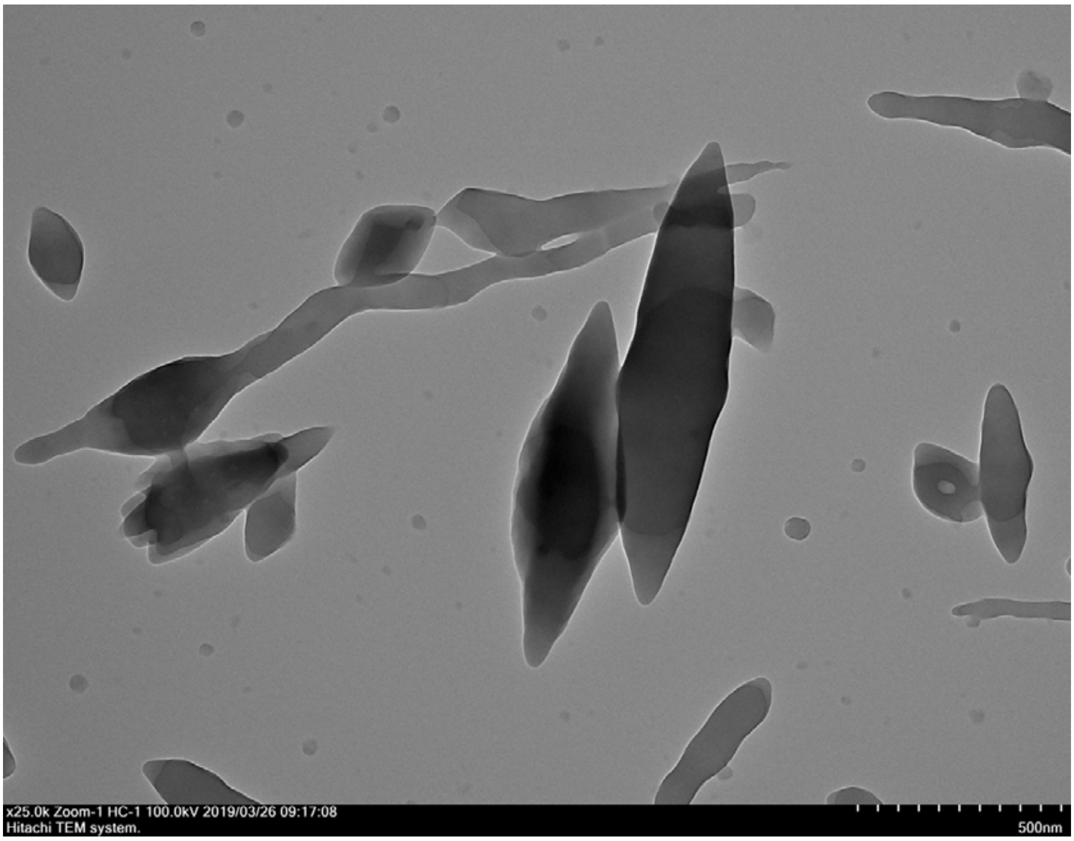

Fig. S20. TEM image of SLN-**5** after the solvent evaporation.

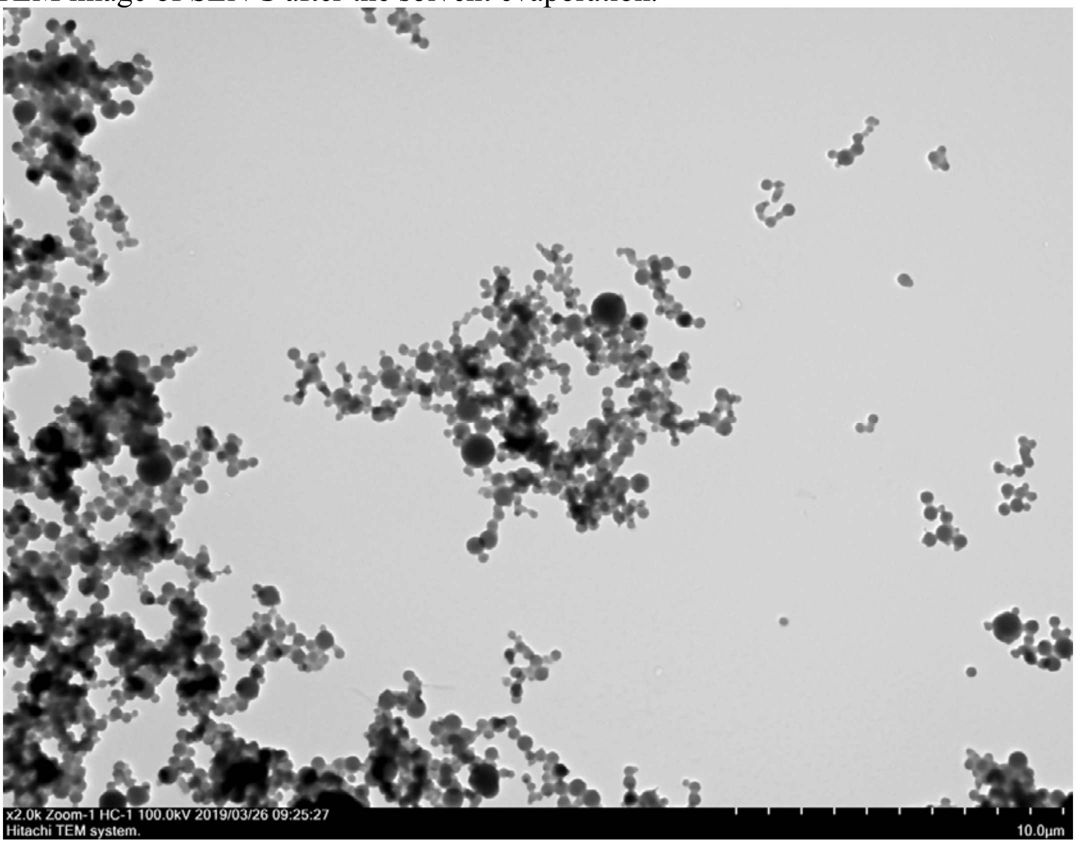

Fig. S21. TEM image of SLN-**6** after the solvent evaporation.

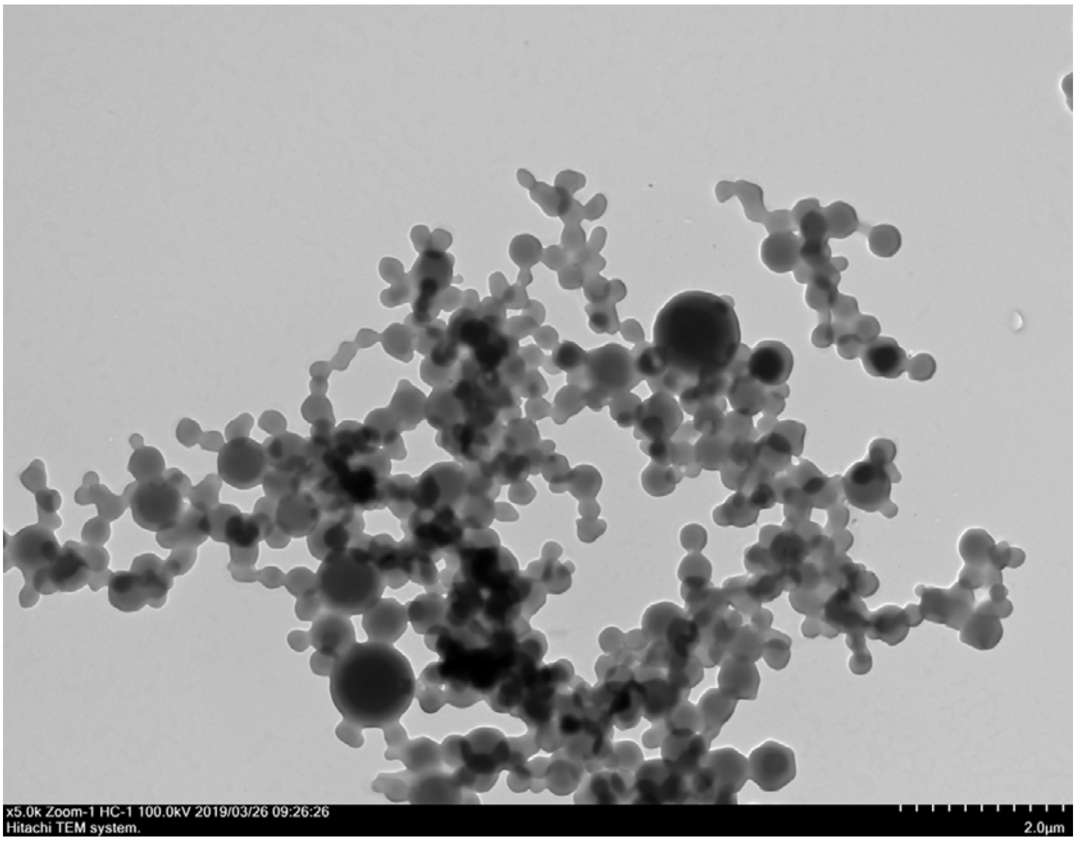

Fig. S22. TEM image of SLN-**6** after the solvent evaporation.

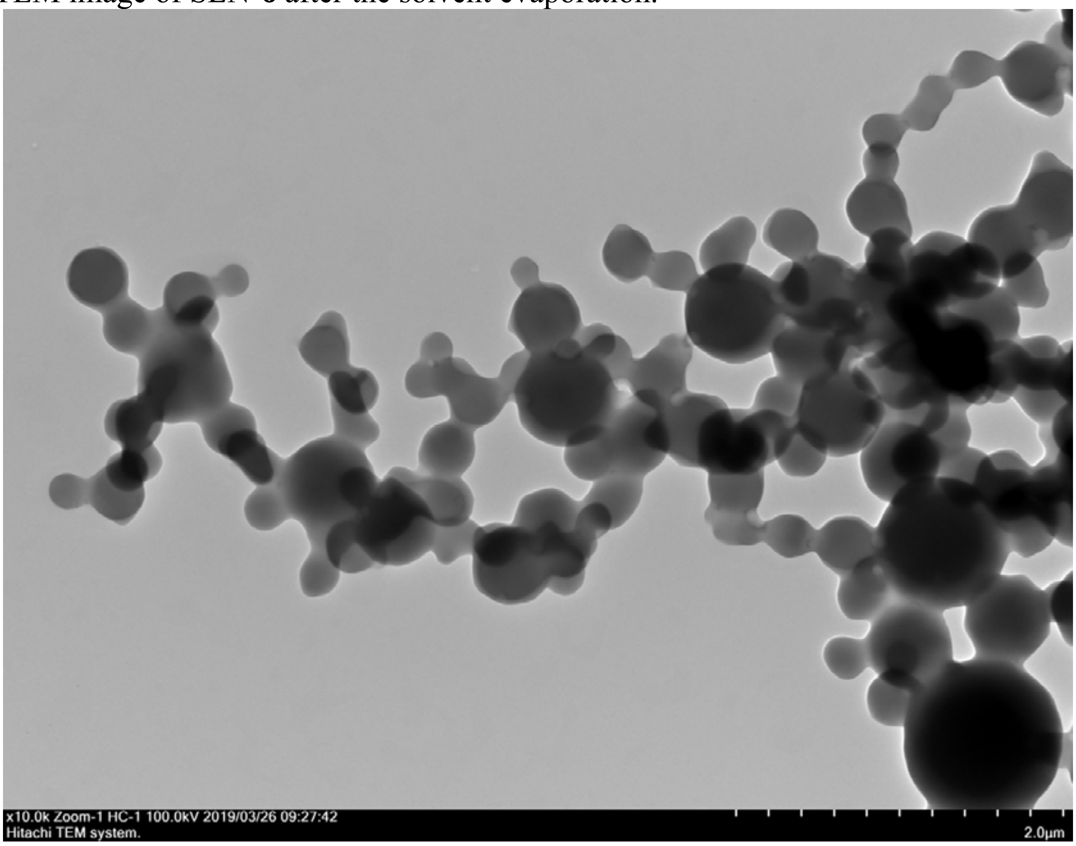

Fig. S23. TEM image of SLN-**6** after the solvent evaporation.

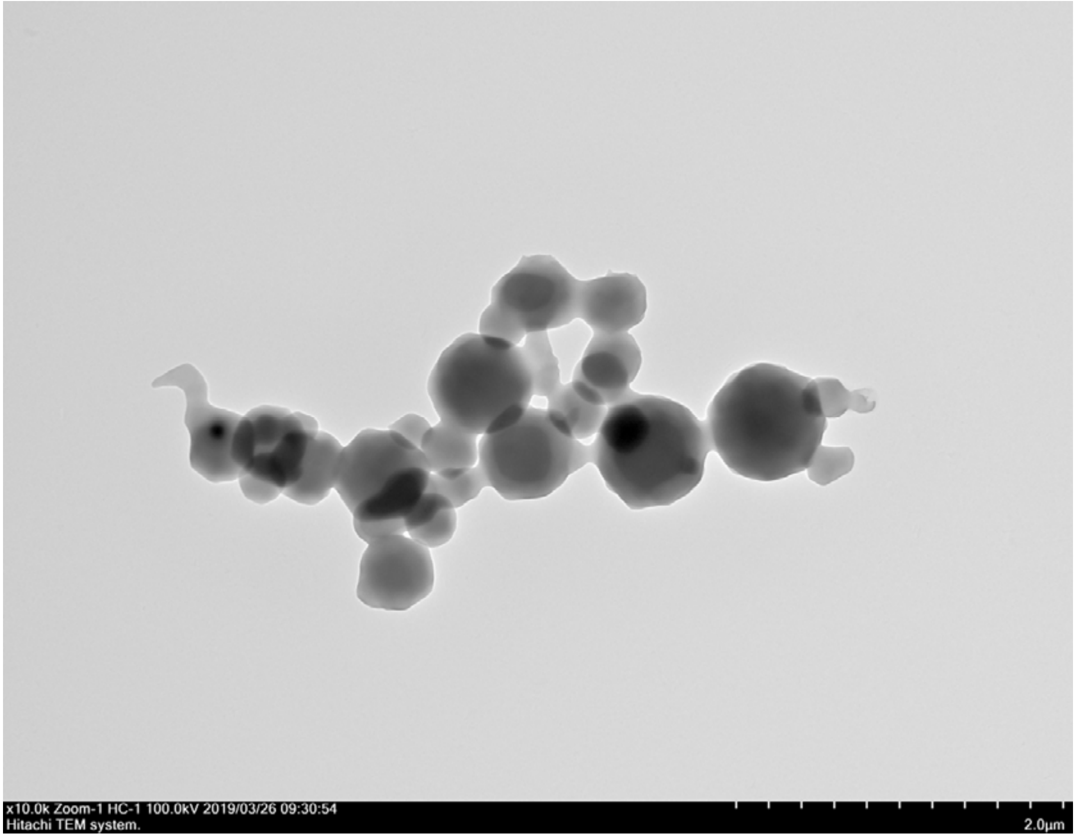

Fig. S24. TEM image of SLN-**6** after the solvent evaporation.

TEM analysis of SLN-[3-6]-Flu

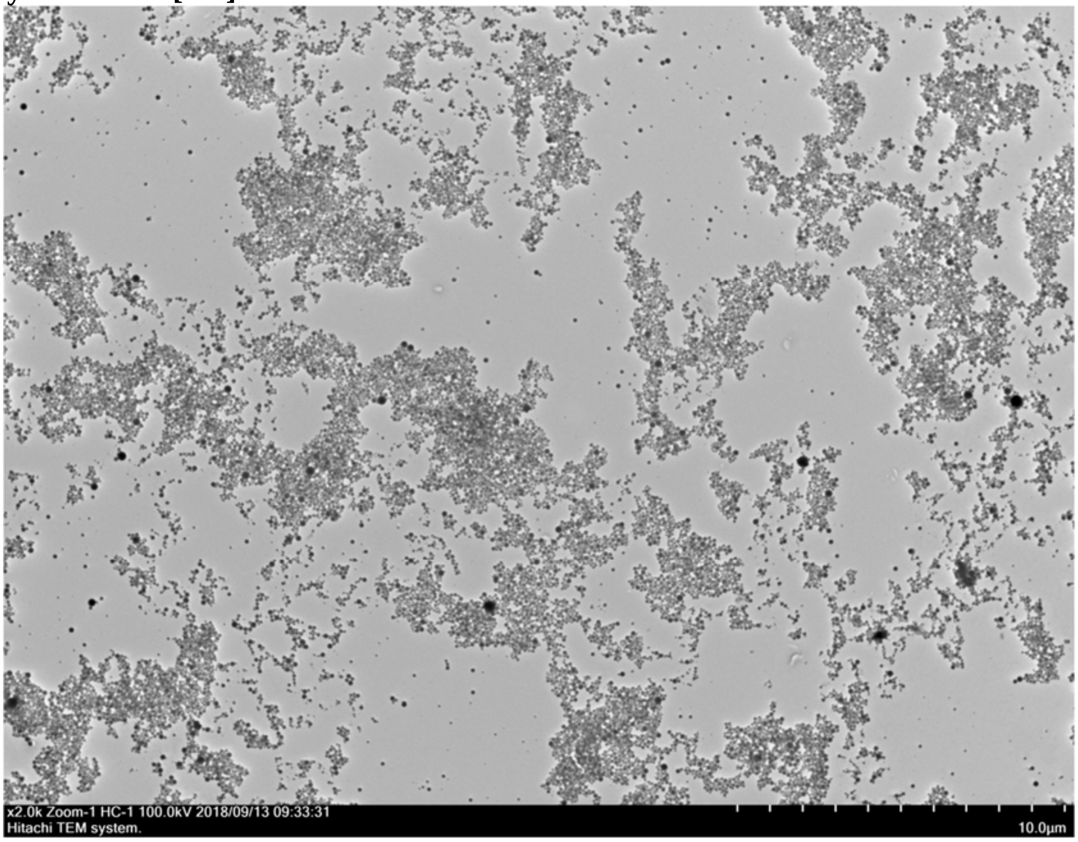

Fig. S25. TEM image of SLN-**3**-Flu after the solvent evaporation.

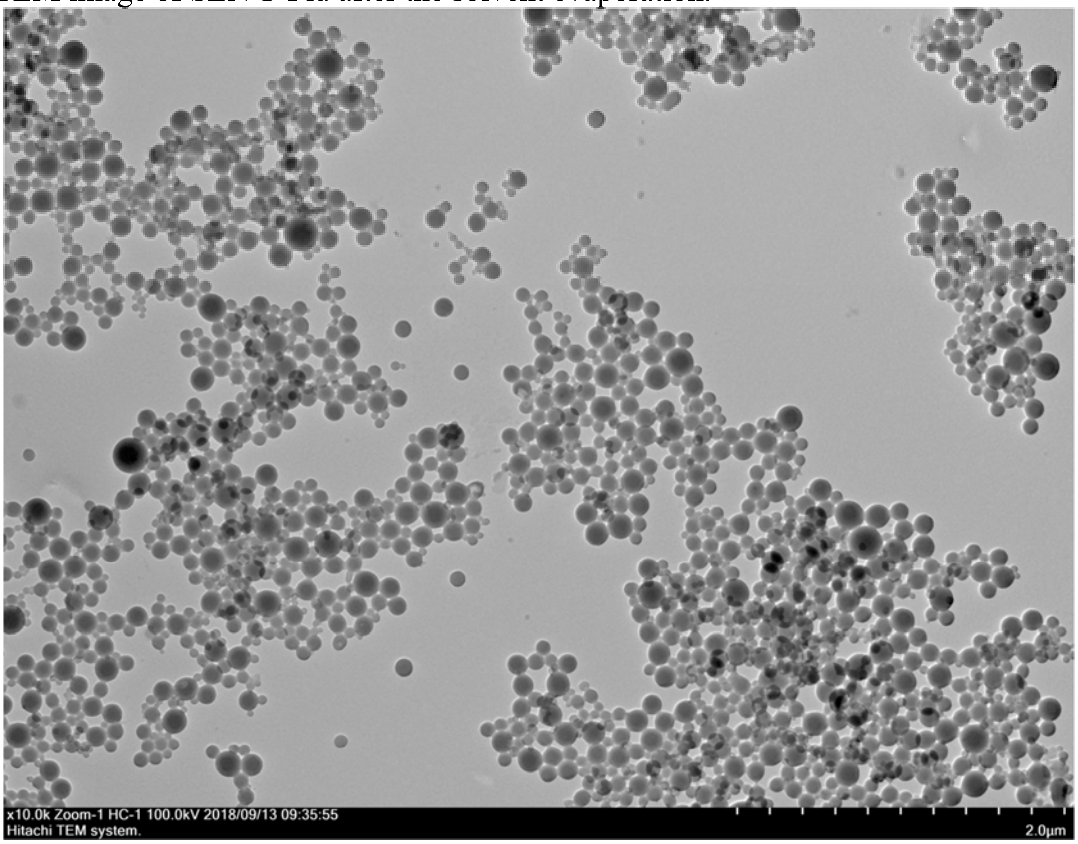

Fig. S26. TEM image of SLN-**3**-Flu after the solvent evaporation.

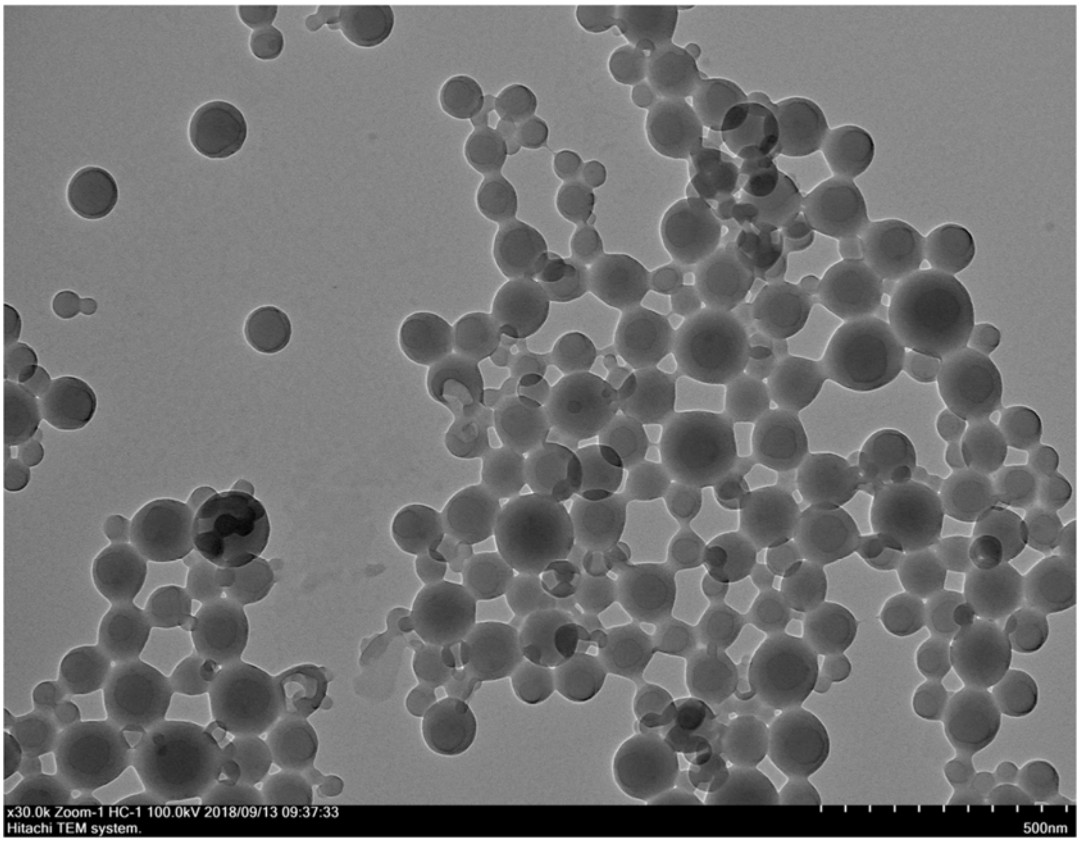

Fig. S27. TEM image of SLN-**3**-Flu after the solvent evaporation.

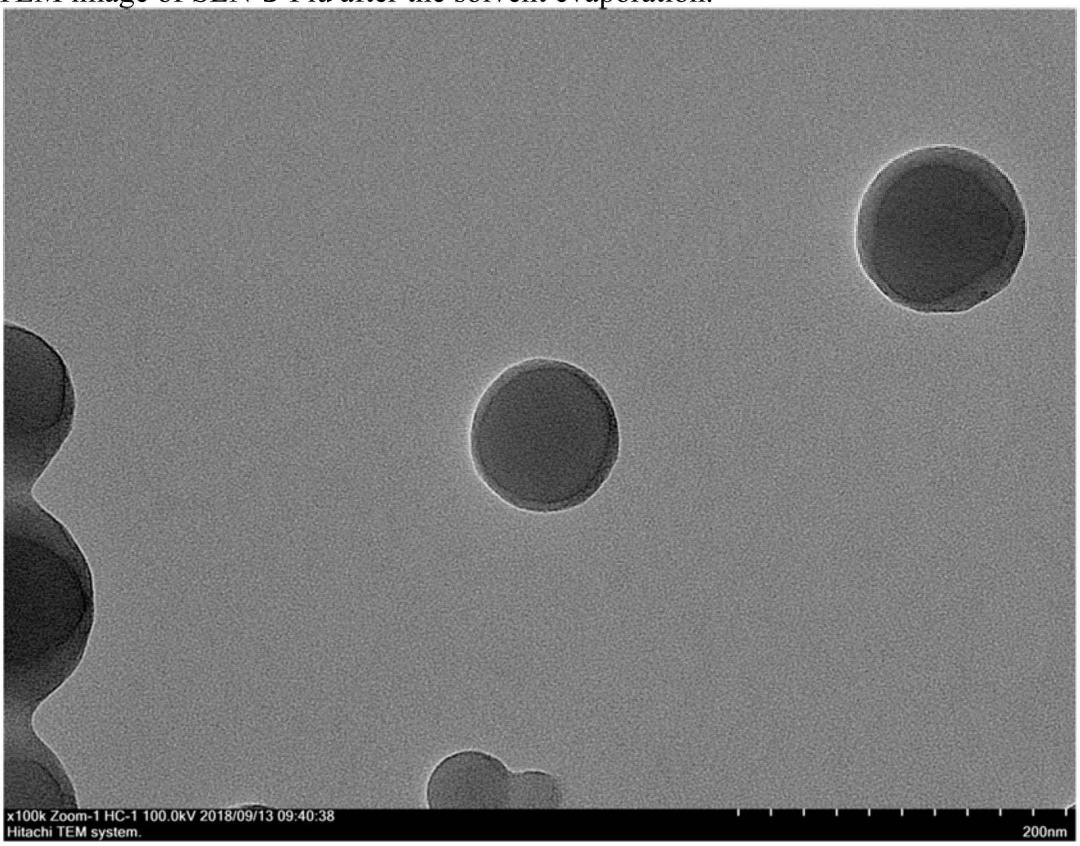

Fig. S28. TEM image of SLN-**3**-Flu after the solvent evaporation.

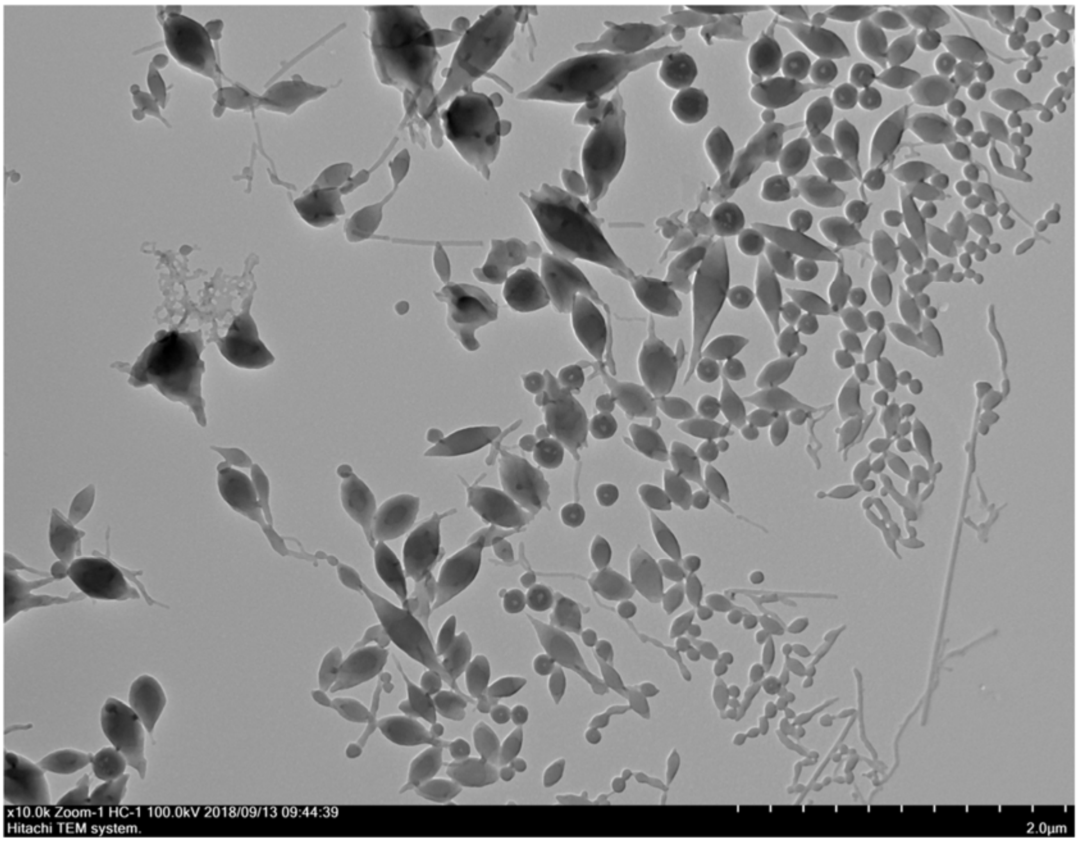

Fig. S29. TEM image of SLN-**4**-Flu after the solvent evaporation.

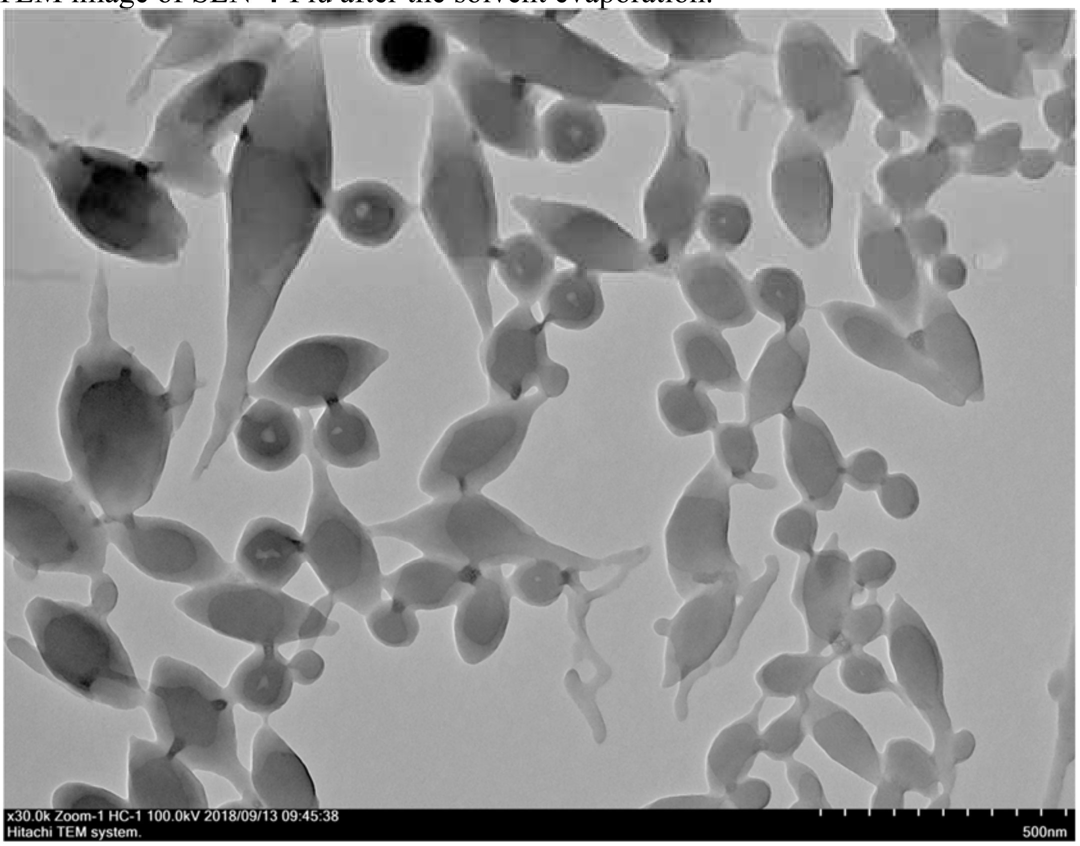

Fig. S30. TEM image of SLN-**4**-Flu after the solvent evaporation.

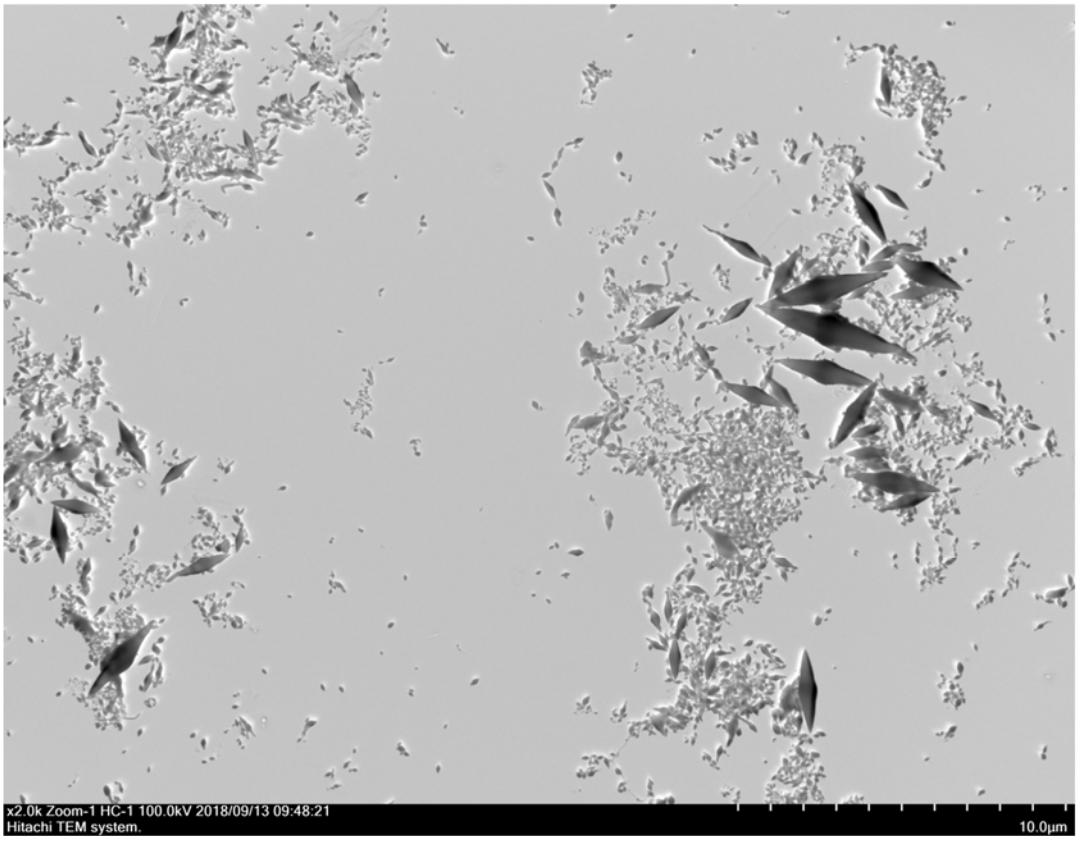

Fig. S31. TEM image of SLN-**5**-Flu after the solvent evaporation.

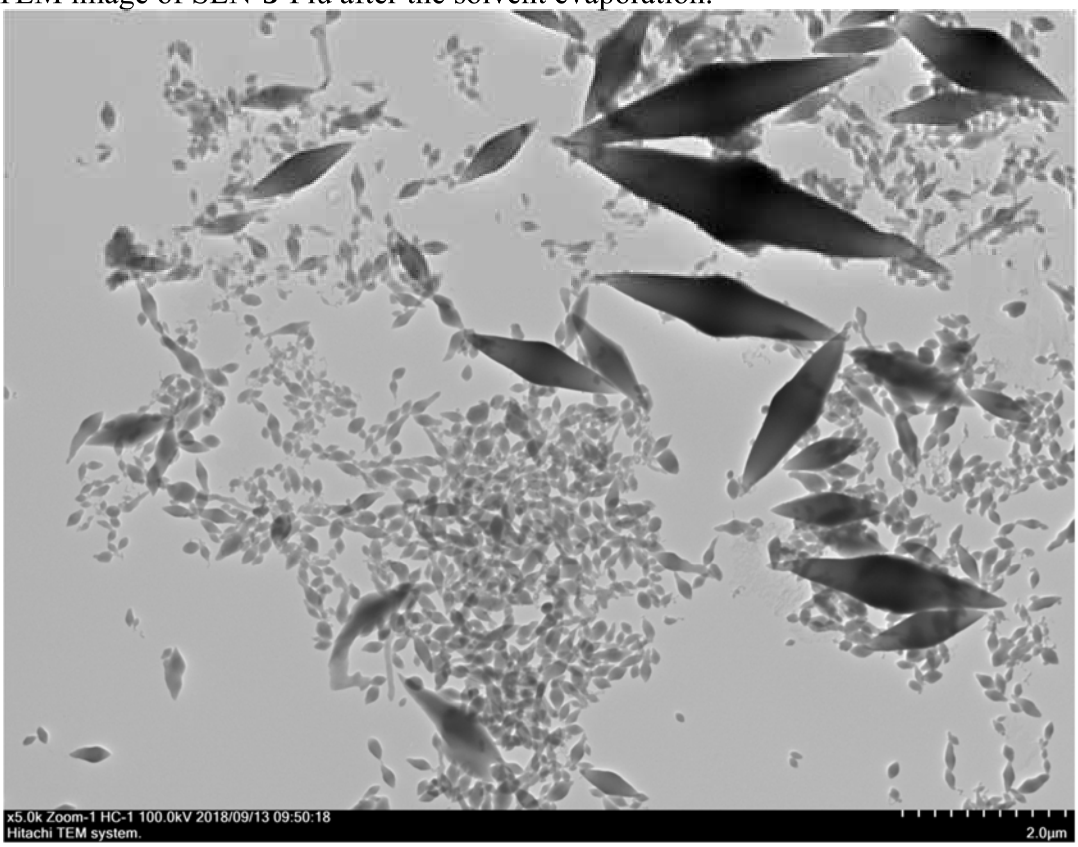

Fig. S32. TEM image of SLN-**5**-Flu after the solvent evaporation.

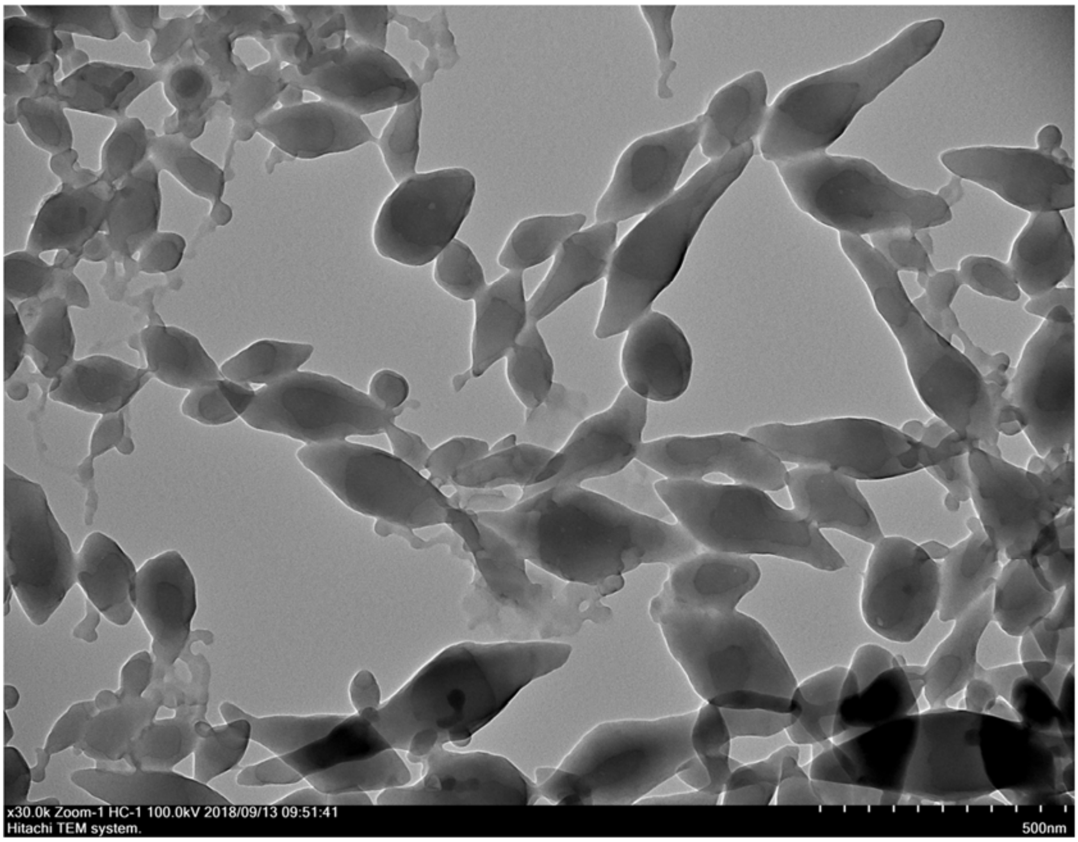

Fig. S33. TEM image of SLN-**5**-Flu after the solvent evaporation.

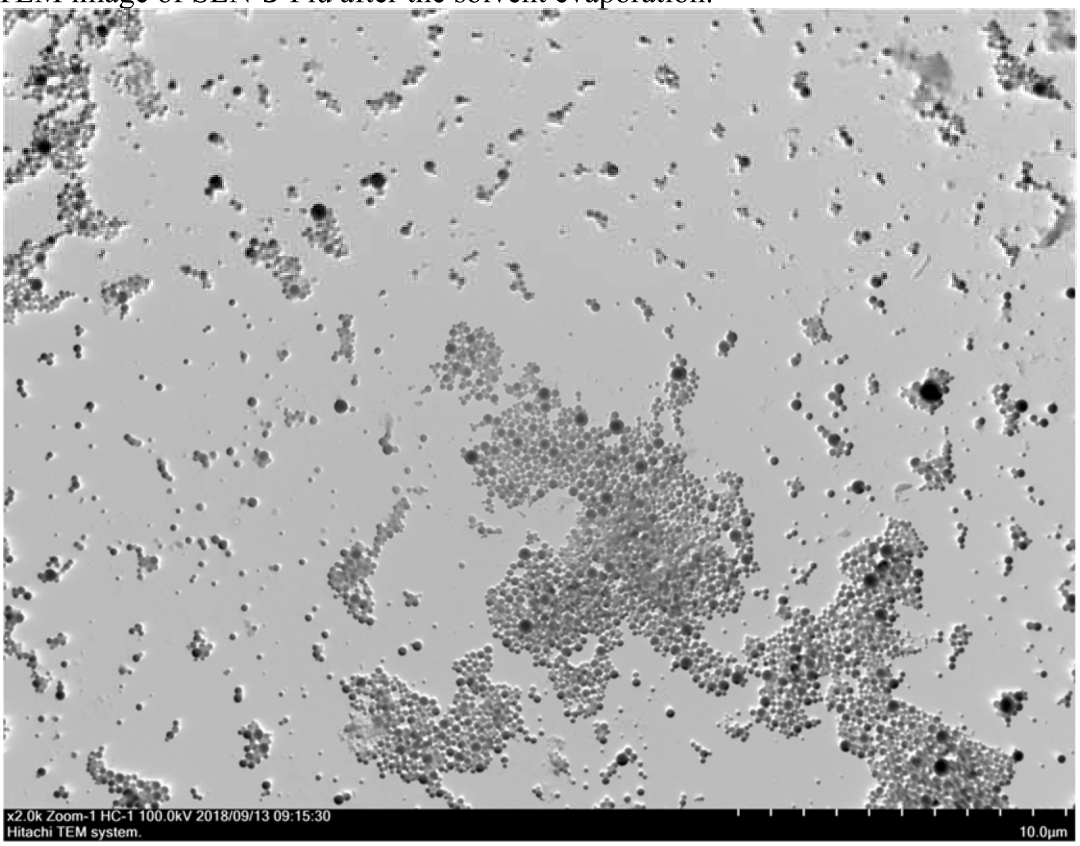

Fig. S34. TEM image of SLN-**6**-Flu after the solvent evaporation.

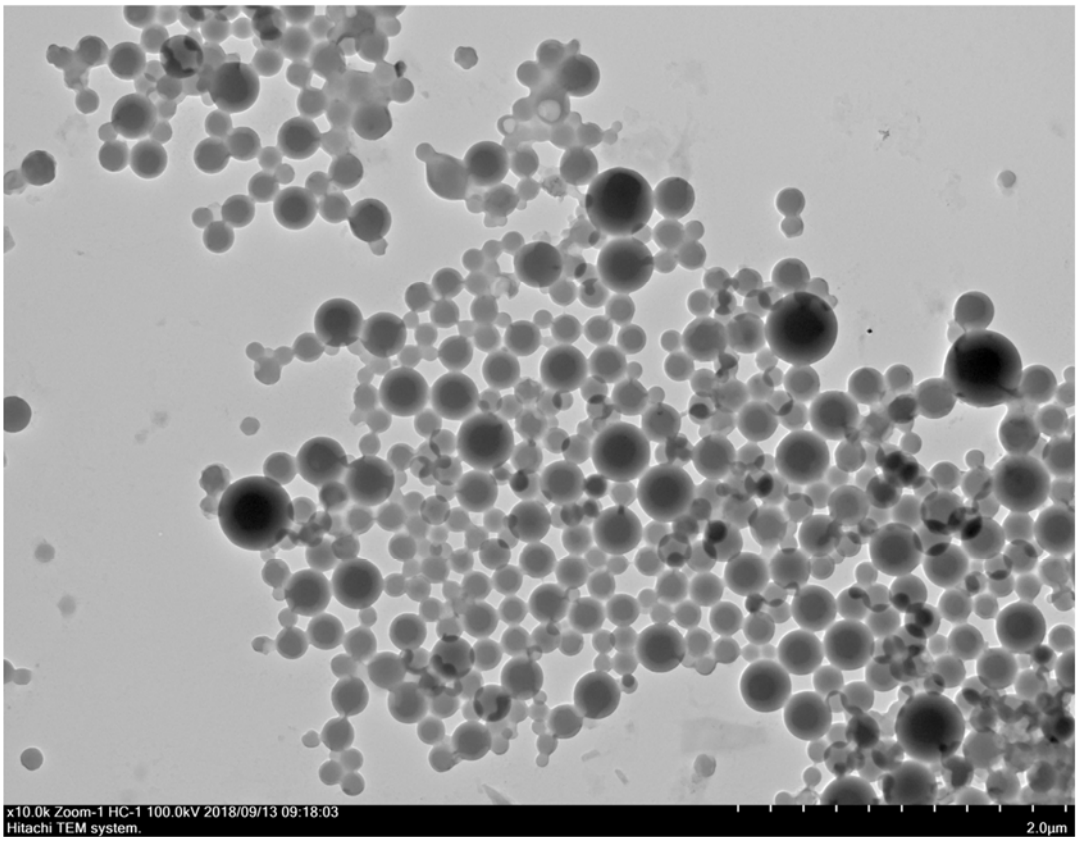

Fig. S35. TEM image of SLN-**6**-Flu after the solvent evaporation.

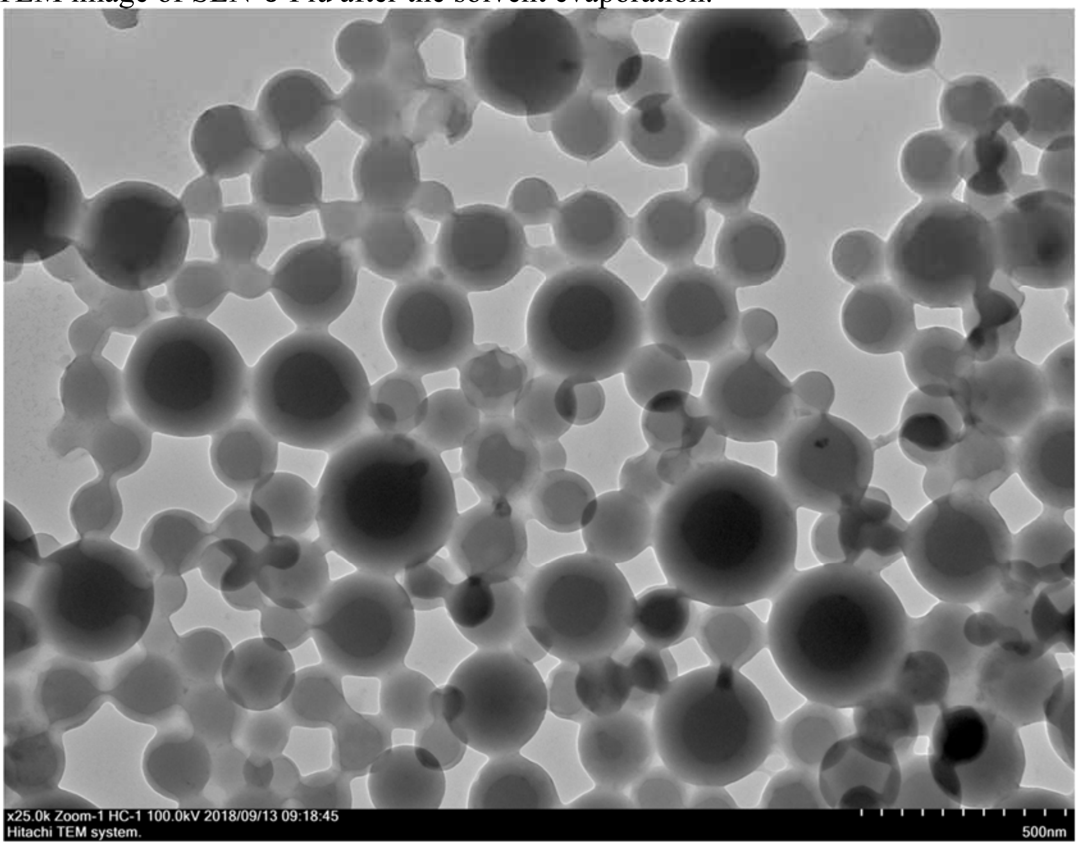

Fig. S36. TEM image of SLN-**6**-Flu after the solvent evaporation.

TEM analysis of SLN-[3-6]-RhB

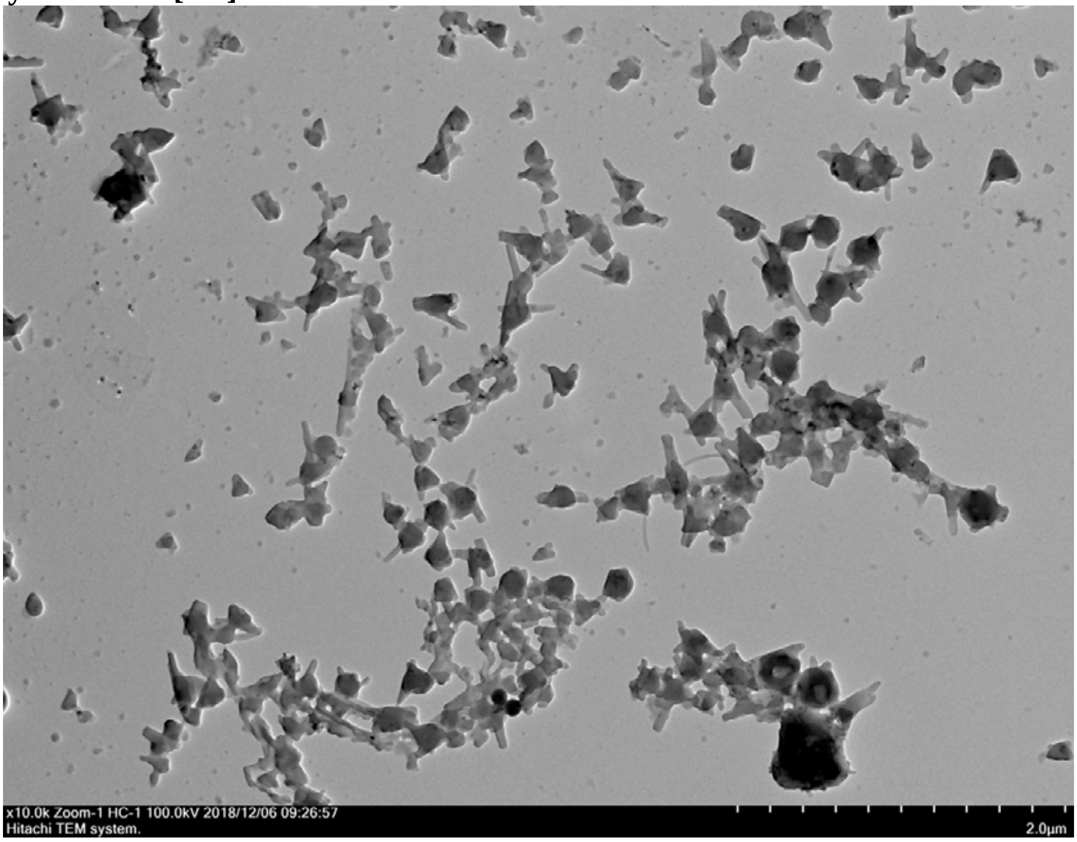

Fig. S37. TEM image of SLN-**3**-RhB after the solvent evaporation.

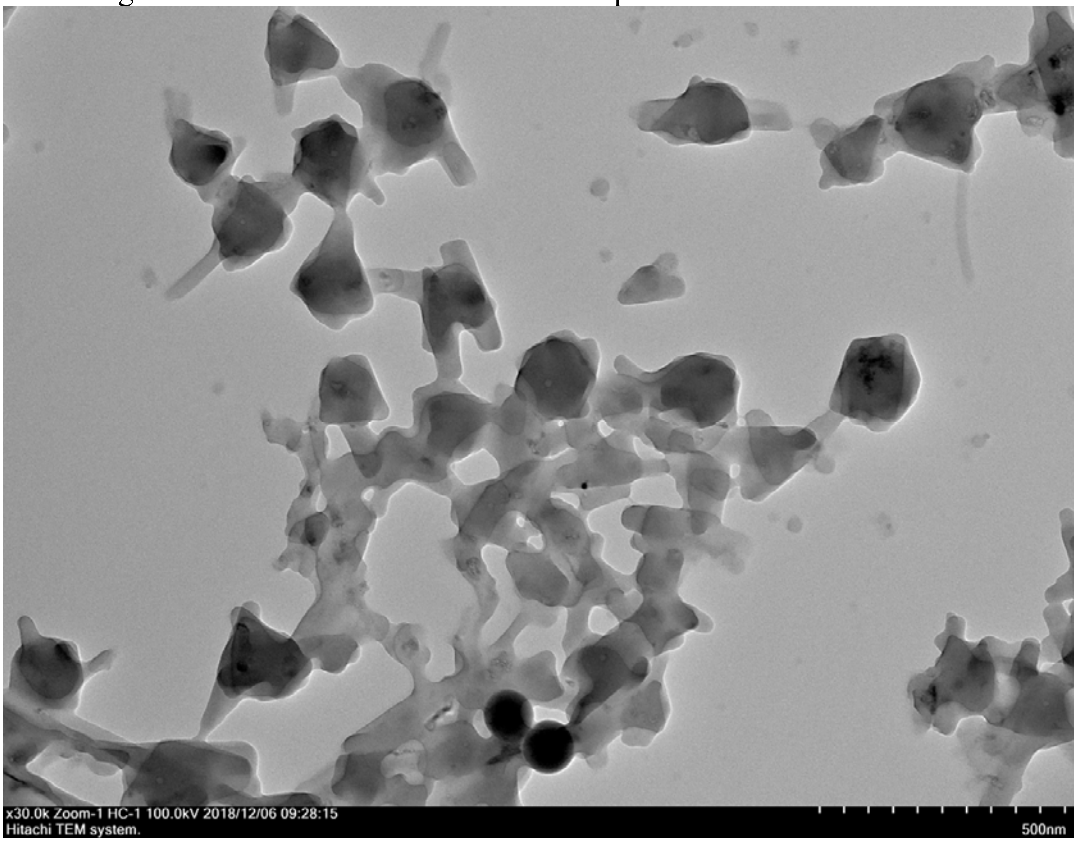

Fig. S38. TEM image of SLN-**3**-RhB after the solvent evaporation.

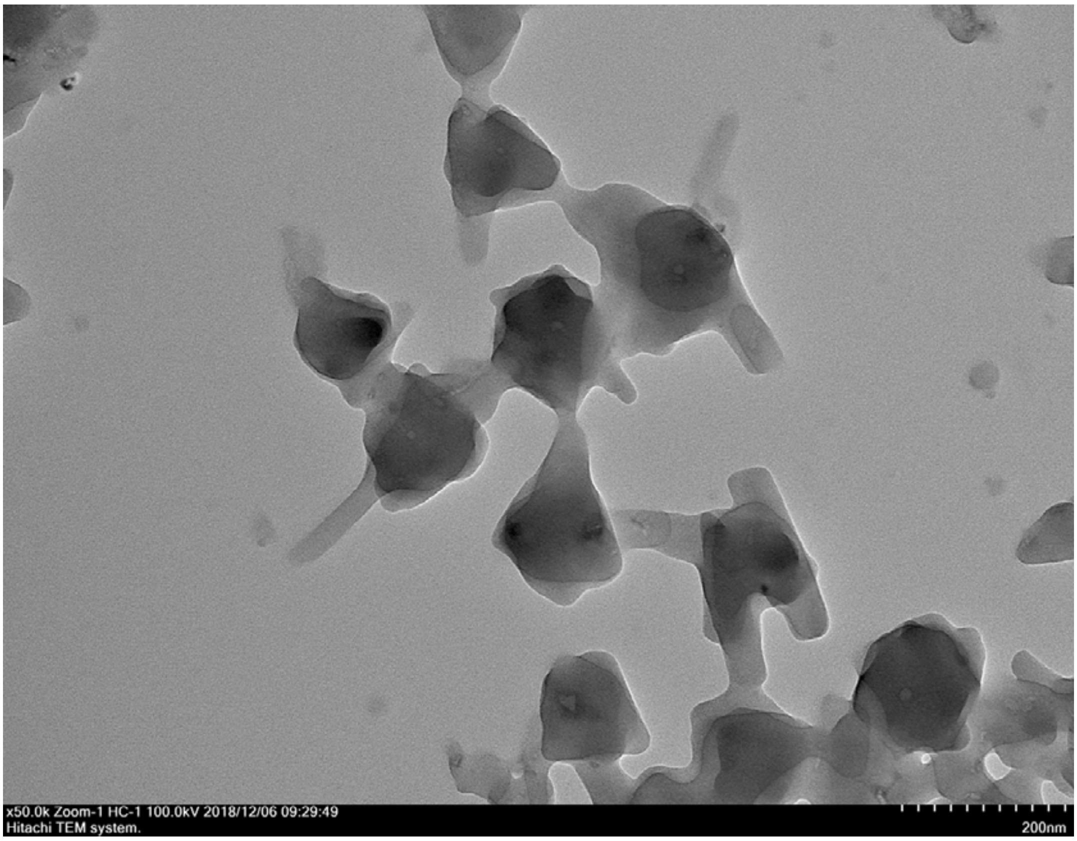

Fig. S39. TEM image of SLN-**3**-RhB after the solvent evaporation.

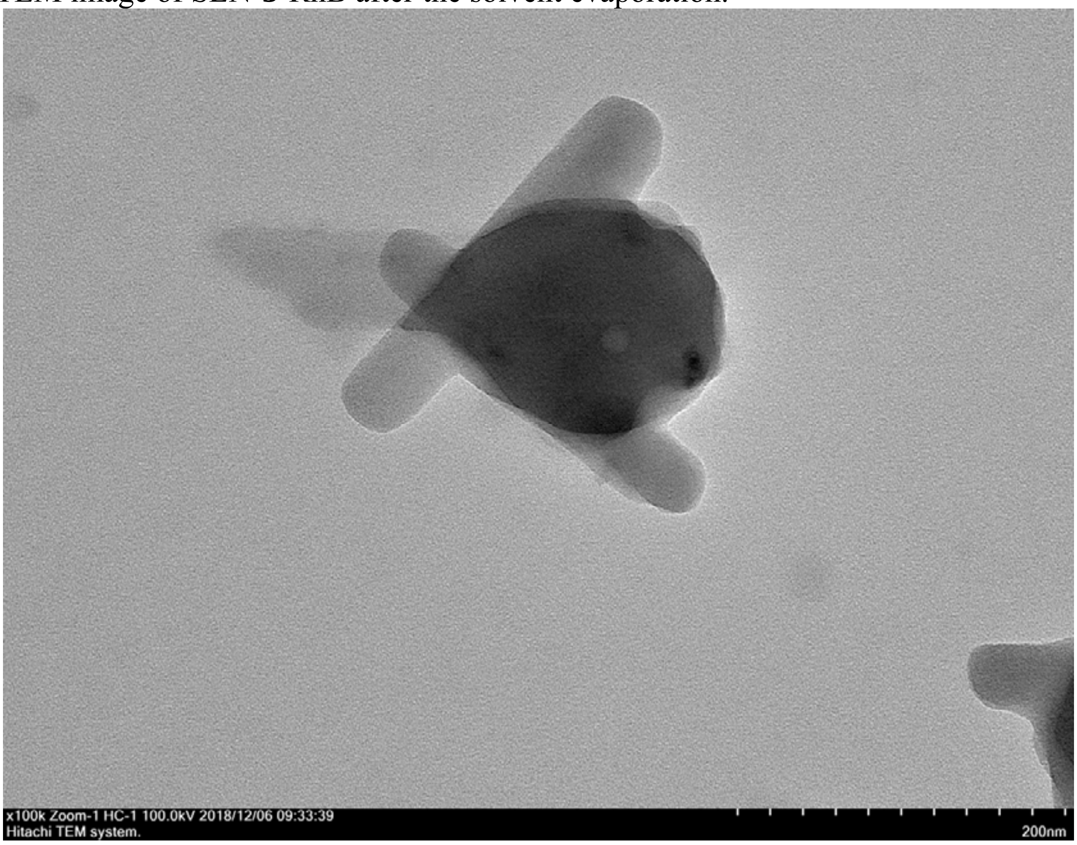

Fig. S40. TEM image of SLN-**3**-RhB after the solvent evaporation.

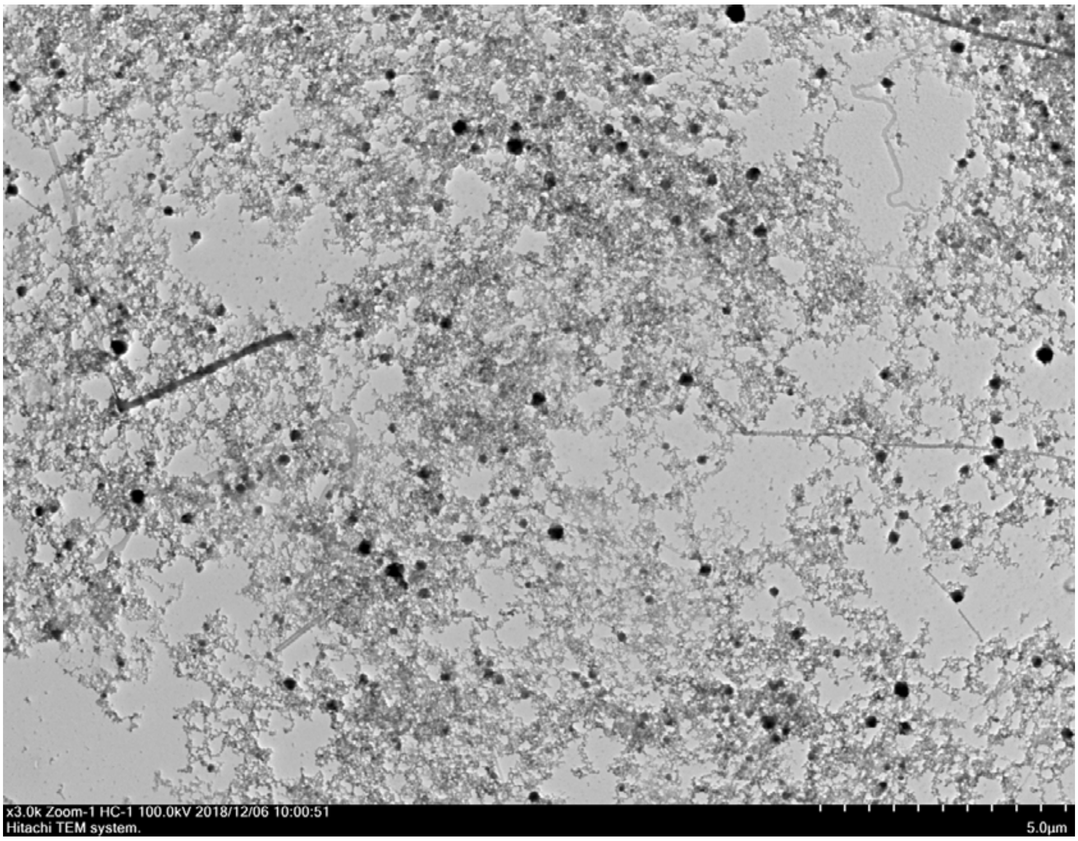

Fig. S41. TEM image of SLN-**4**-RhB after the solvent evaporation.

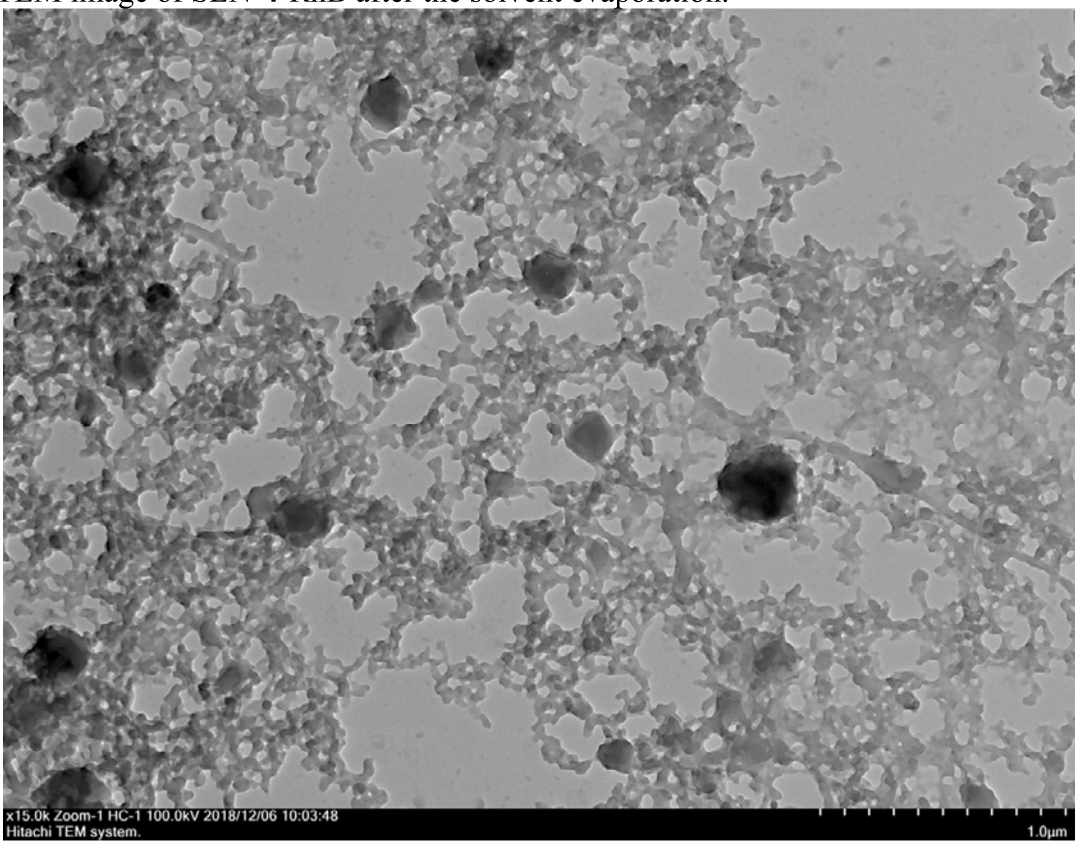

Fig. S42. TEM image of SLN-**4**-RhB after the solvent evaporation.

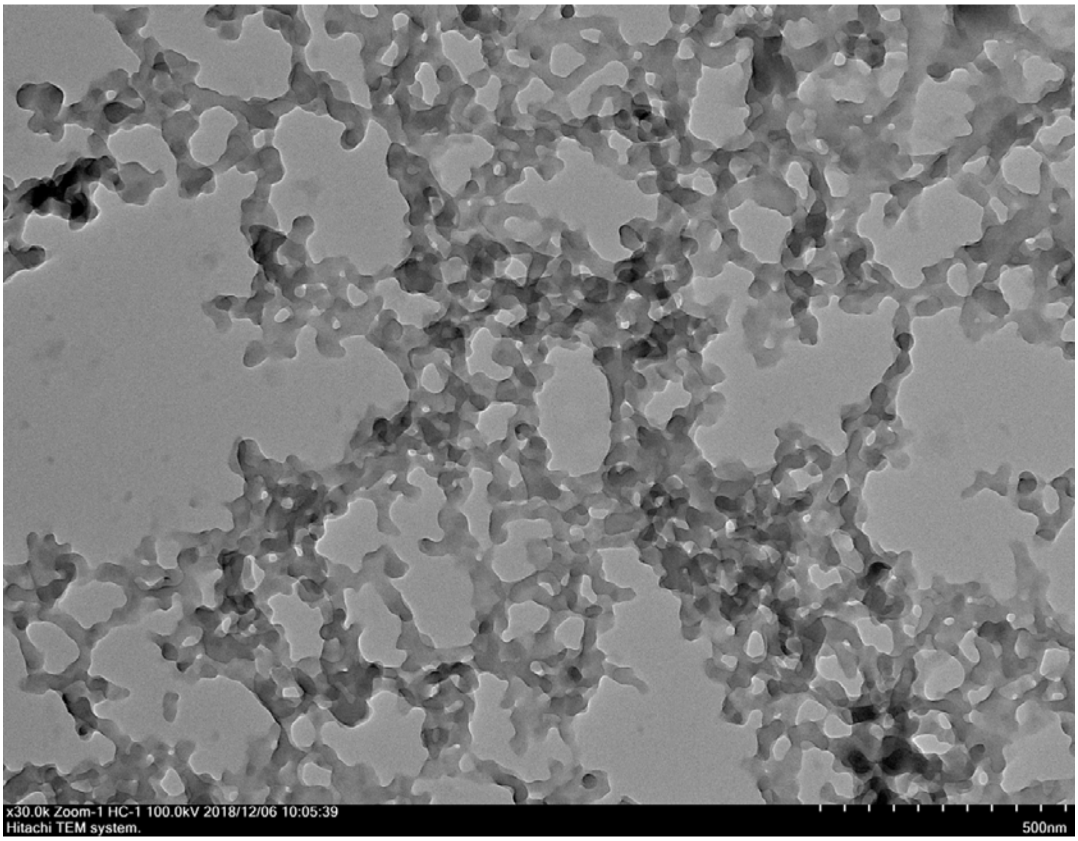

Fig. S43. TEM image of SLN-**4**-RhB after the solvent evaporation.

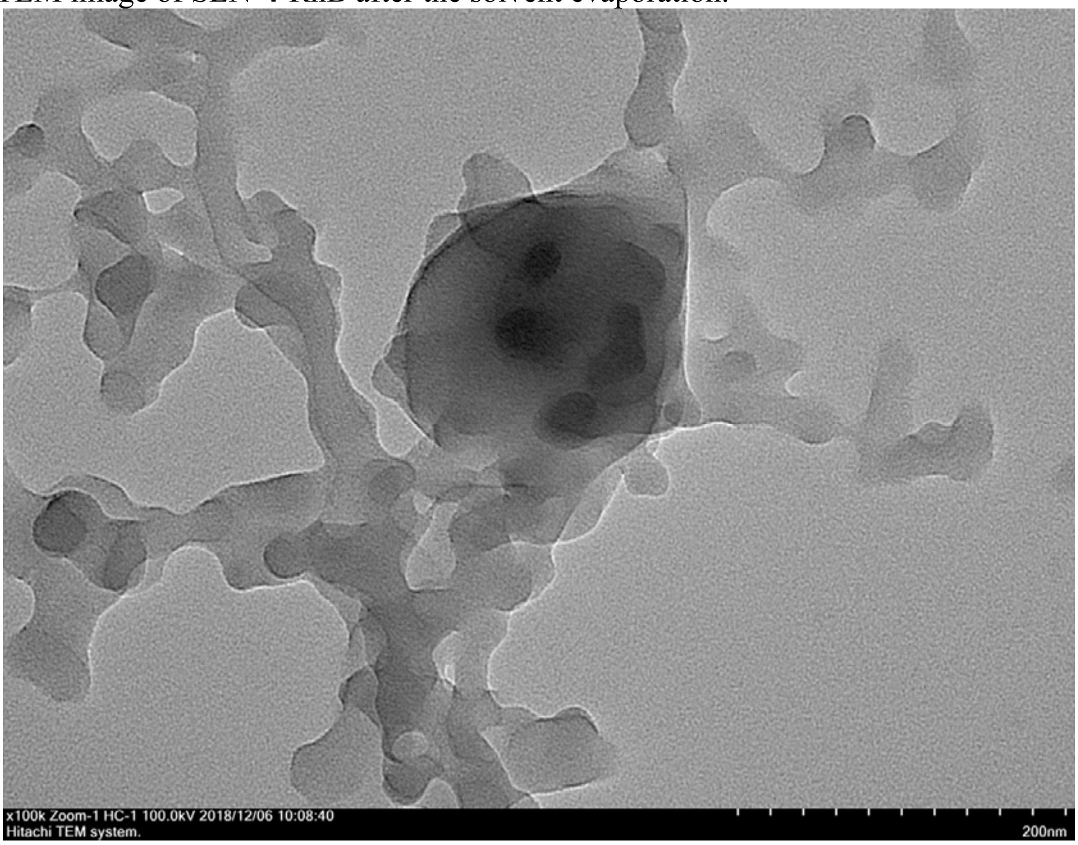

Fig. S44. TEM image of SLN-**4**-RhB after the solvent evaporation.

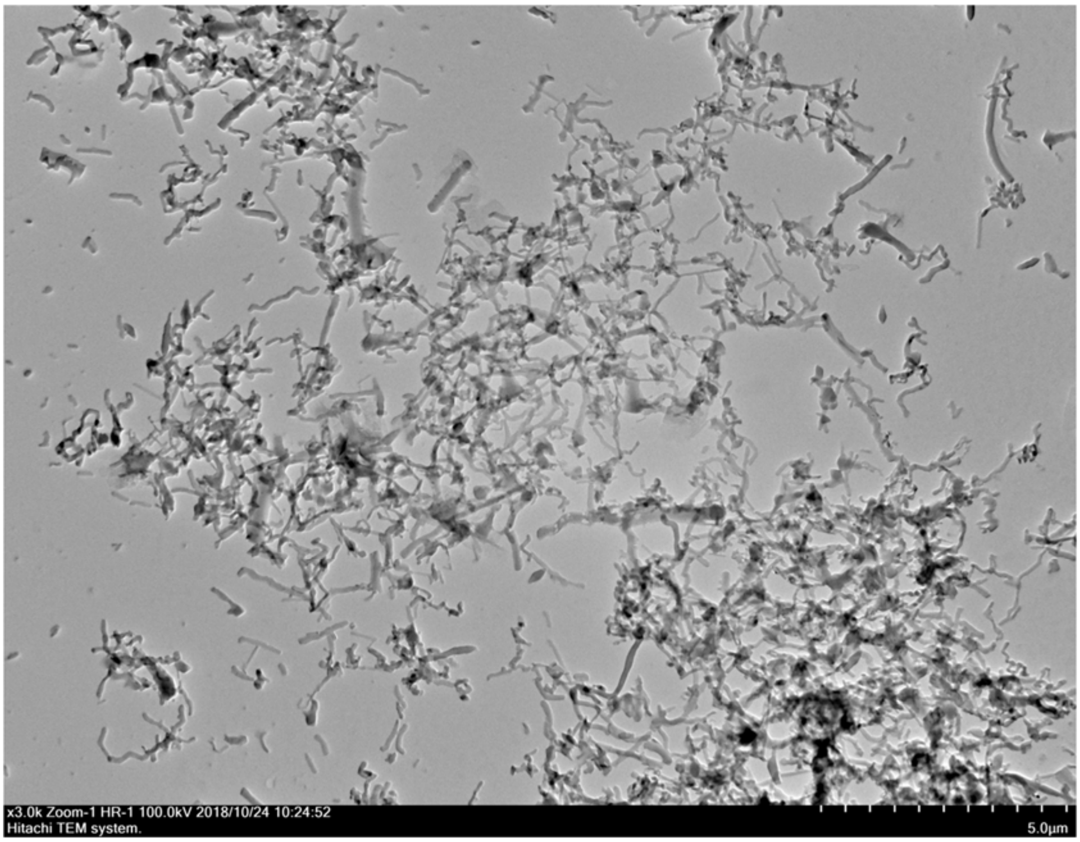

Fig. S45. TEM image of SLN-**5**-RhB after the solvent evaporation.

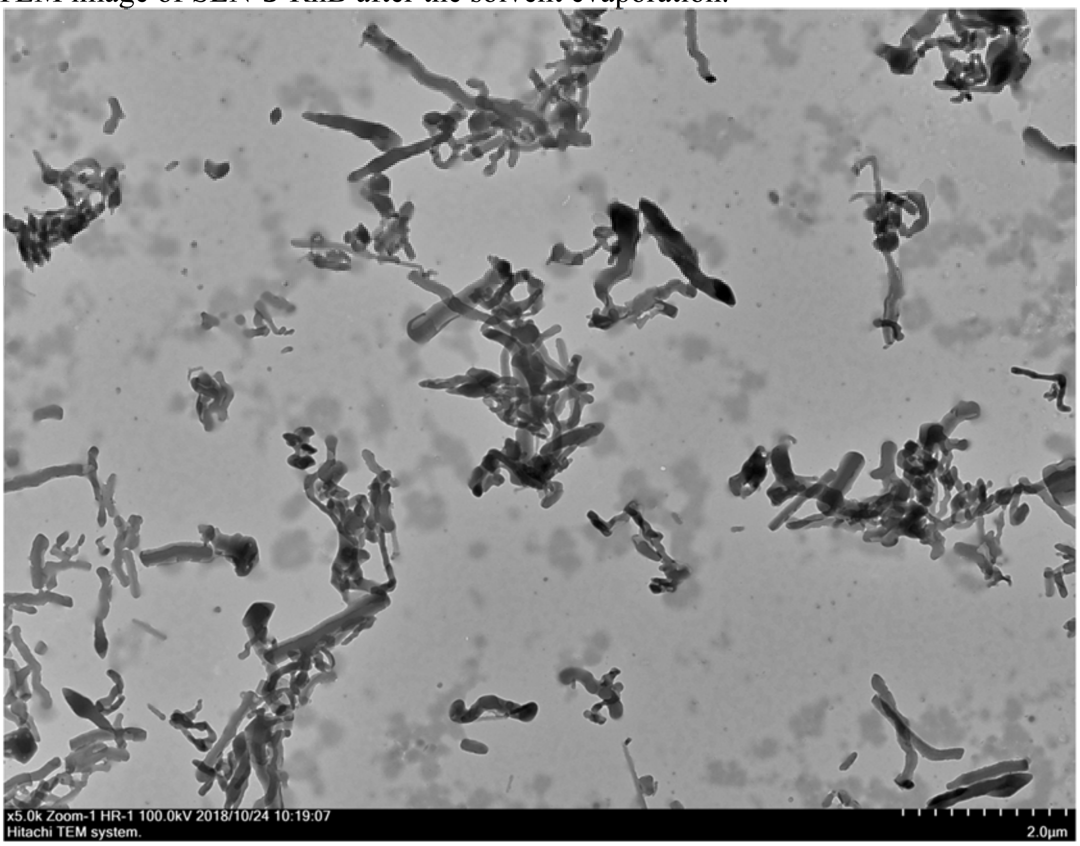

Fig. S46. TEM image of SLN-**5**-RhB after the solvent evaporation.

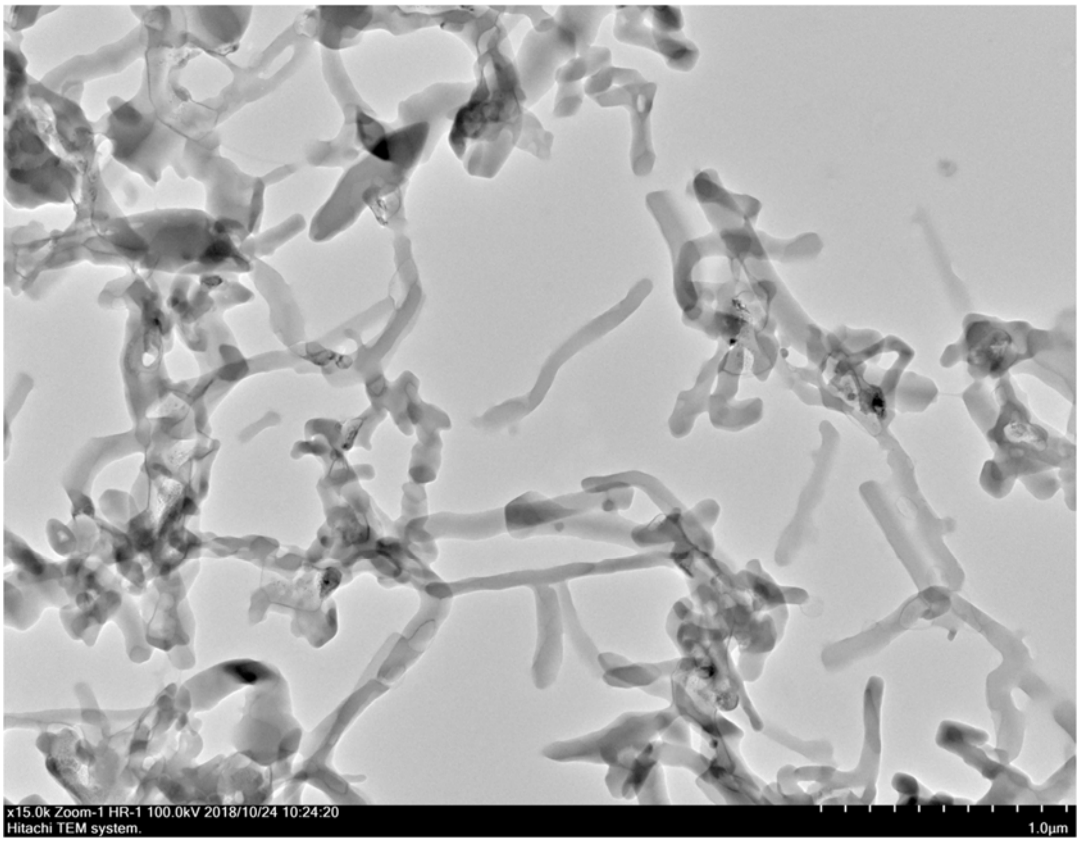

Fig. S47. TEM image of SLN-**5**-RhB after the solvent evaporation.

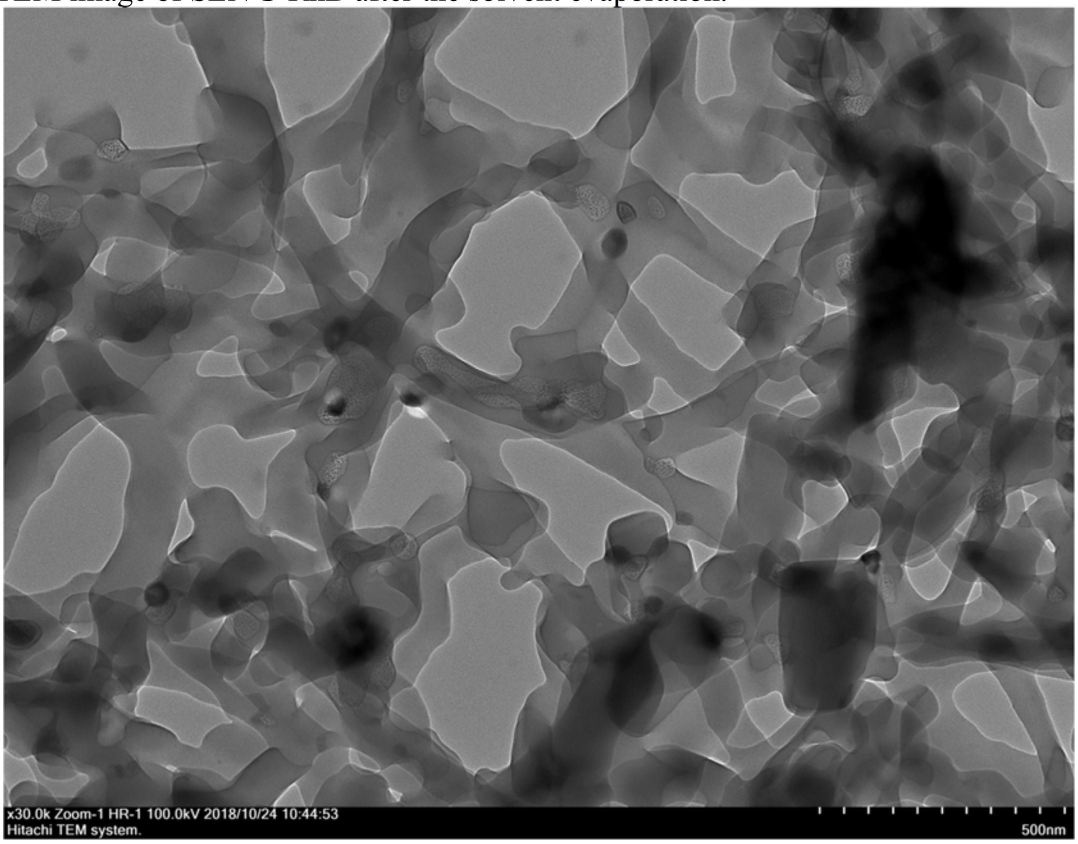

Fig. S48. TEM image of SLN-**5**-RhB after the solvent evaporation.

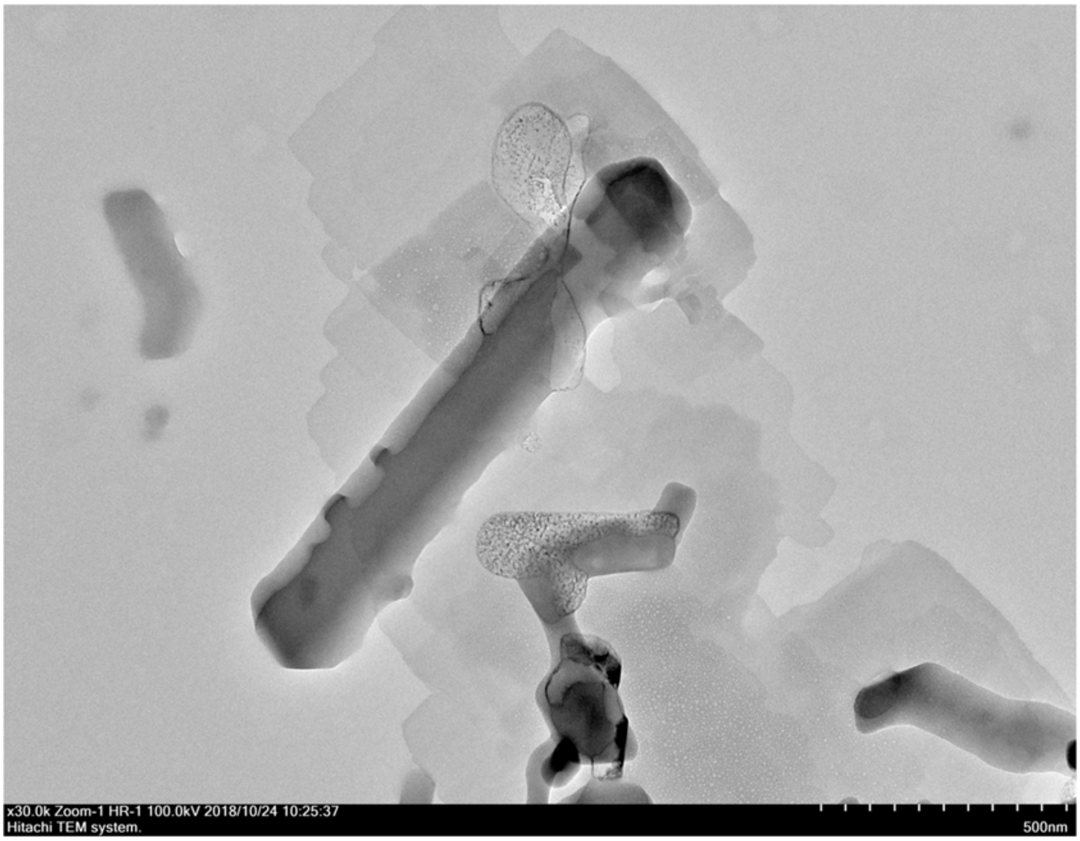

Fig. S49. TEM image of SLN-**5**-RhB after the solvent evaporation.

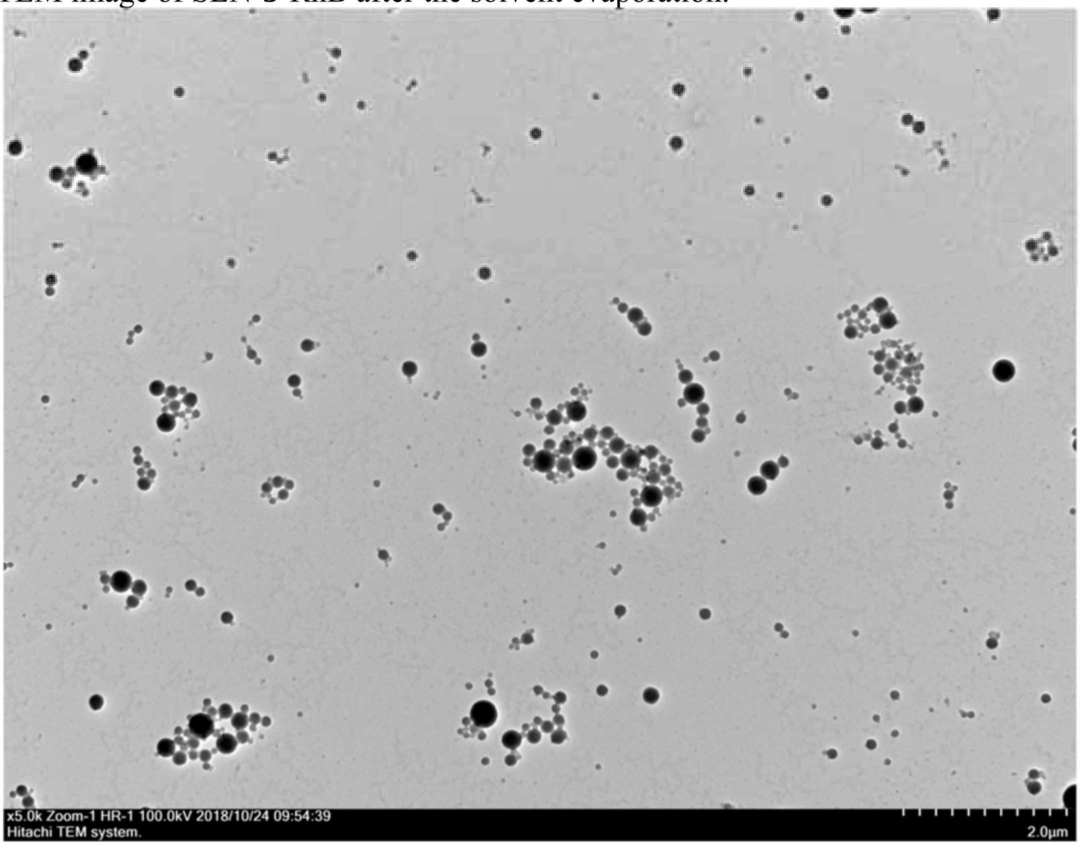

Fig. S50. TEM image of SLN-**6**-RhB after the solvent evaporation.

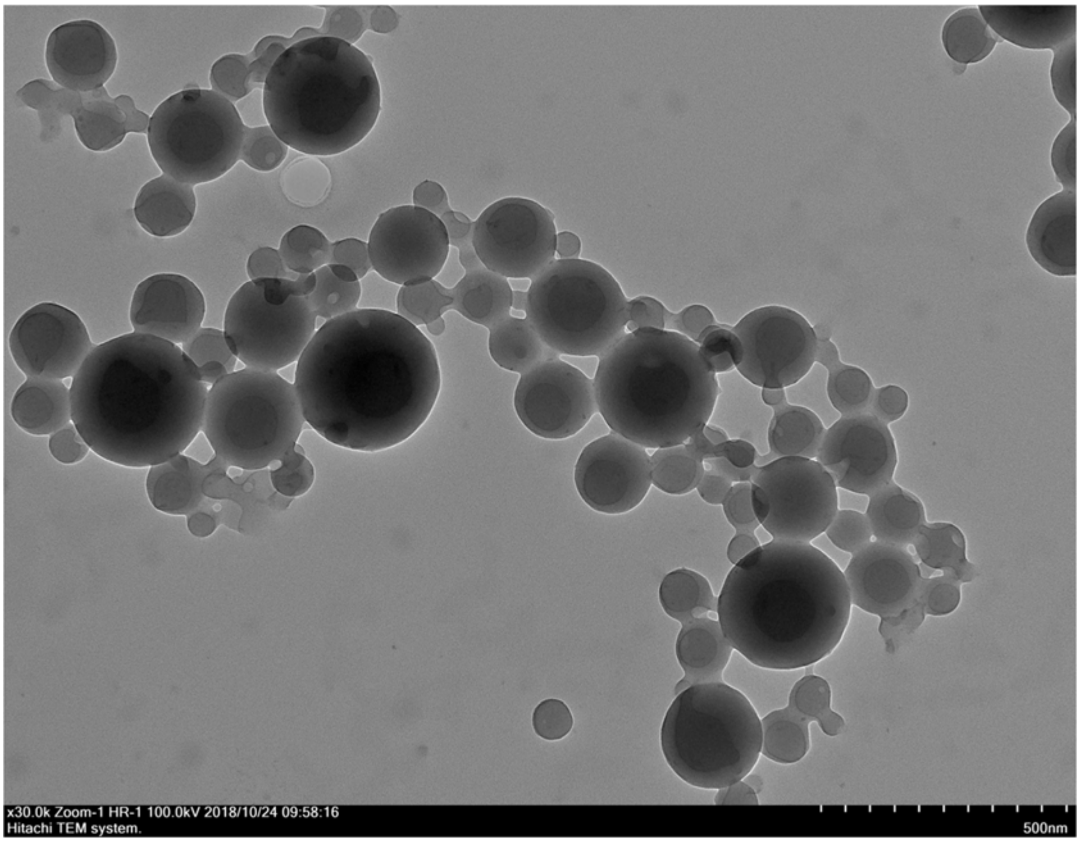

Fig. S51. TEM image of SLN-**6**-RhB after the solvent evaporation.

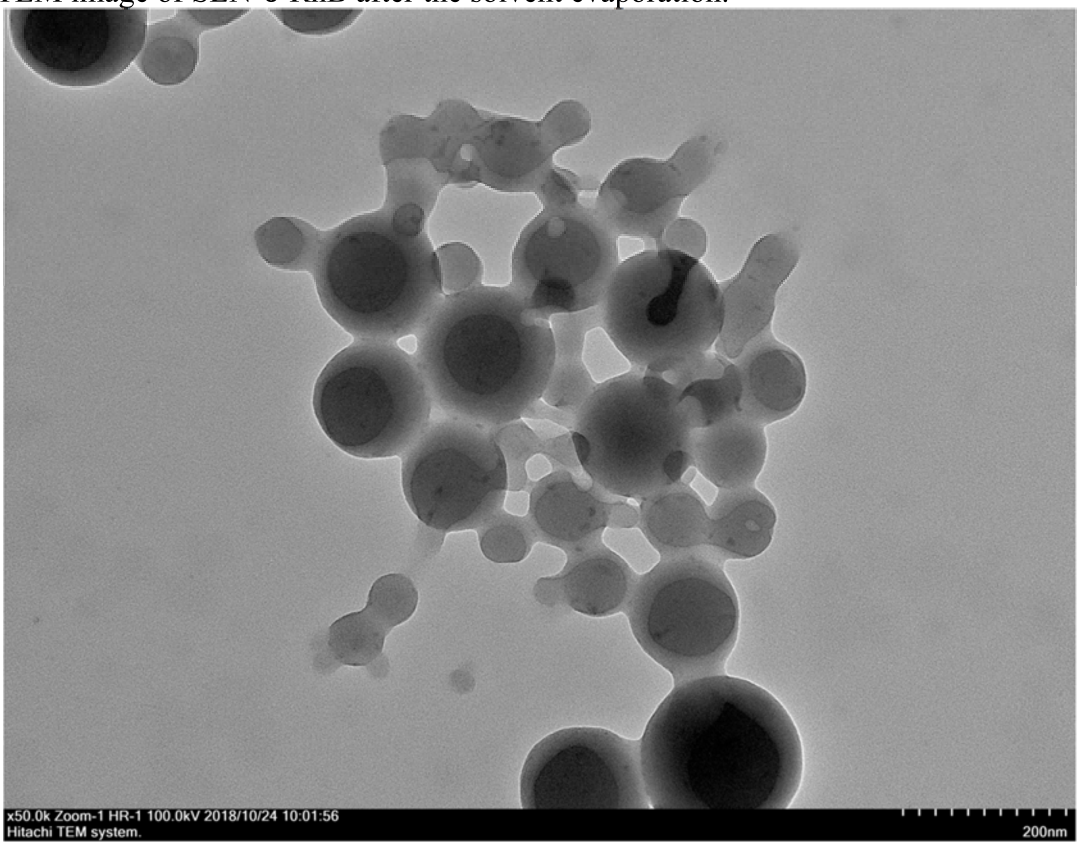

Fig. S52. TEM image of SLN-**6**-RhB after the solvent evaporation.

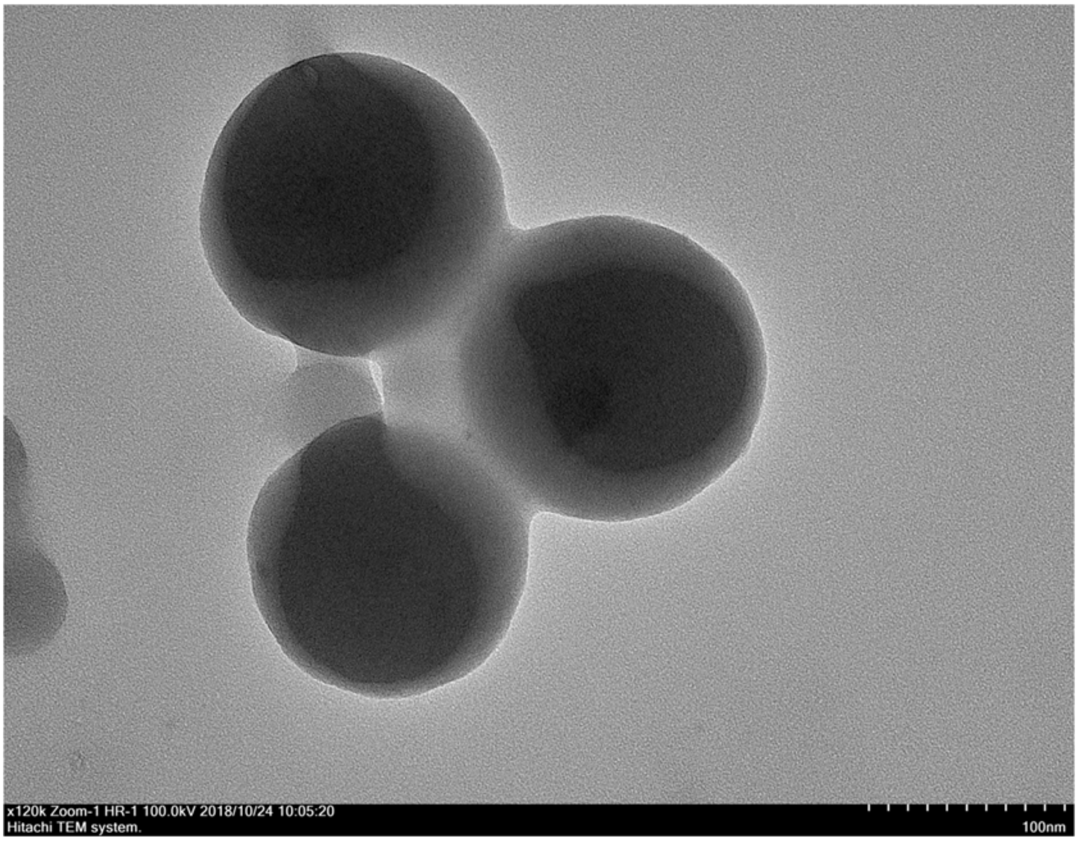

Fig. S53. TEM image of SLN-**6**-RhB after the solvent evaporation.

TEM analysis of SLN-[3-6]-Rh6G

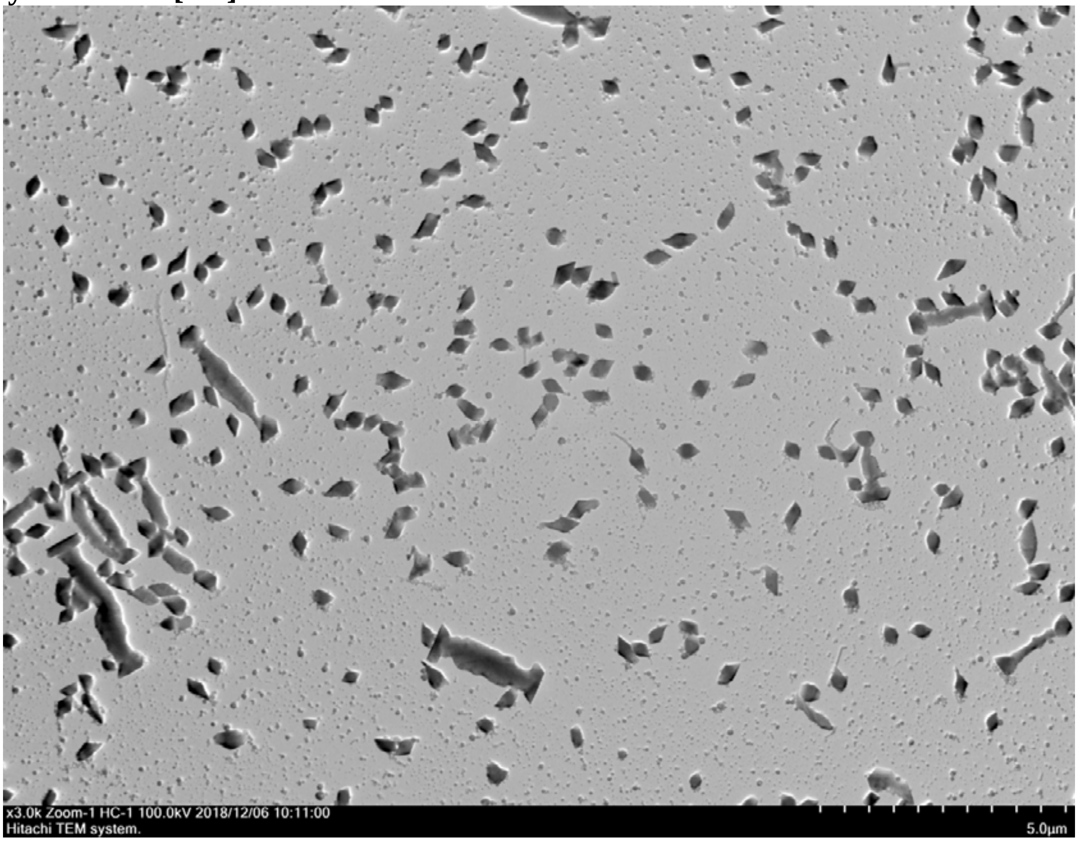

Fig. S54. TEM image of SLN-**3**-Rh6G after the solvent evaporation.

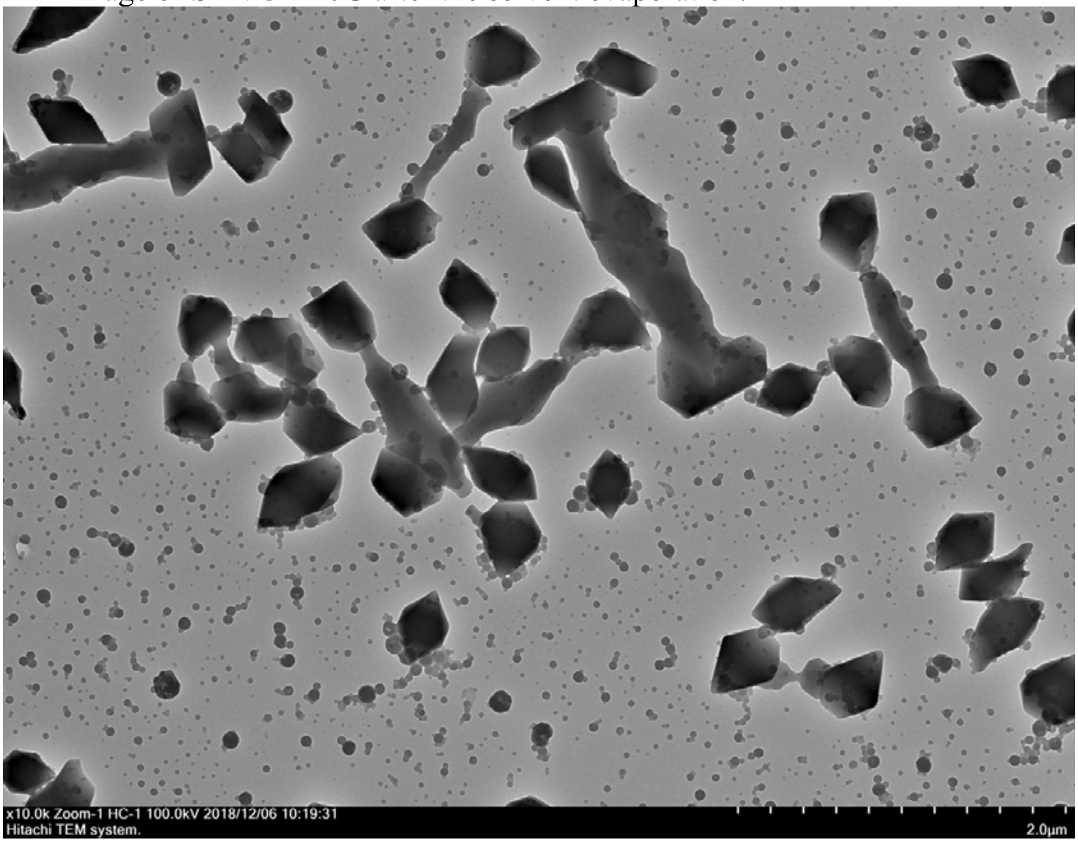

Fig. S55. TEM image of SLN-**3**-Rh6G after the solvent evaporation.

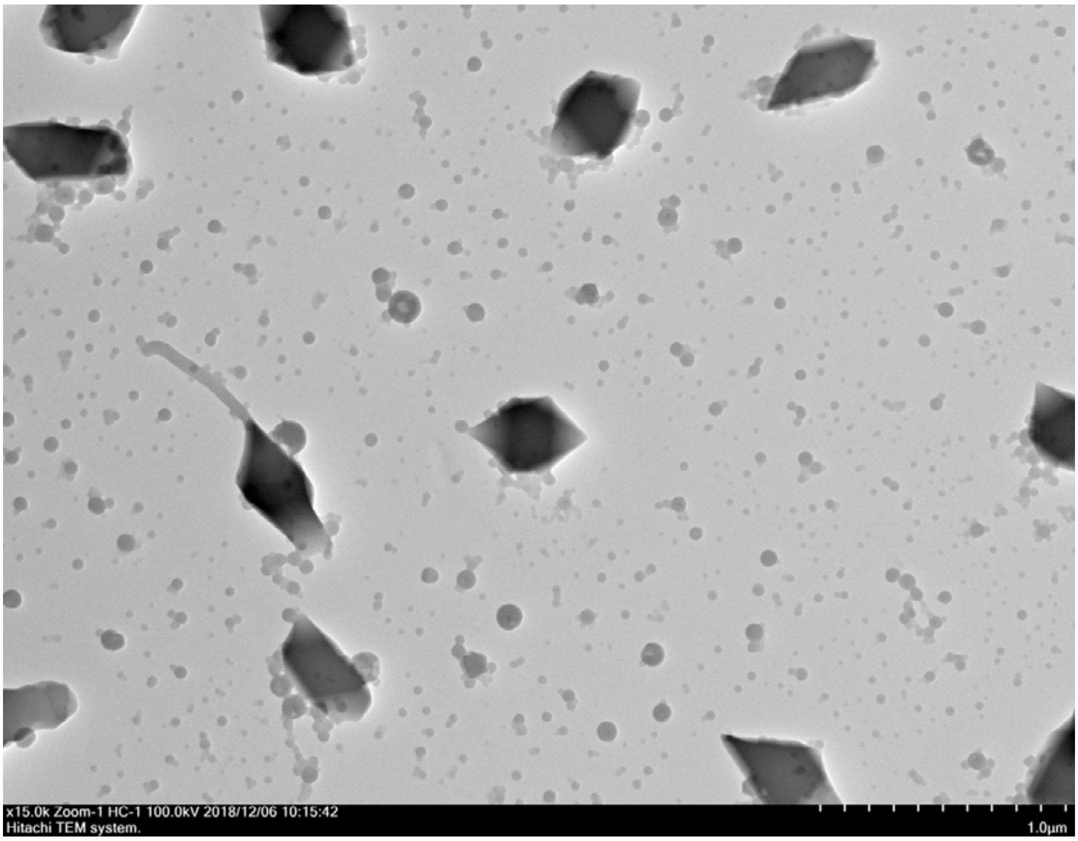

Fig. S56. TEM image of SLN-**3**-Rh6G after the solvent evaporation.

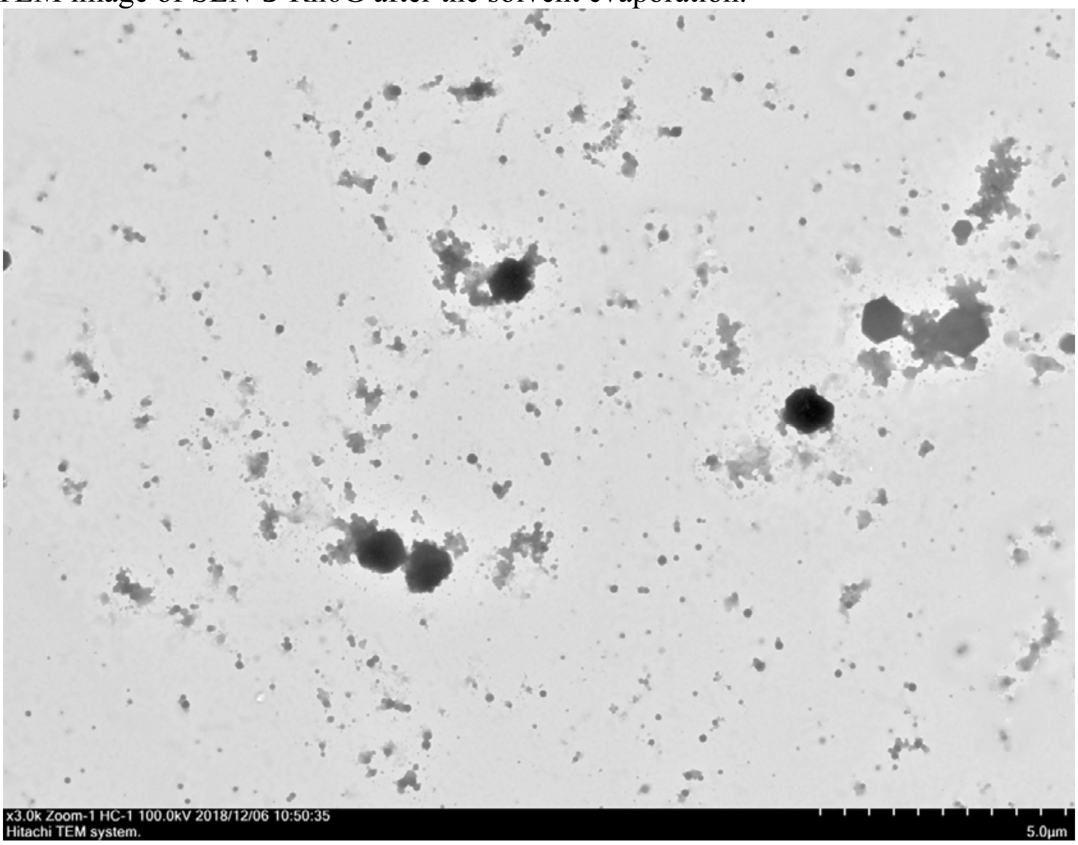

Fig. S57. TEM image of SLN-**4**-Rh6G after the solvent evaporation.

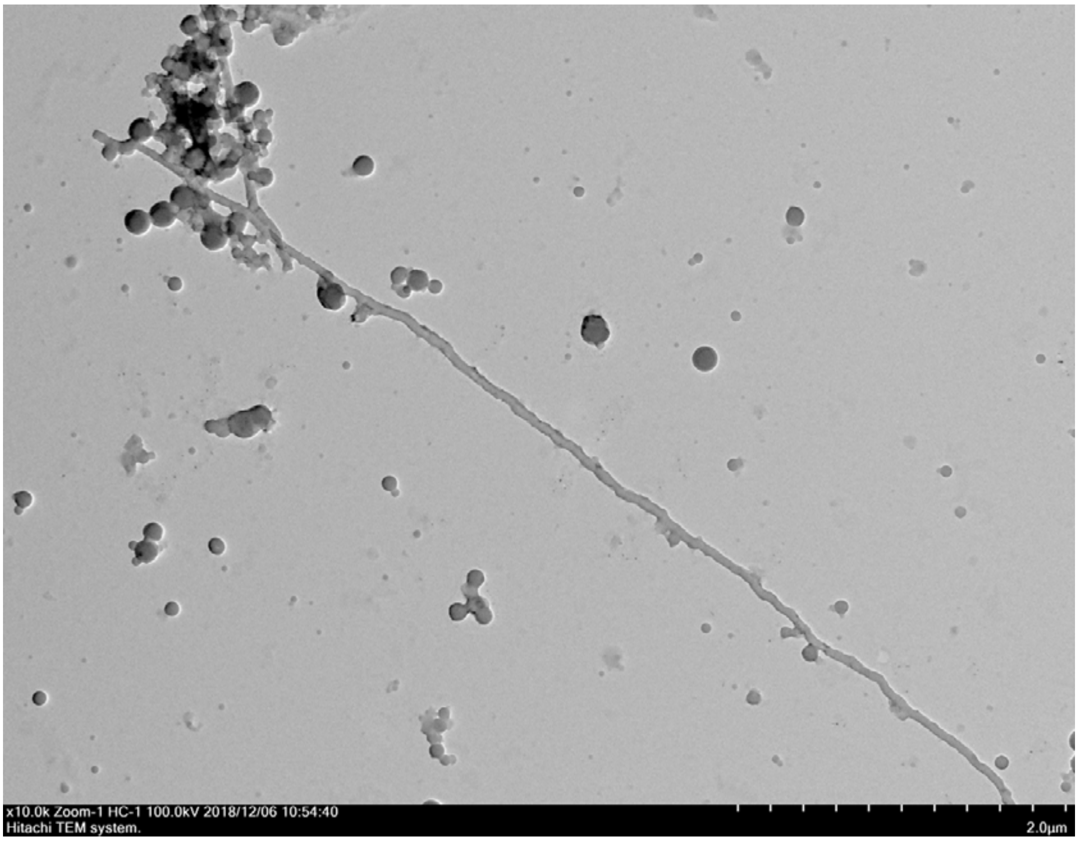

Fig. S58. TEM image of SLN-**4**-Rh6G after the solvent evaporation.

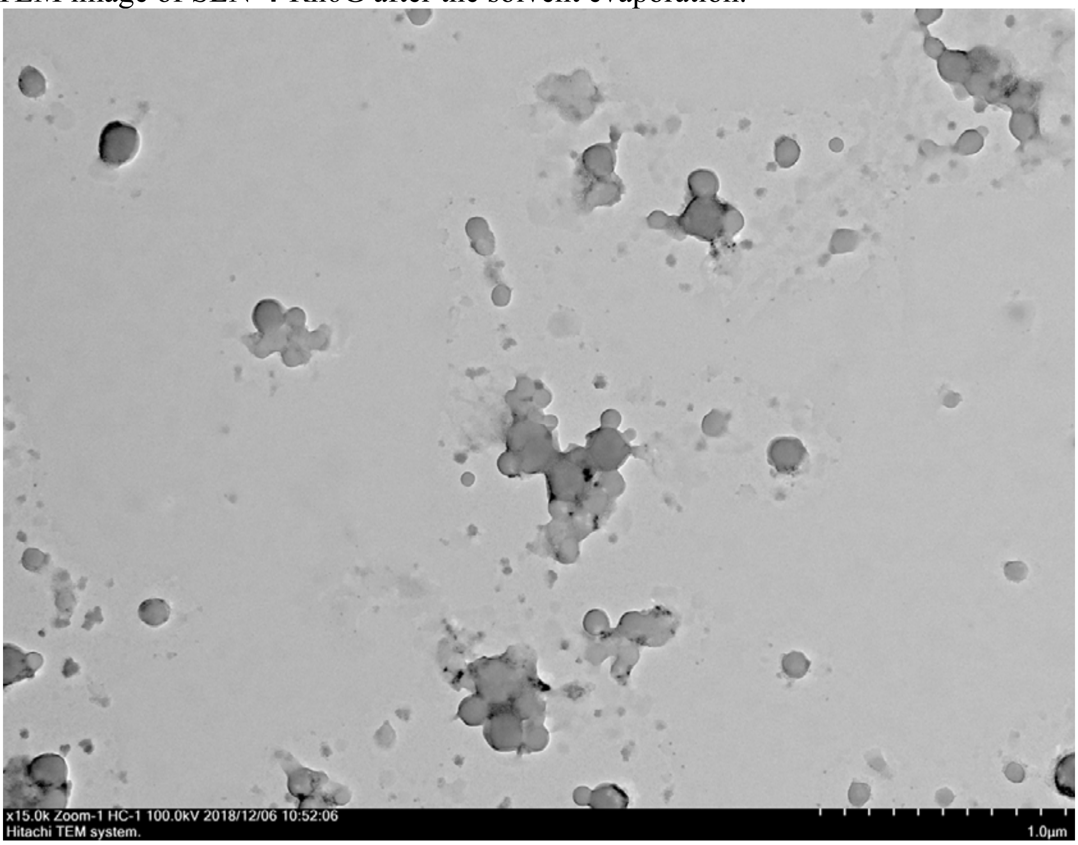

Fig. S59. TEM image of SLN-**4**-Rh6G after the solvent evaporation.

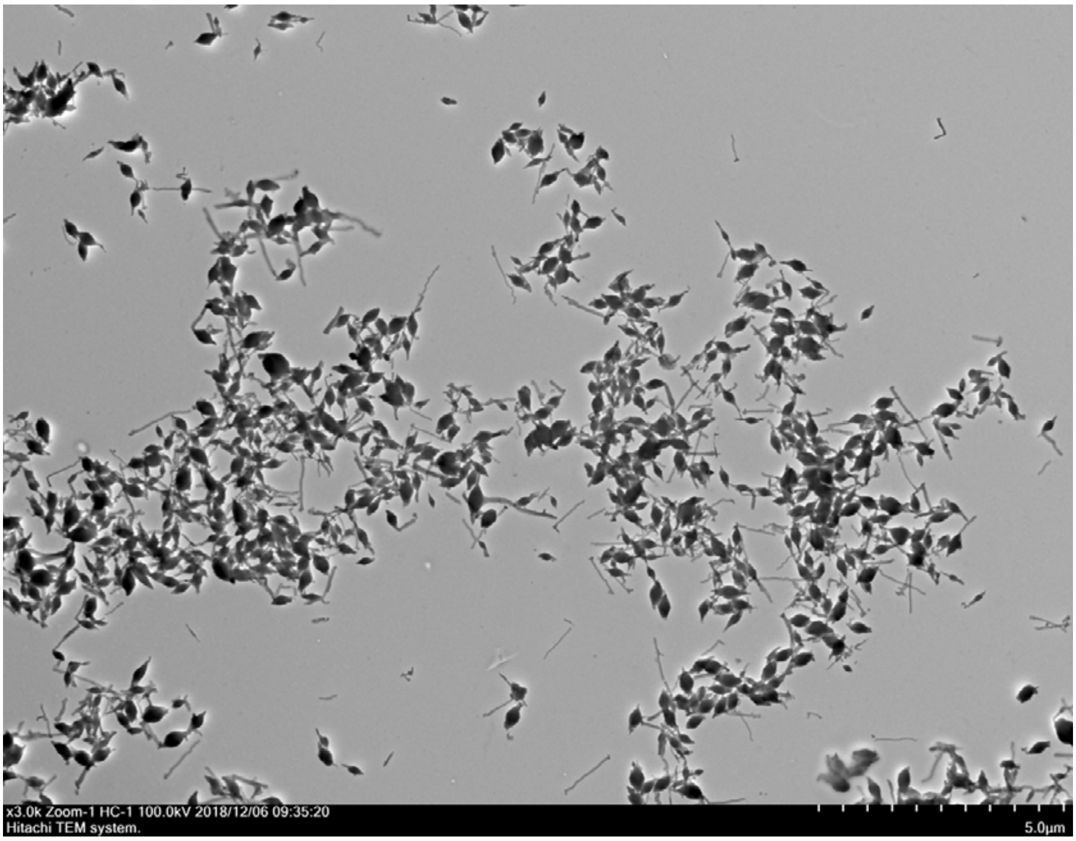

Fig. S60. TEM image of SLN-**5**-Rh6G after the solvent evaporation.

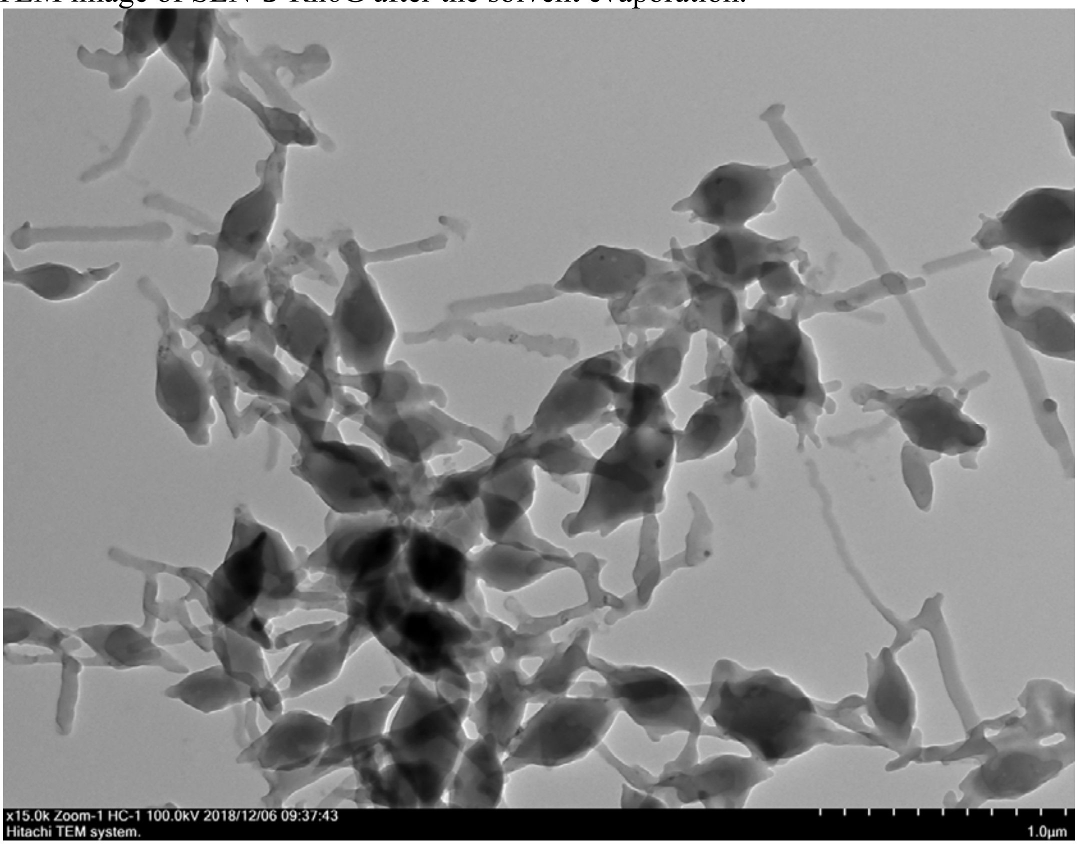

Fig. S61. TEM image of SLN-**5**-Rh6G after the solvent evaporation.

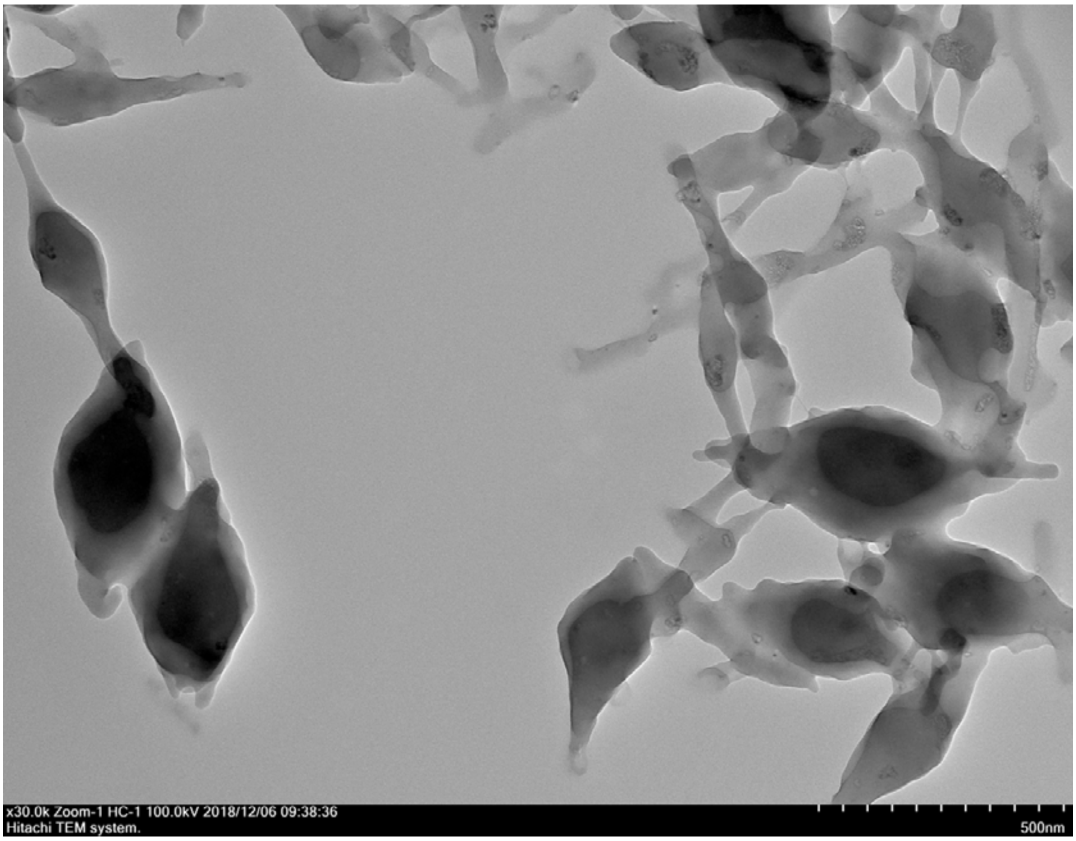

Fig. S62. TEM image of SLN-**5**-Rh6G after the solvent evaporation.

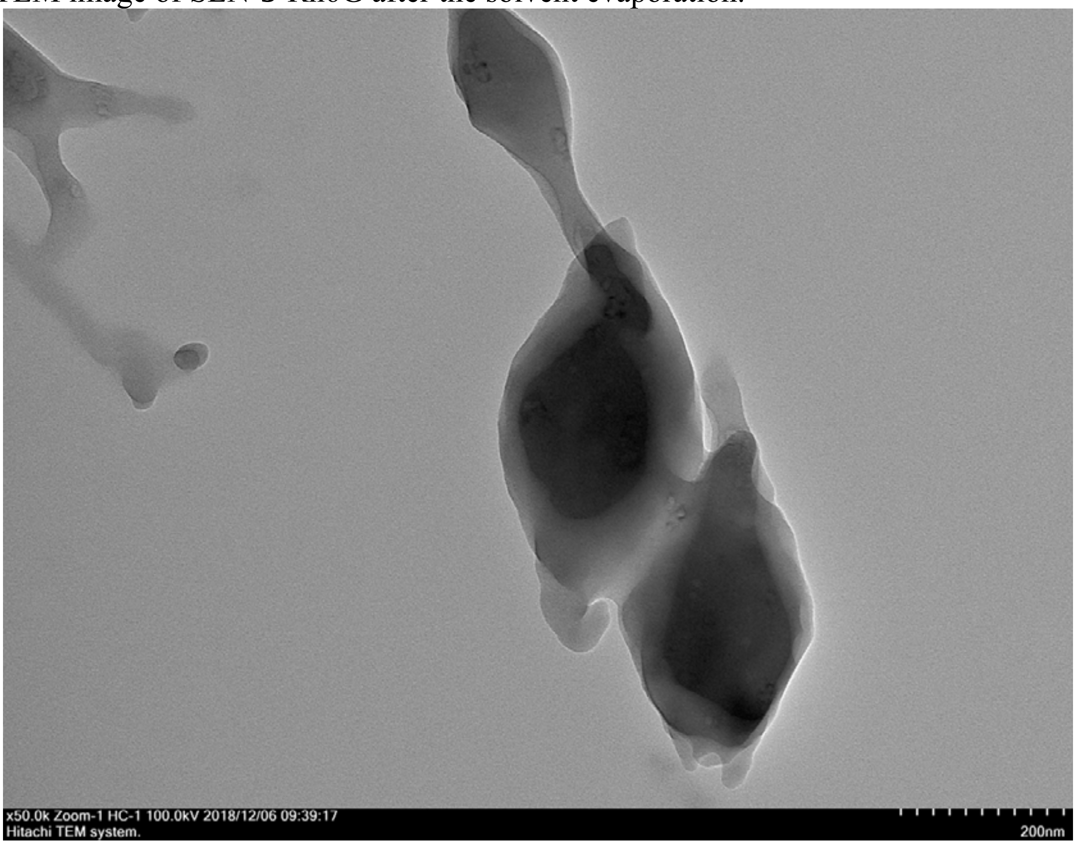

Fig. S63. TEM image of SLN-**5**-Rh6G after the solvent evaporation.

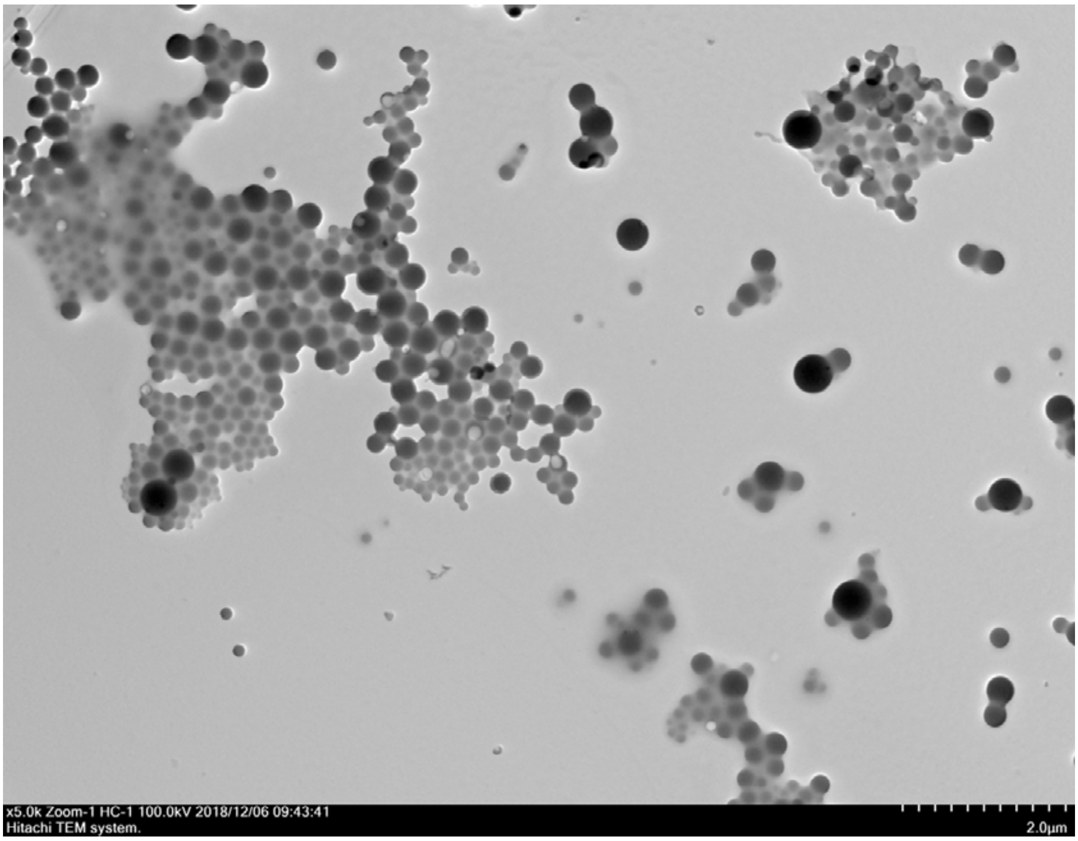

Fig. S64. TEM image of SLN-**6**-Rh6G after the solvent evaporation.

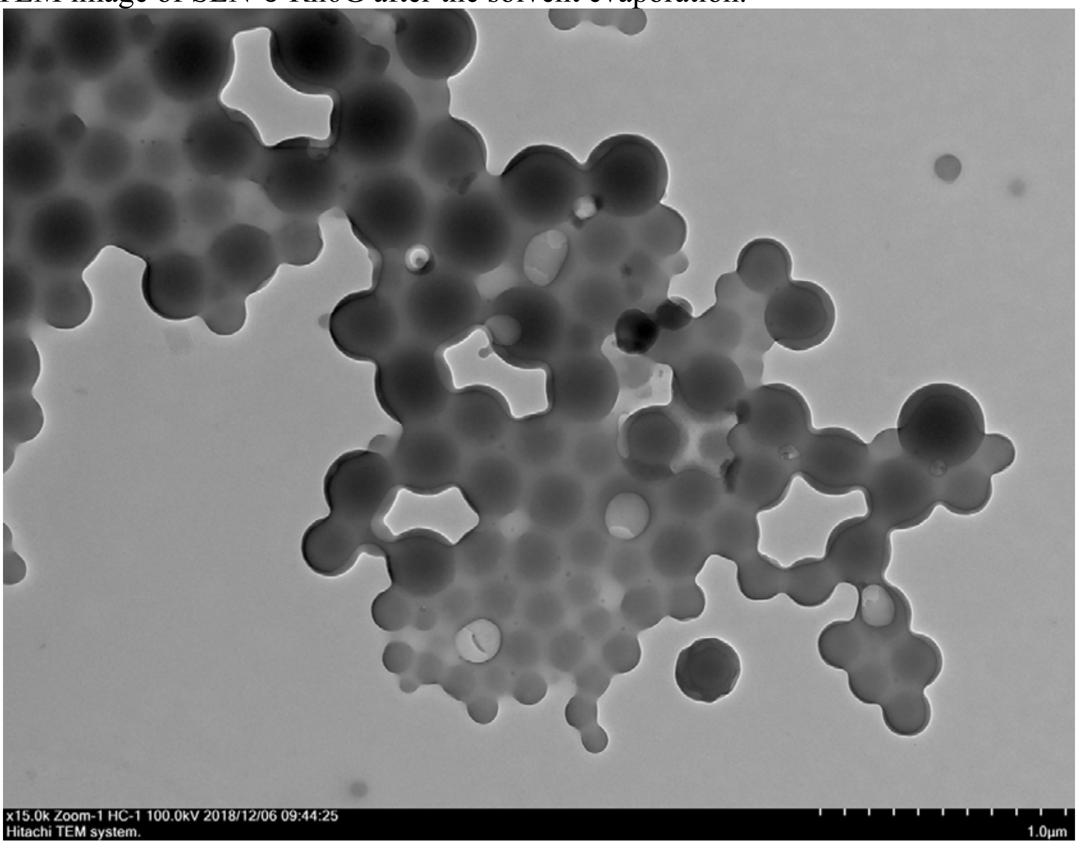

Fig. S65. TEM image of SLN-**6**-Rh6G after the solvent evaporation.

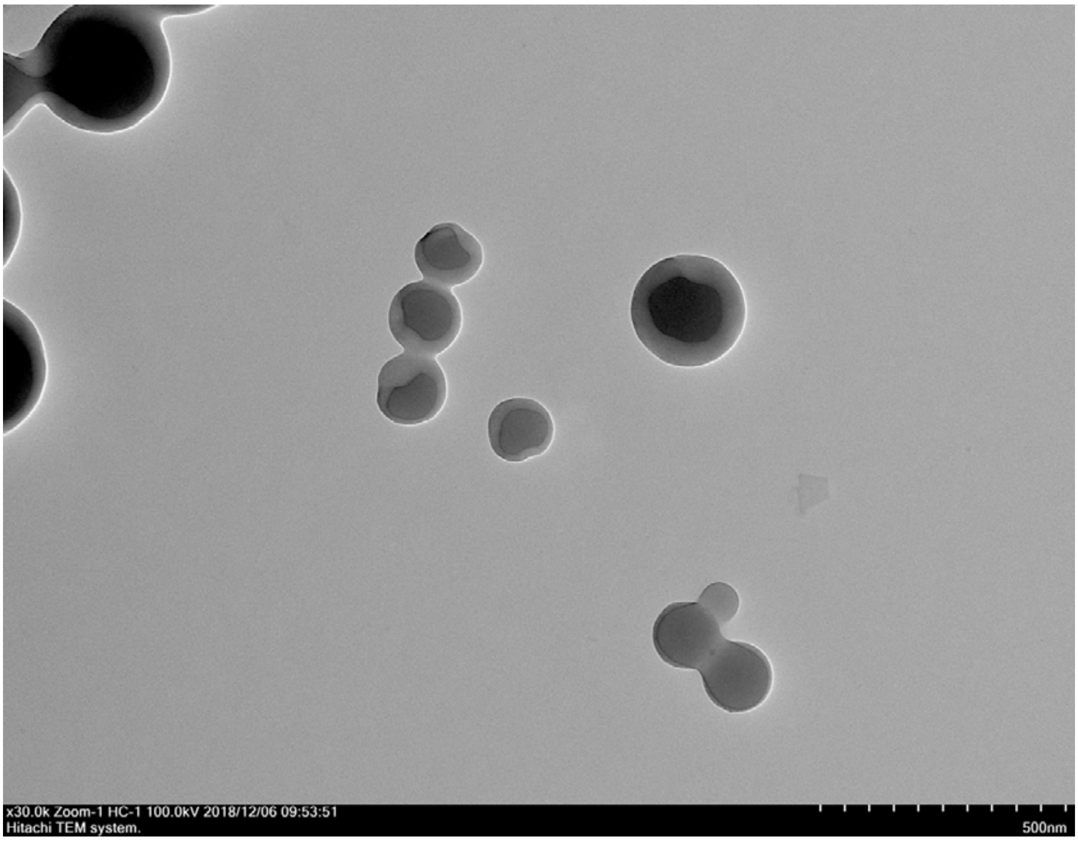

Fig. S66. TEM image of SLN-**6**-Rh6G after the solvent evaporation.

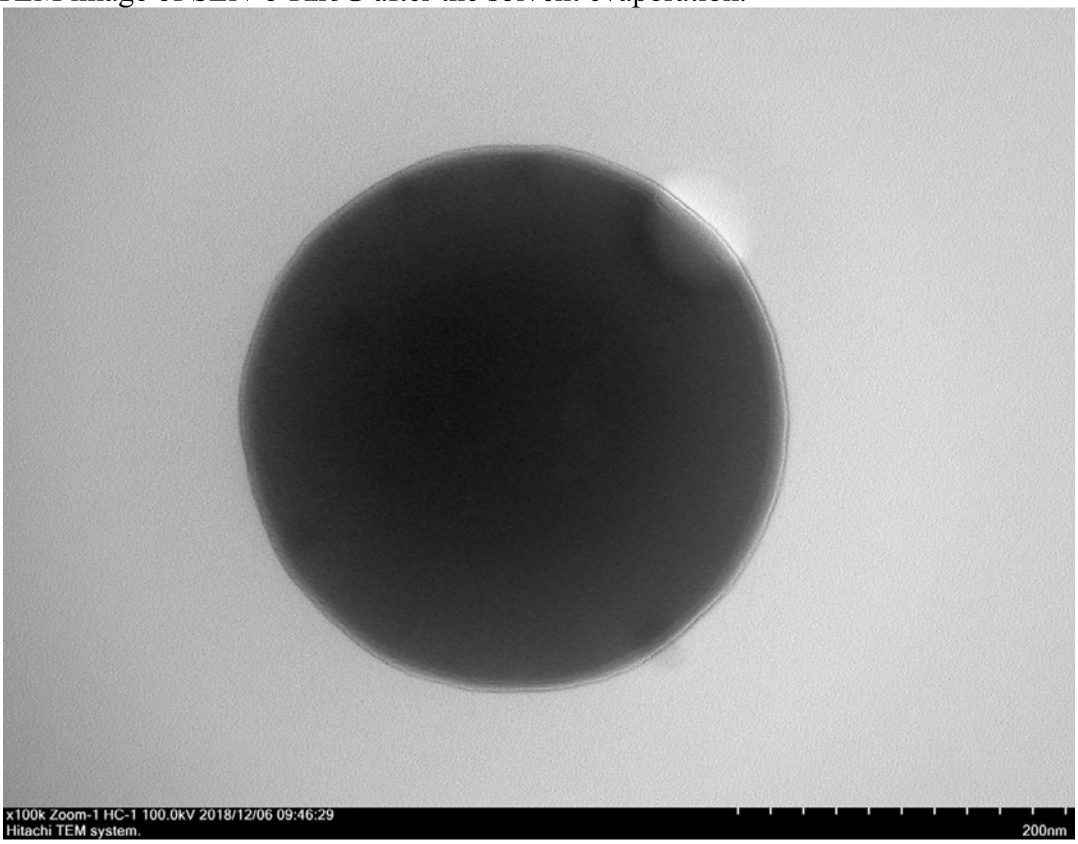

Fig. S67. TEM image of SLN-**6**-Rh6G after the solvent evaporation.

3. Scanning electron microscopy (SEM) analysis of SLNs

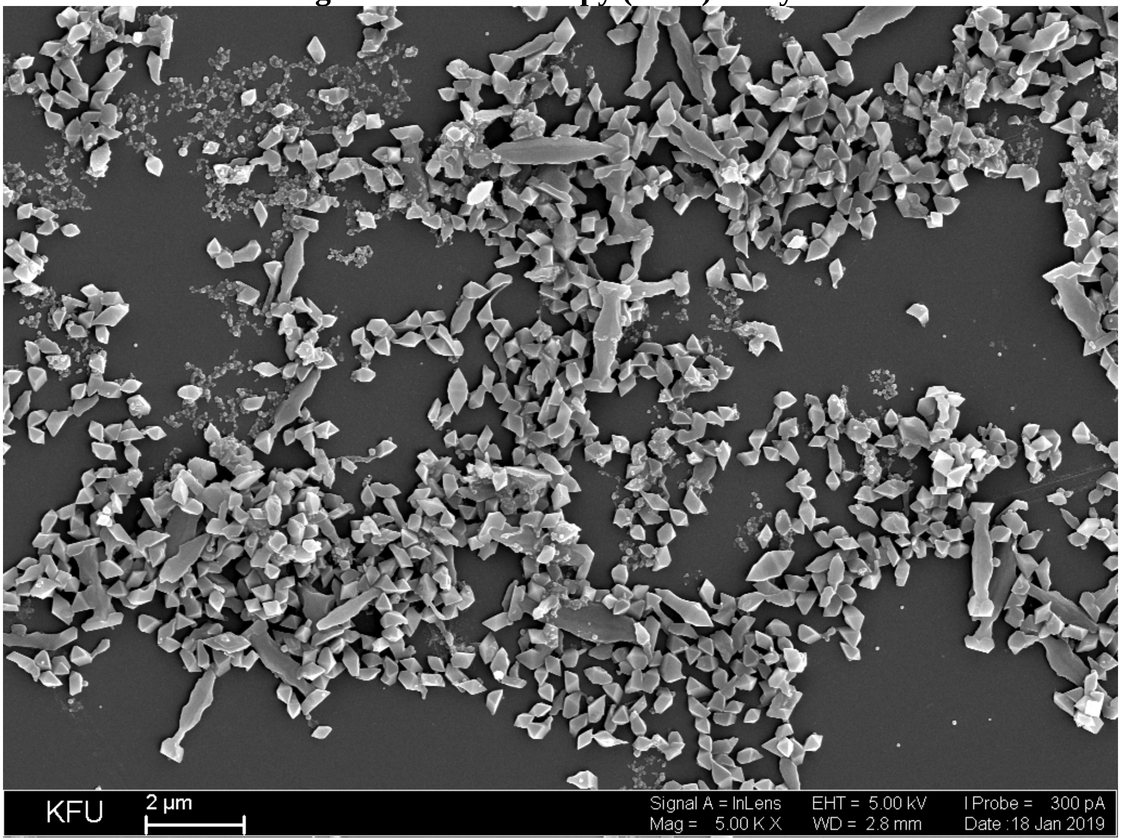

Fig. S68. SEM image of SLN-**3**-Rh6G after the solvent evaporation.

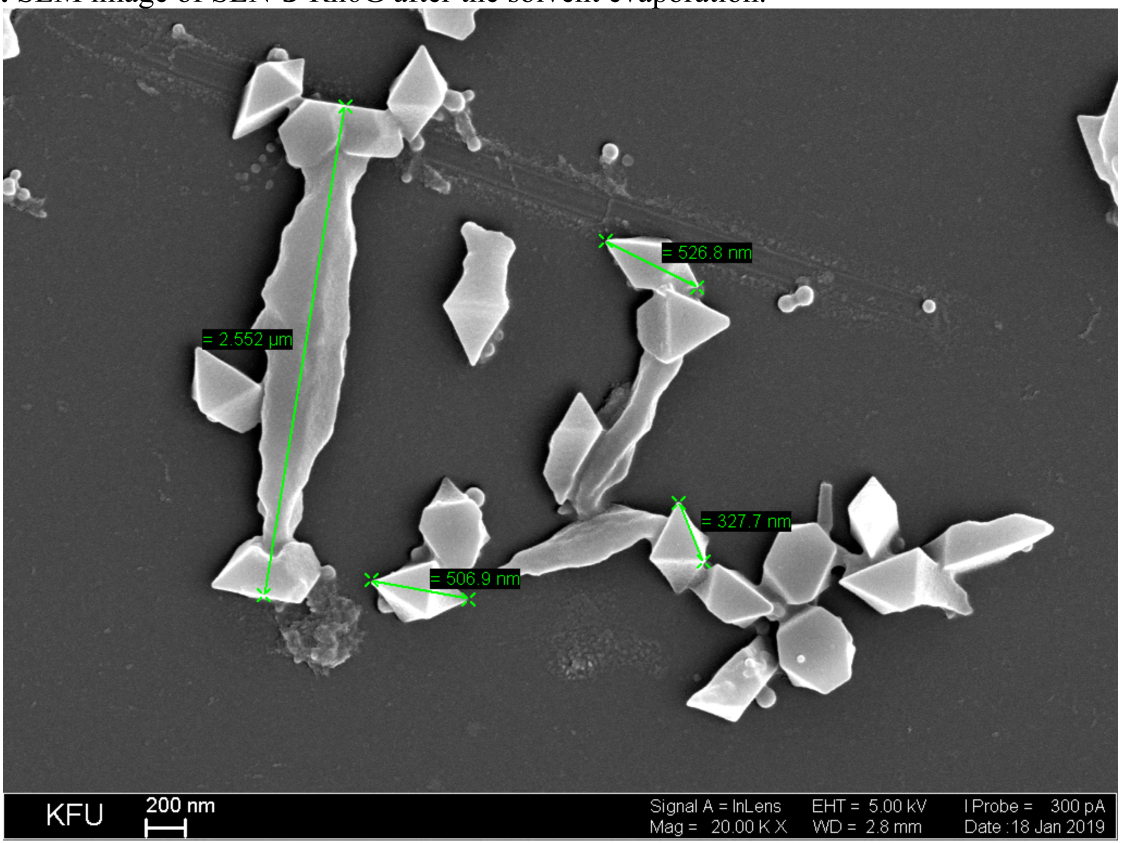

Fig. S69. SEM image of SLN-**3**-Rh6G after the solvent evaporation.

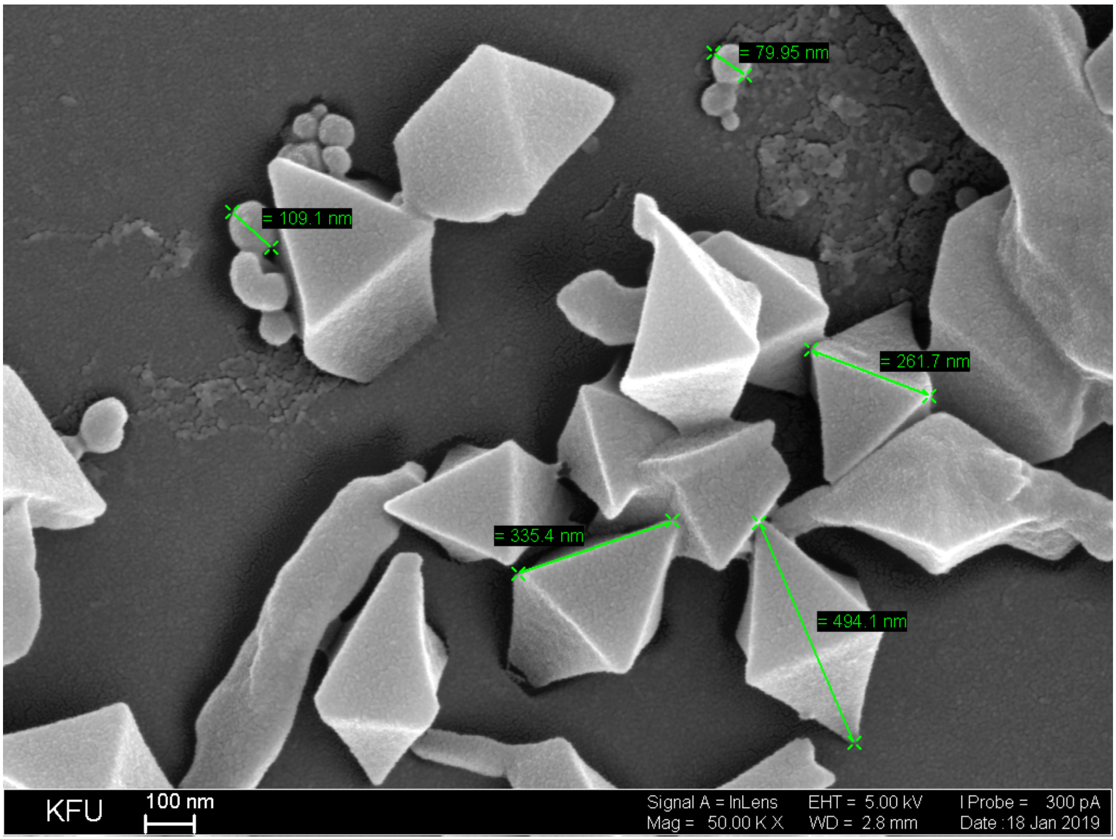

Fig. S70. SEM image of SLN-**3**-Rh6G after the solvent evaporation.

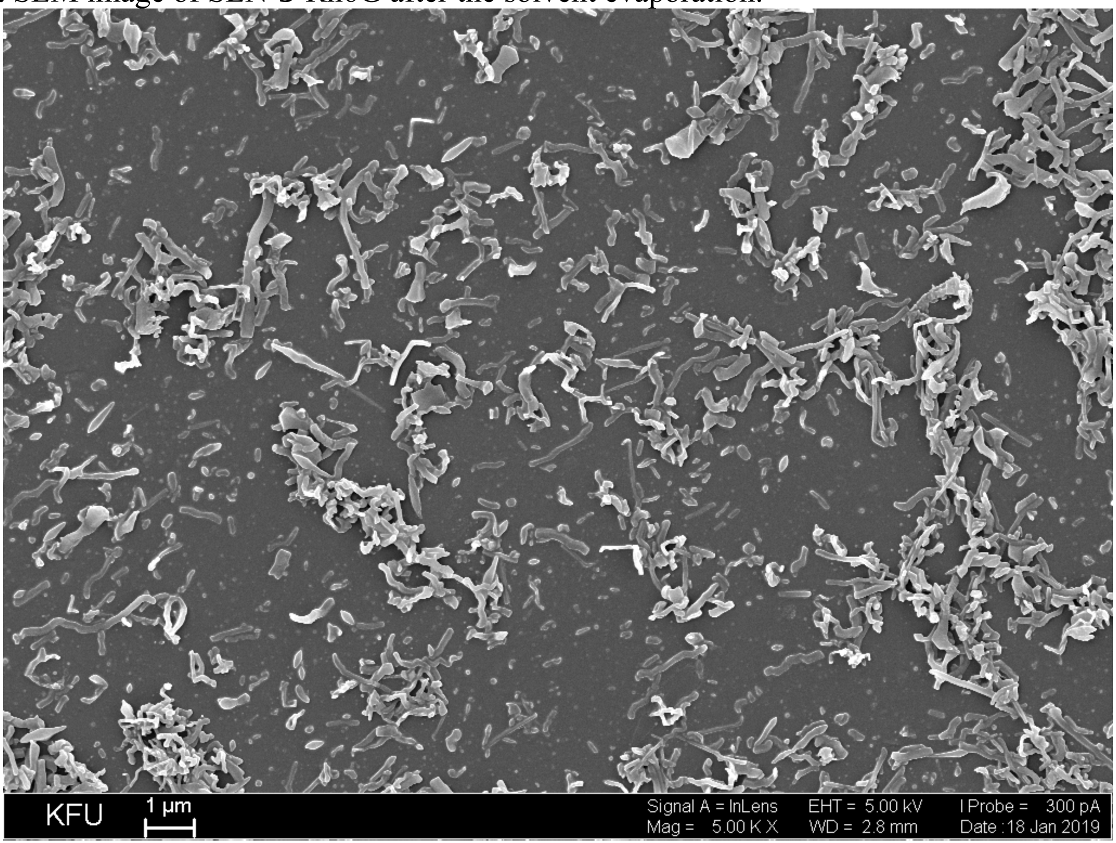

Fig. S71. SEM image of SLN-**5**-RhB after the solvent evaporation.

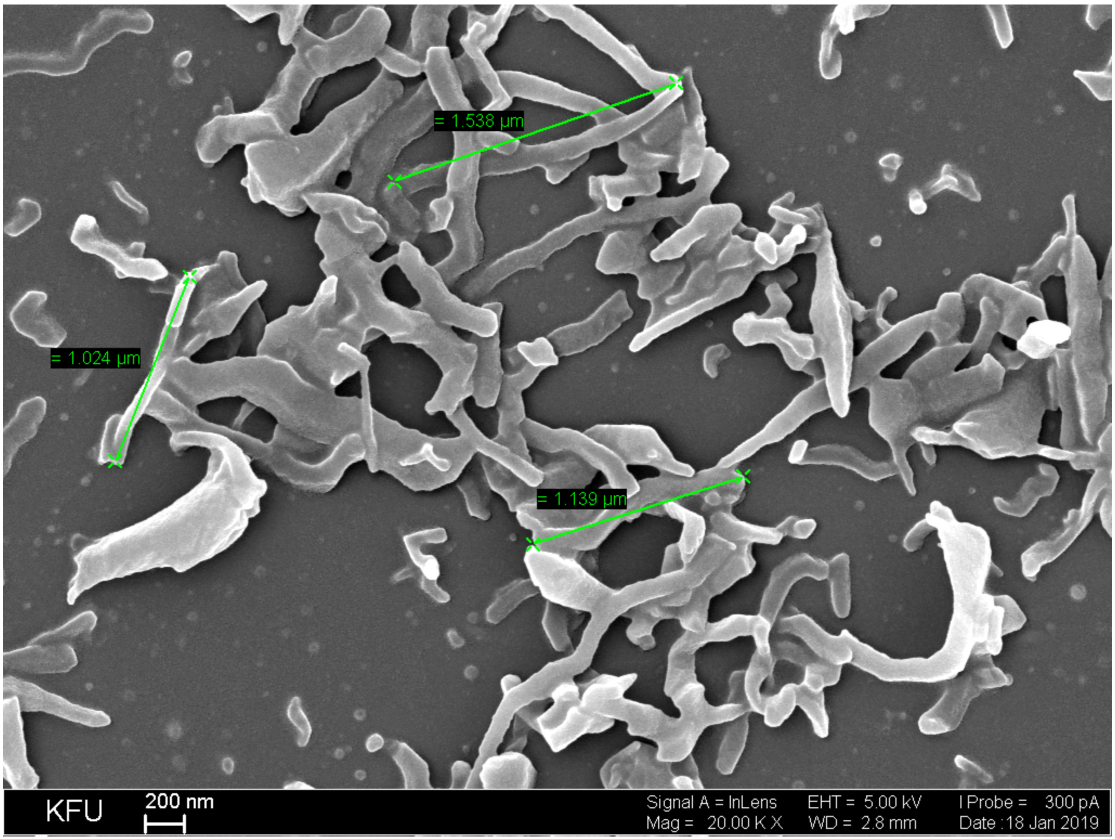

Fig. S72. SEM image of SLN-**5**-RhB after the solvent evaporation.

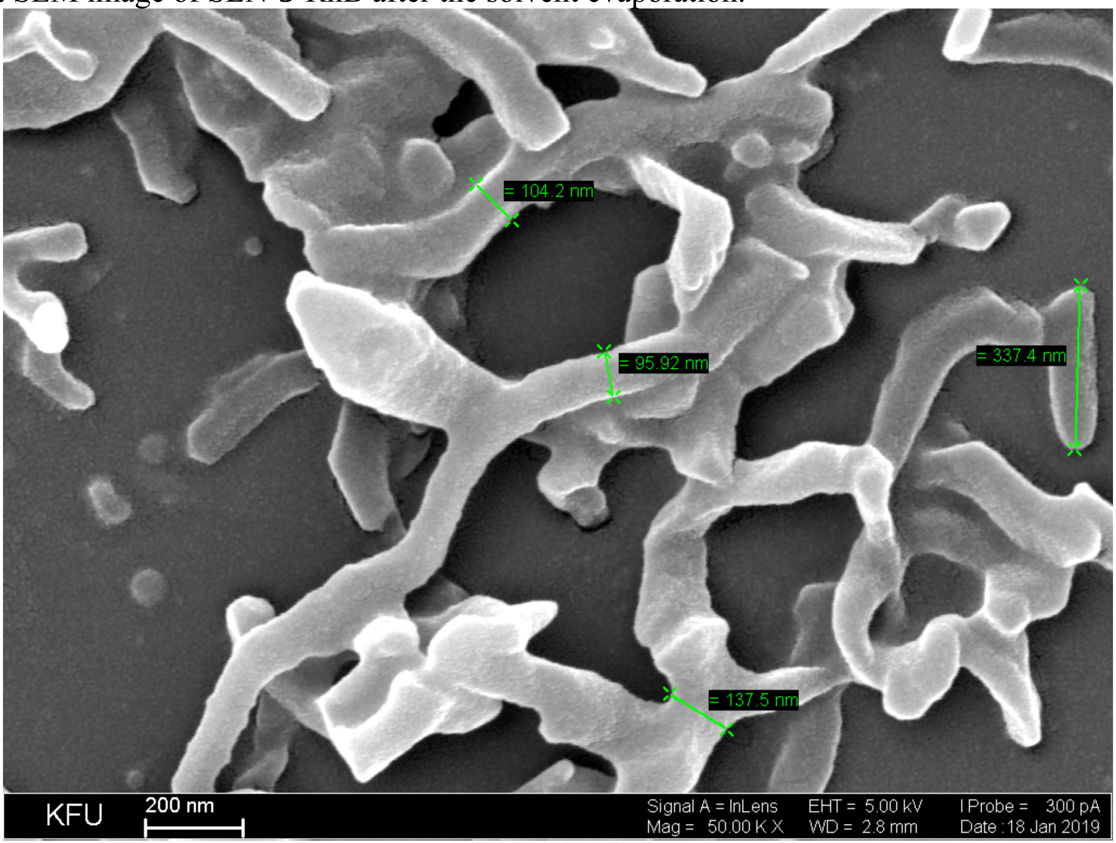

Fig. S73. SEM image of SLN-**5**-RhB after the solvent evaporation.

4. Dynamic light scattering

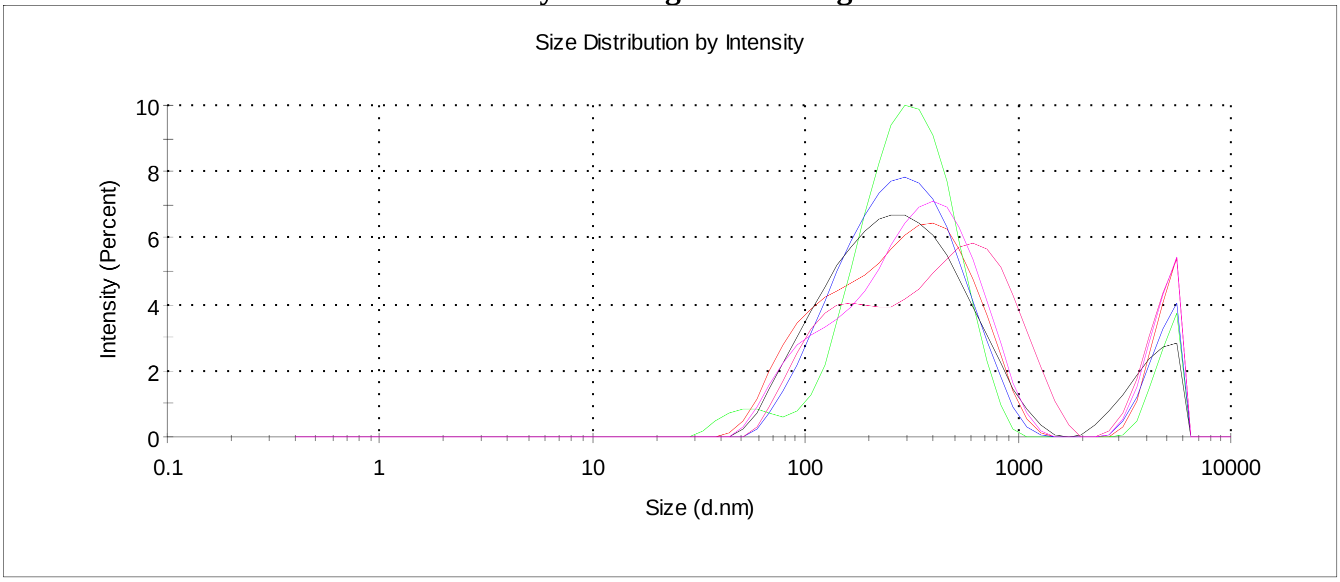

Fig. S74. Size distribution by intensity for **3** (1×10^{-3}M) in $CHCl_3$.

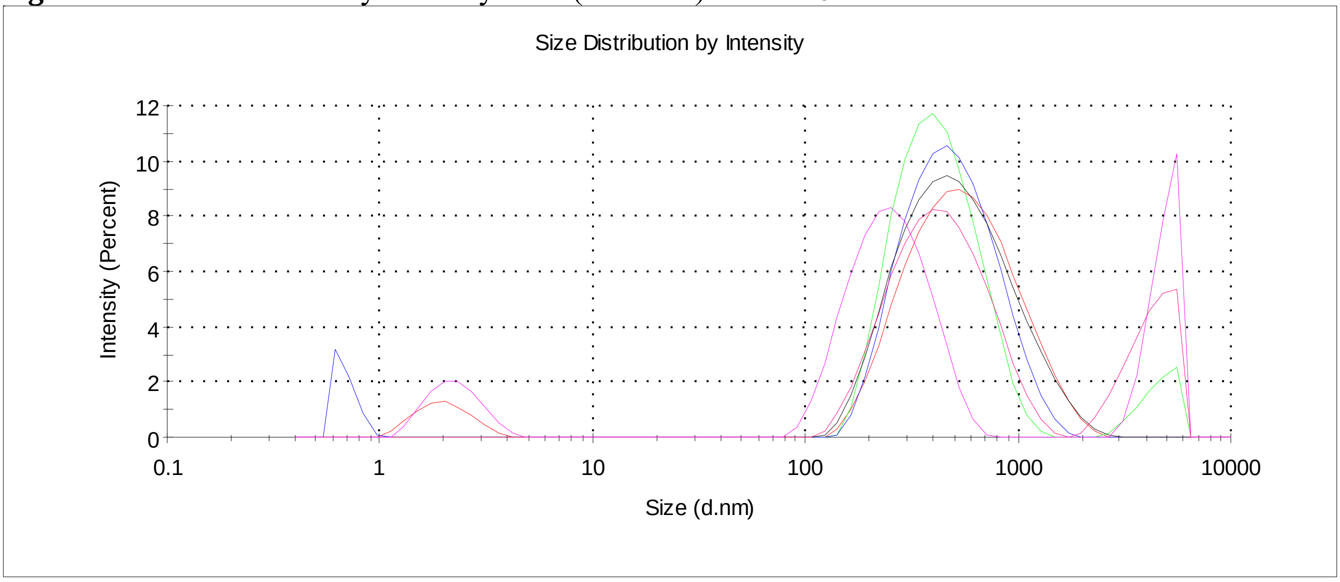

Fig. S75. Size distribution by intensity for **3** (1×10^{-3}M) in DMSO.

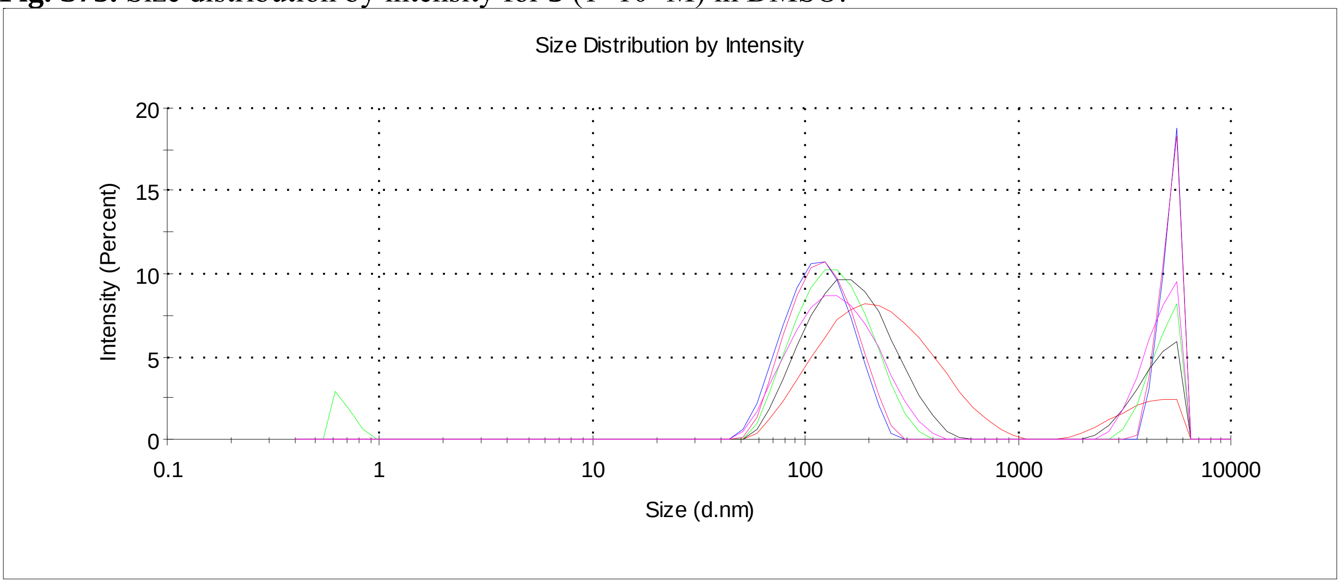

Fig. S76. Size distribution by intensity for **4** (1×10^{-3}M) in $CHCl_3$.

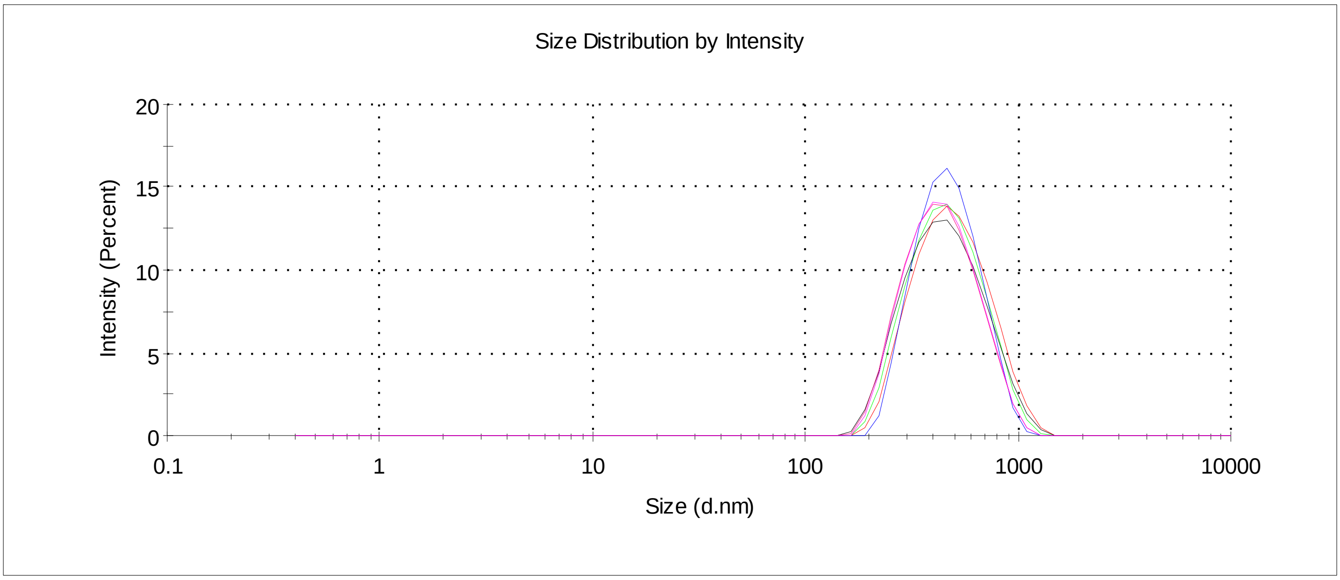

Fig. S77. Size distribution by intensity for **4** (1×10^{-3}M) in DMSO.

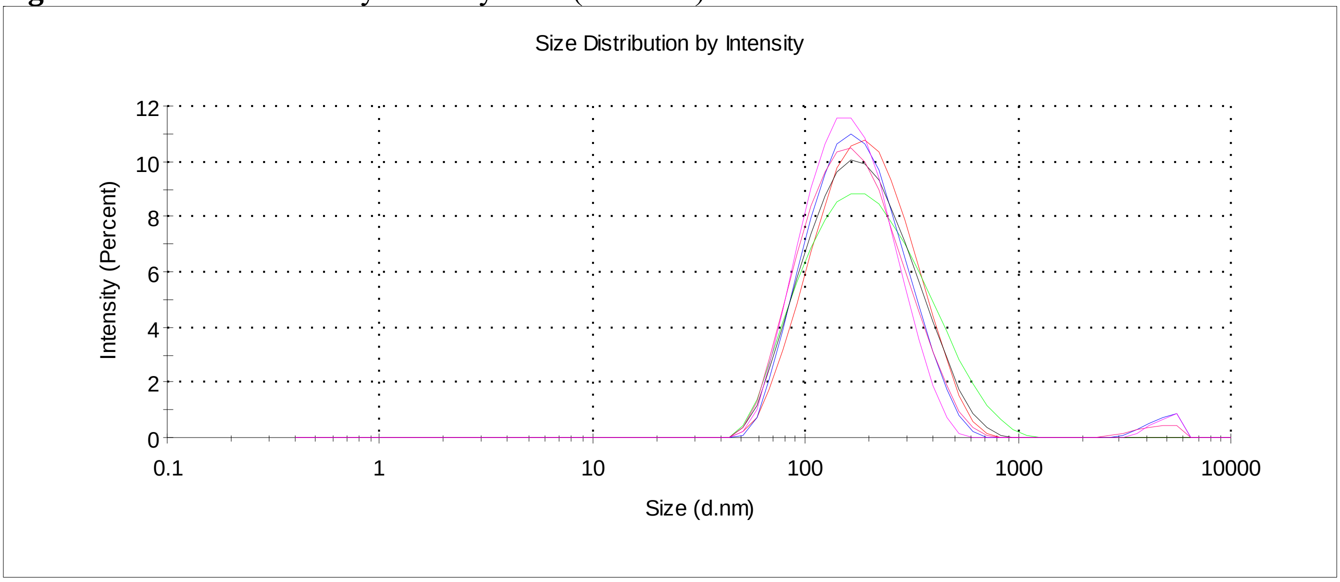

Fig. S78. Size distribution by intensity for **5** (1×10^{-3}M) in $CHCl_3$.

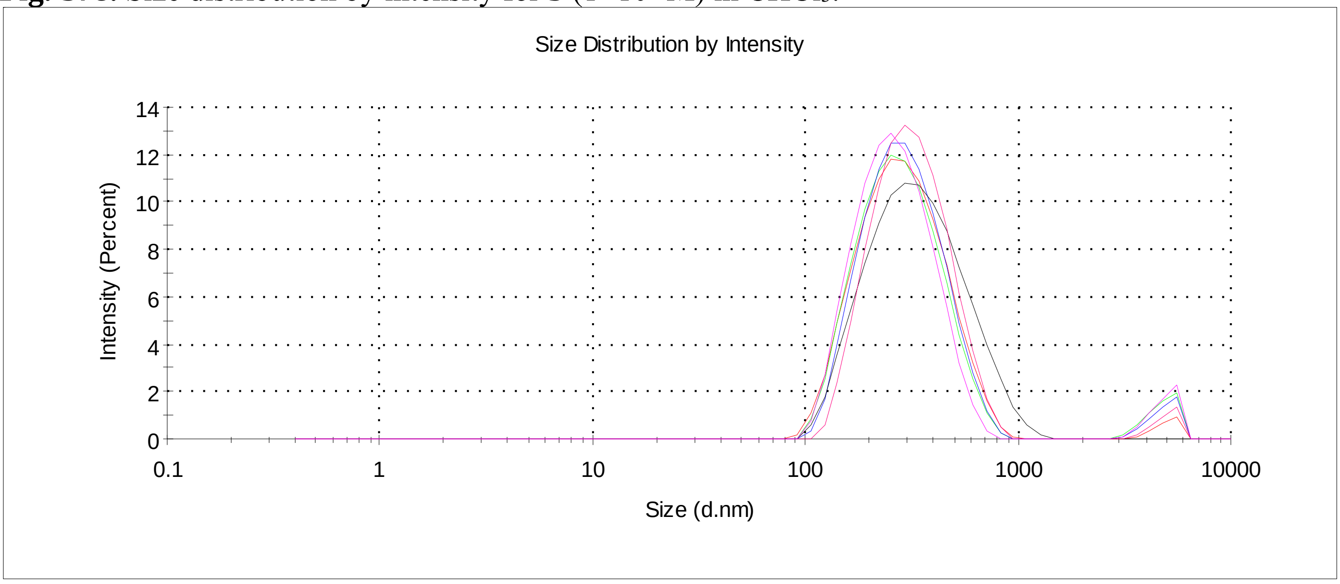

Fig. S79. Size distribution by intensity for **5** (1×10^{-3}M) in DMSO.

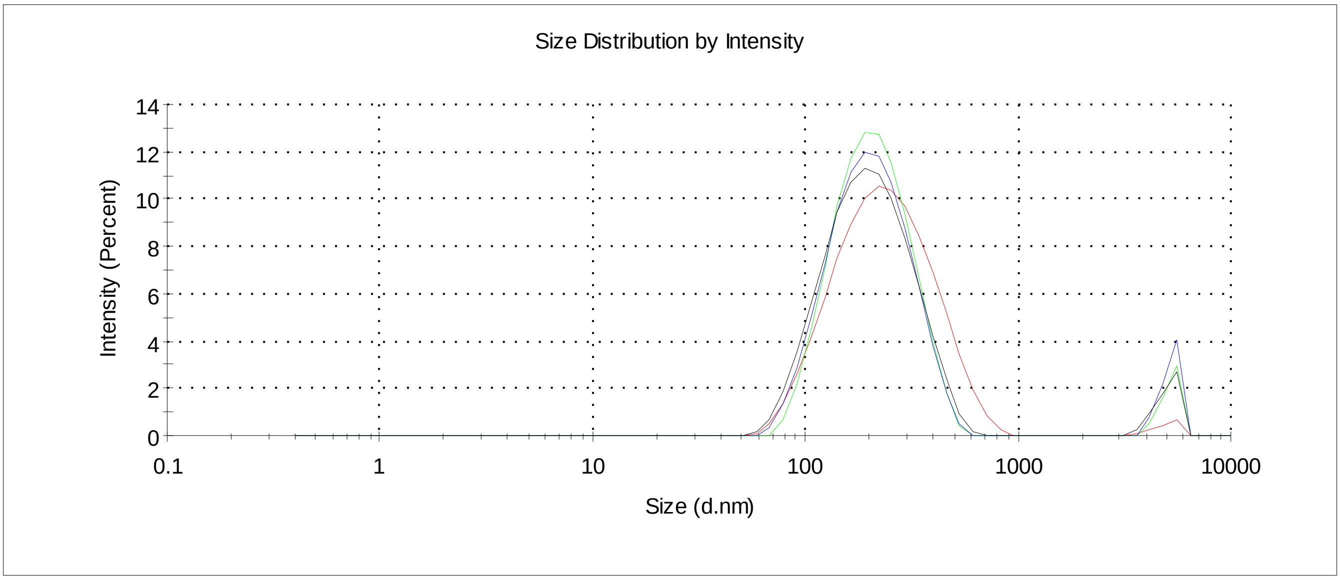

Fig. S80. Size distribution by intensity for **6** (1×10^{-3}M) in $CHCl_3$.

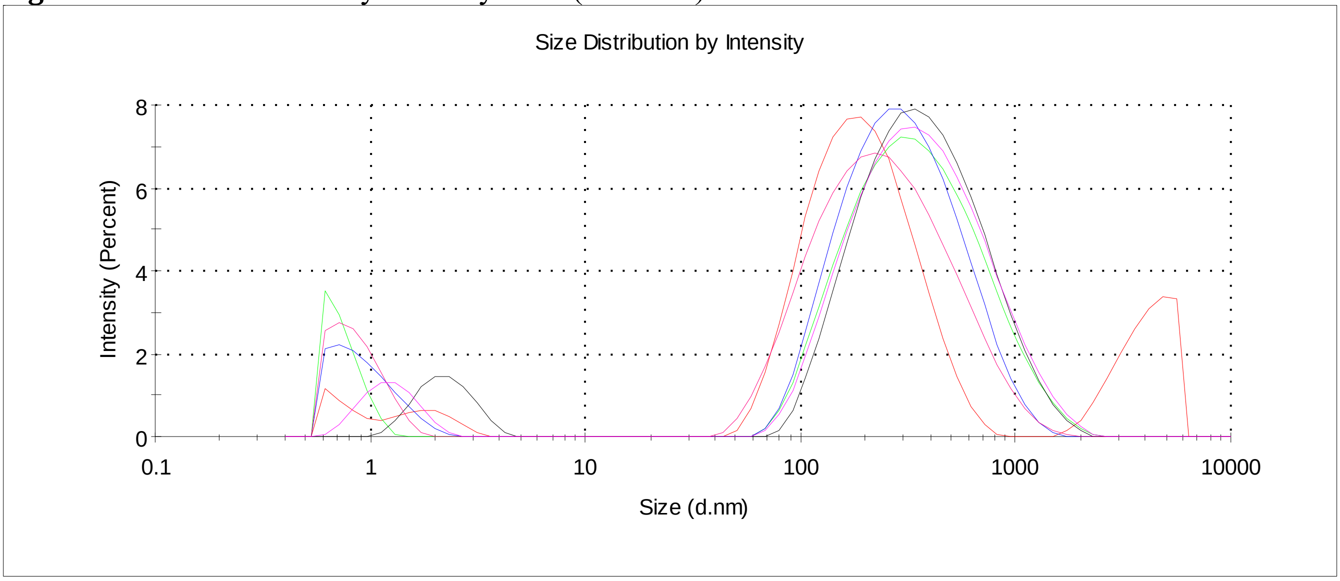

Fig. S81. Size distribution by intensity for **6** (1×10^{-3}M) in DMSO.

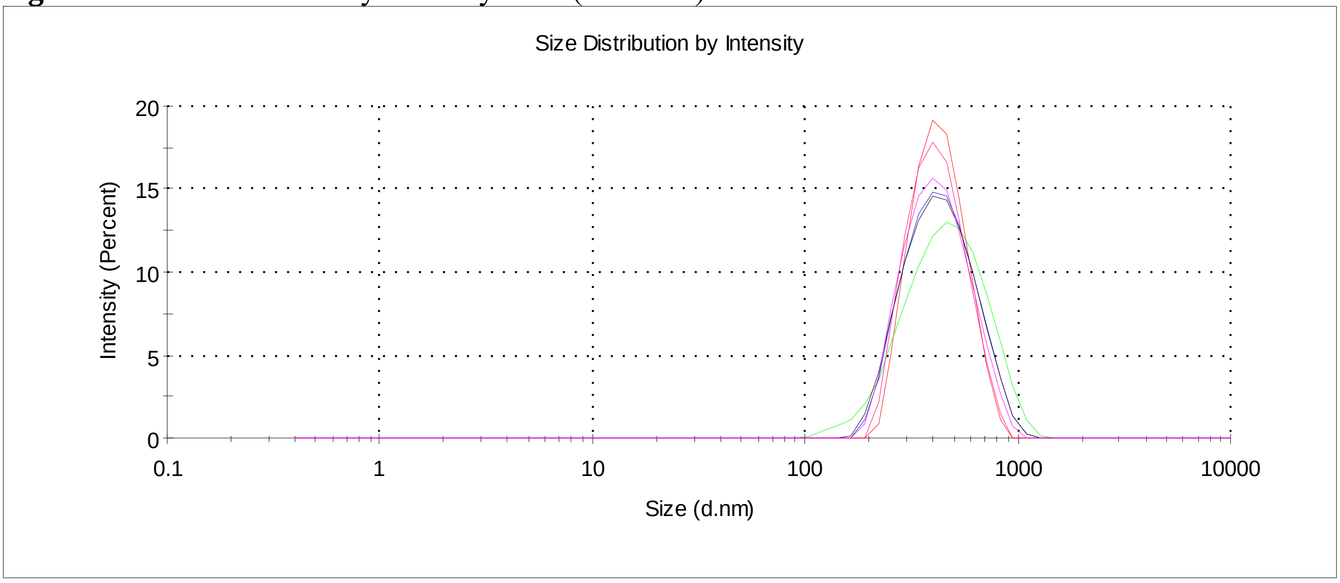

Fig. S82. Size distribution of the particles by intensity for SLN-**3** (3×10^{-5}M) in water.

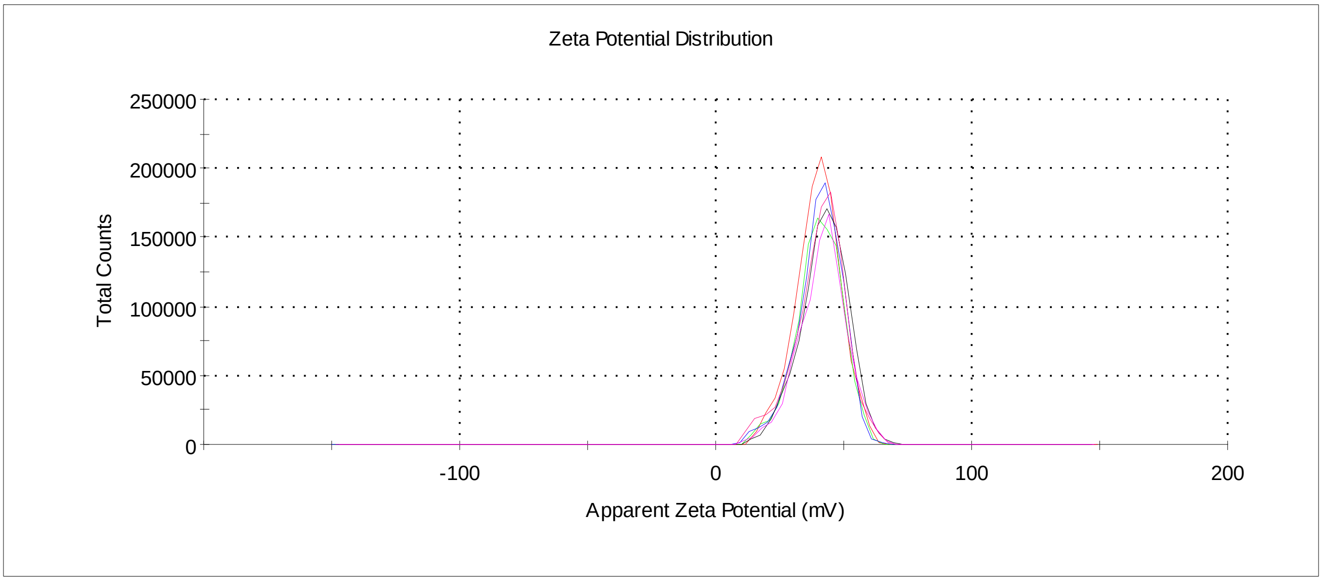

Fig. S83. Zeta potential distribution of the particles SLN-**3** (3×10^{-5}M) in water.

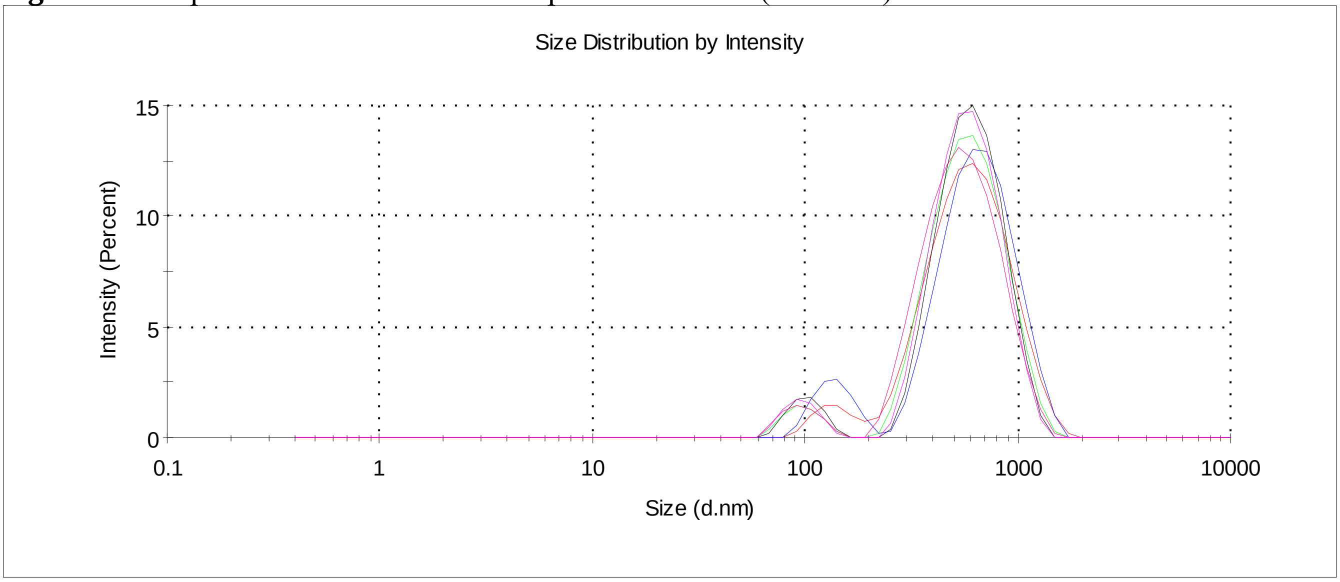

Fig. S84. Size distribution of the particles by intensity for SLN-**4** (3×10^{-5}M) in water.

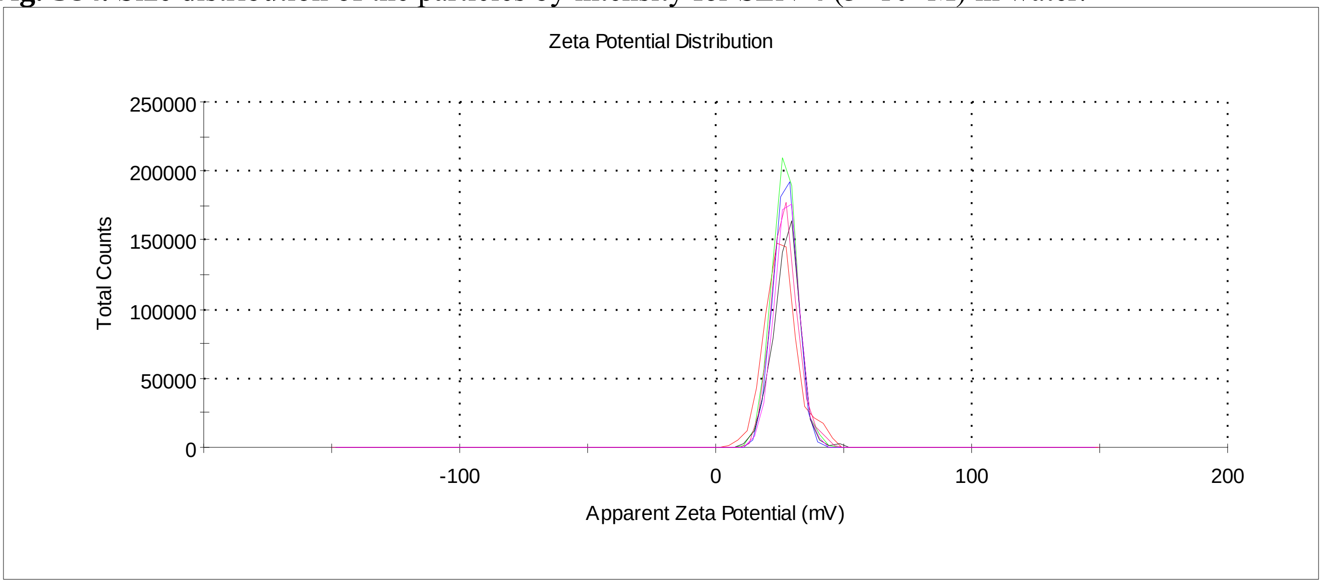

Fig. S85. Zeta potential distribution of the particles SLN-**4** (3×10^{-5}M) in water.

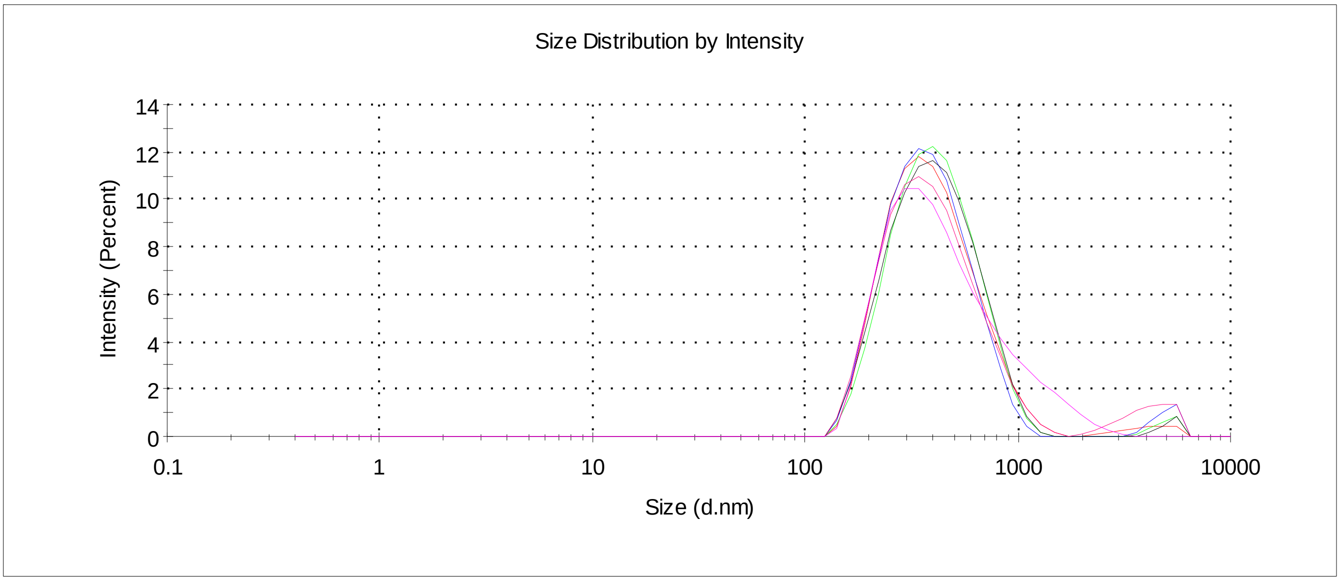

Fig. S86. Size distribution of the particles by intensity for SLN-**5** (3×10^{-5}M) in water.

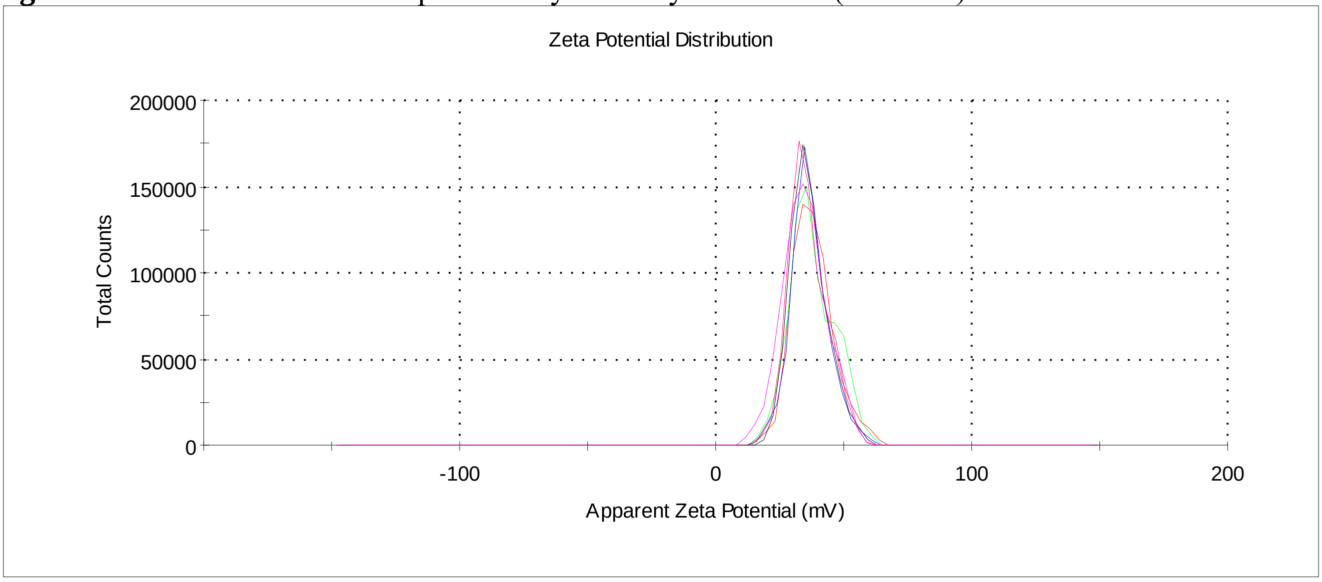

Fig. S87. Zeta potential distribution of the particles SLN-**5** (3×10^{-5}M) in water.

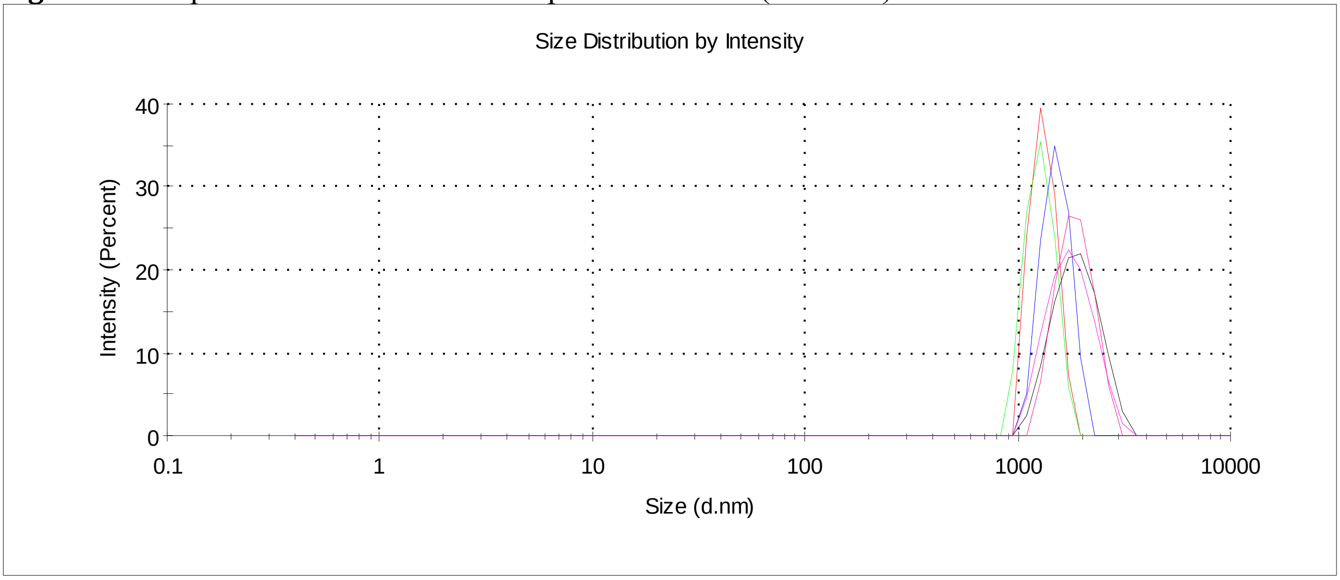

Fig. S88. Size distribution of the particles by intensity for SLN-**6** (3×10^{-5}M) in water.

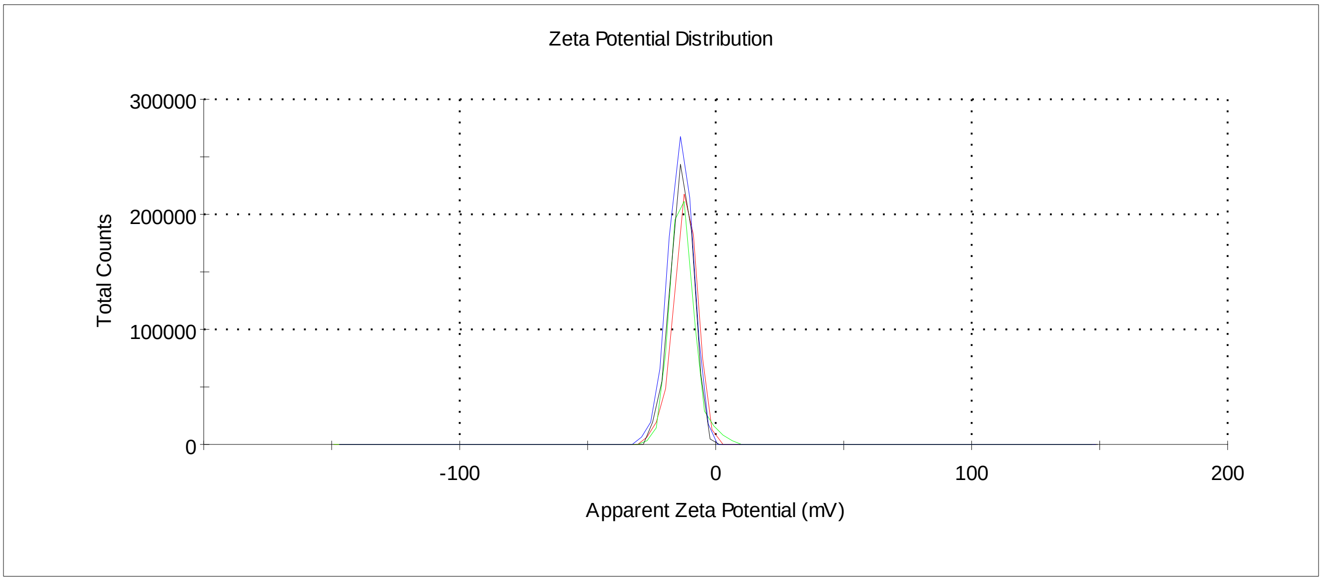

Fig. S89. Zeta potential distribution of the particles SLN-**6** (3×10^{-5}M) in water.

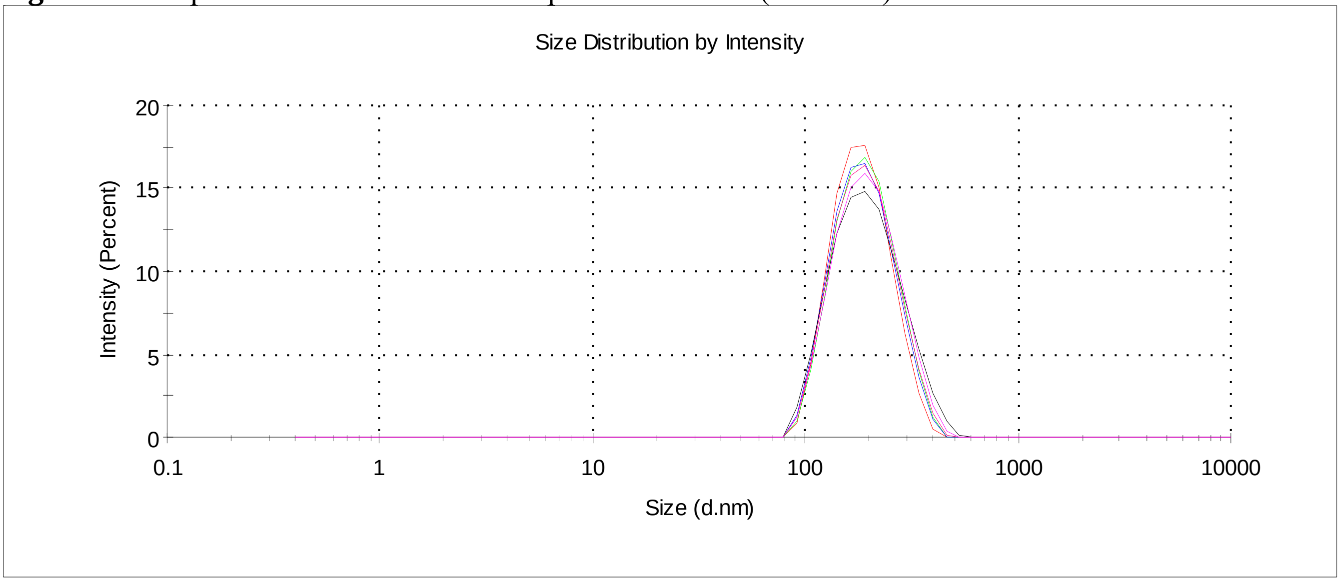

Fig. S90. Size distribution of the particles by intensity for SLN-**3**-Flu (3×10^{-5}M) in water.

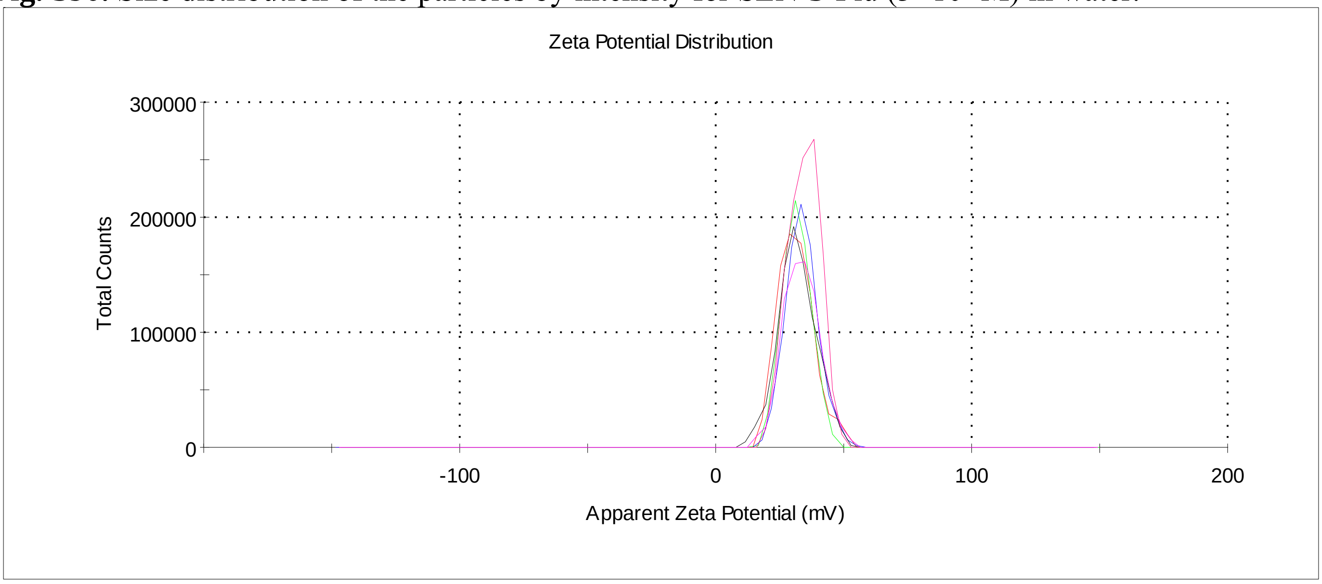

Fig. S91. Zeta potential distribution of the particles SLN-**3**-Flu (3×10^{-5}M) in water.

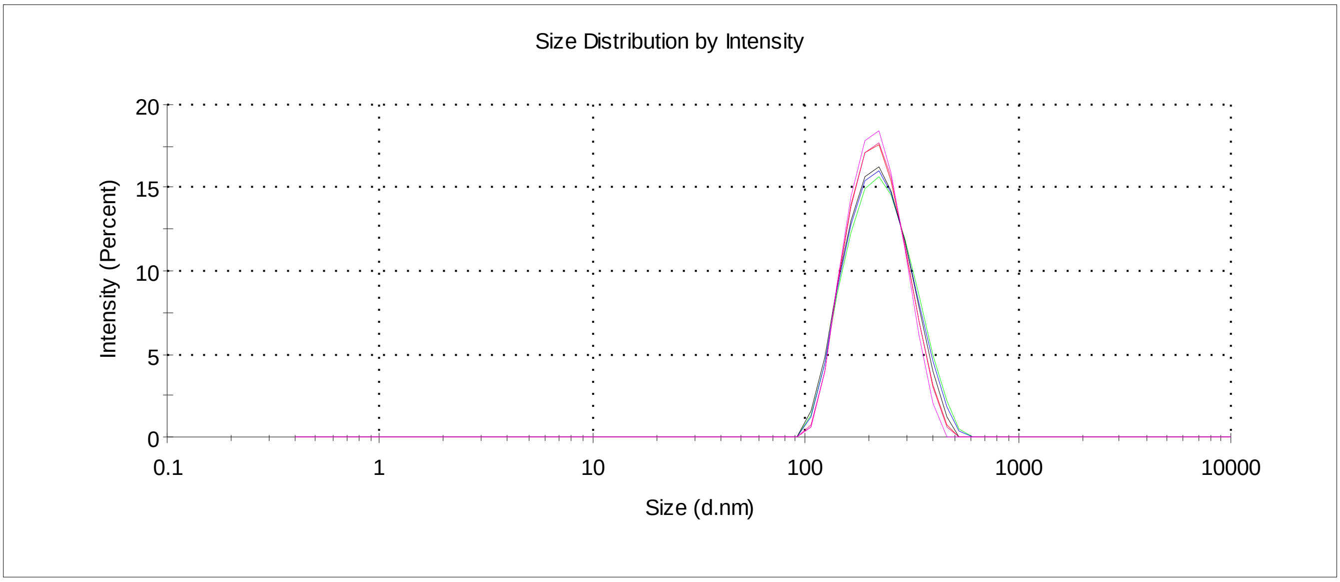

Fig. S92. Size distribution of the particles by intensity for SLN-**4**-Flu (3×10^{-5}M) in water.

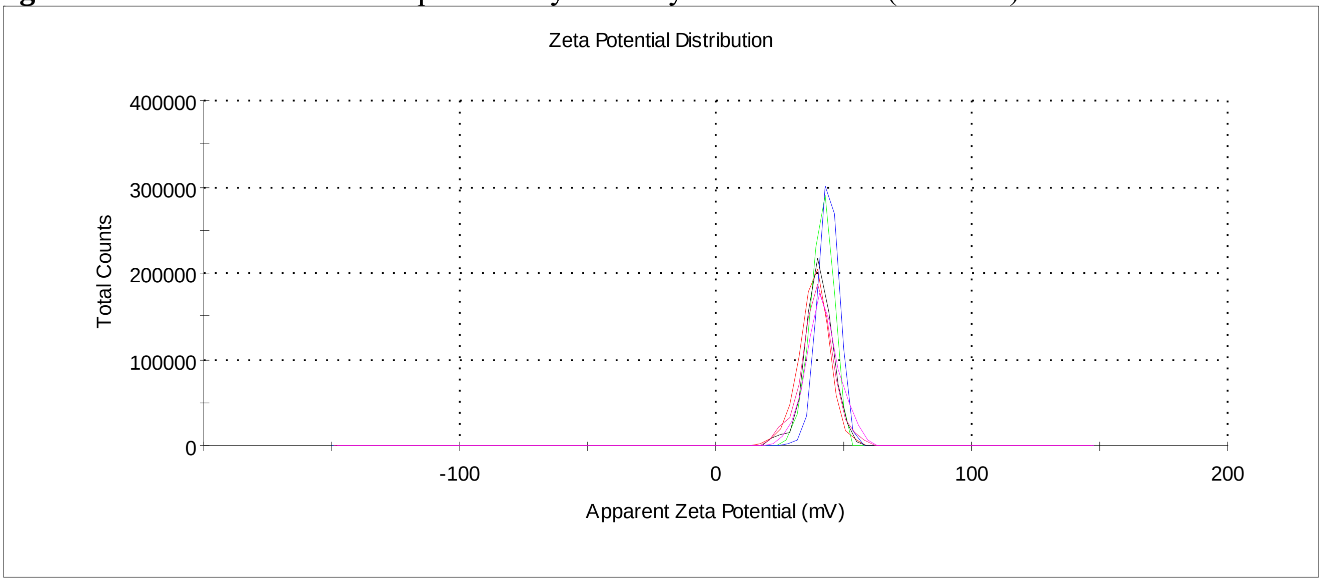

Fig. S93. Zeta potential distribution of the particles SLN-**4**-Flu (3×10^{-5}M) in water.

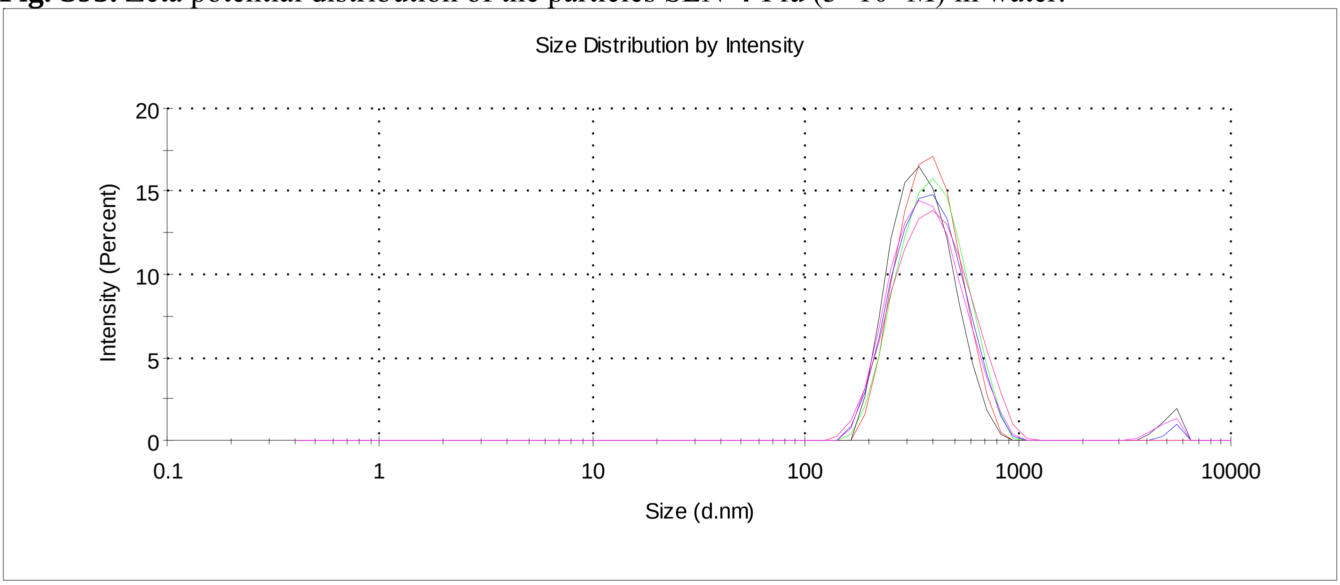

Fig. S94. Size distribution of the particles by intensity for SLN-**5**-Flu (3×10^{-5}M) in water.

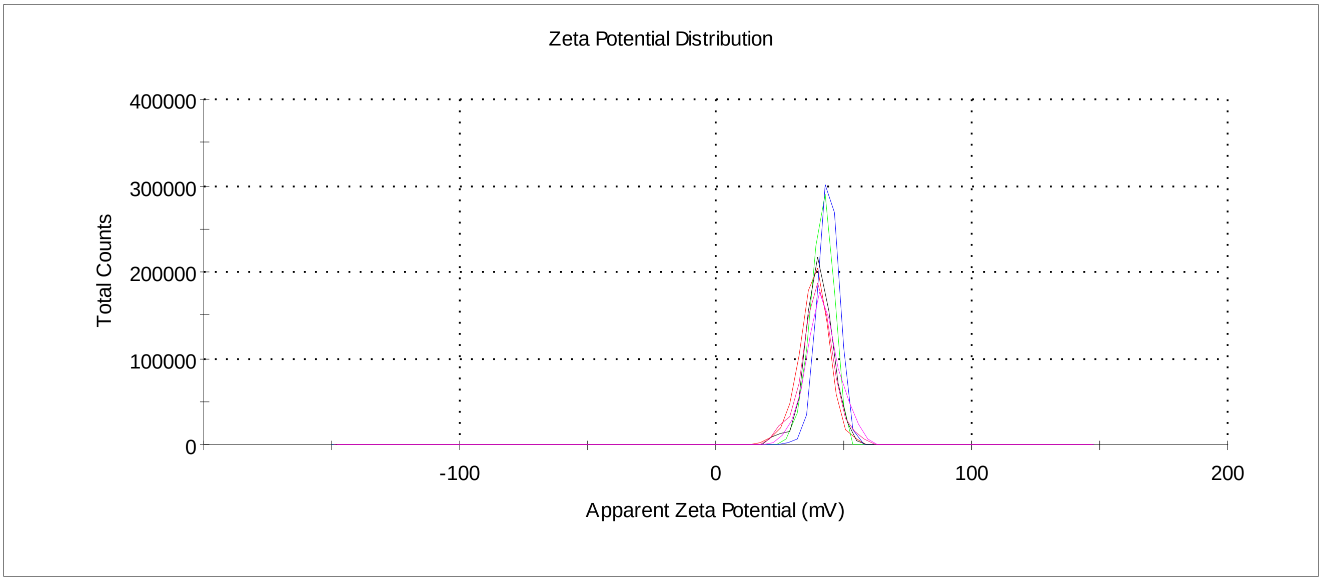

Fig. S95. Zeta potential distribution of the particles SLN-**5**-Flu (3×10^{-5}M) in water.

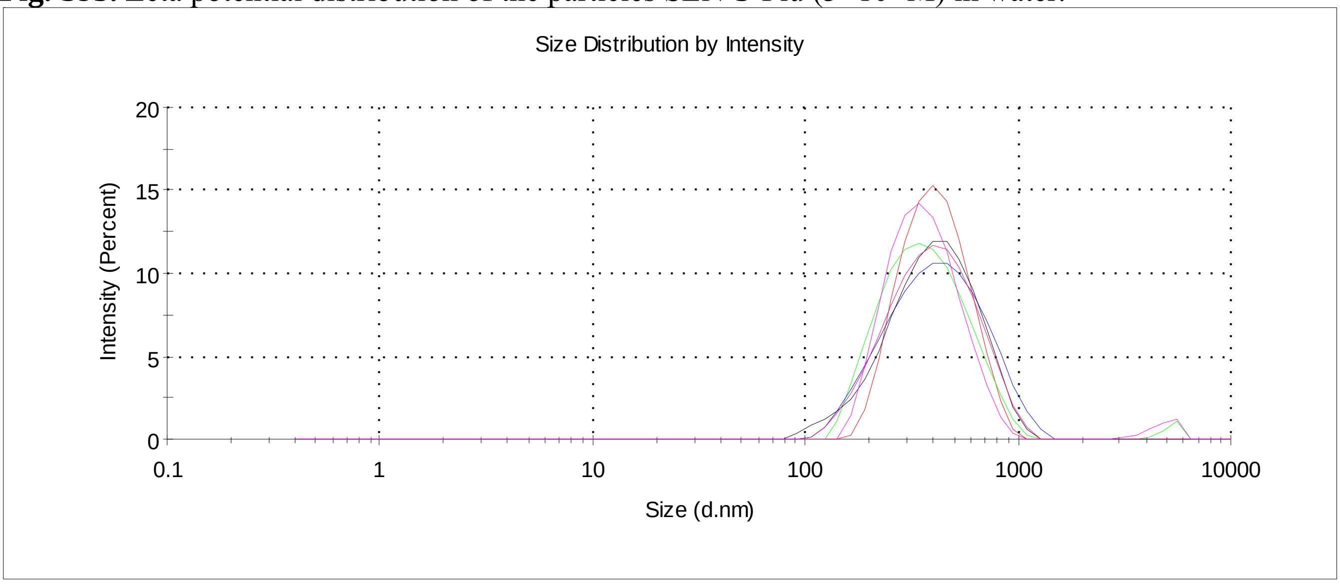

Fig. S96. Size distribution of the particles by intensity for SLN-**6**-Flu (3×10^{-5}M) in water.

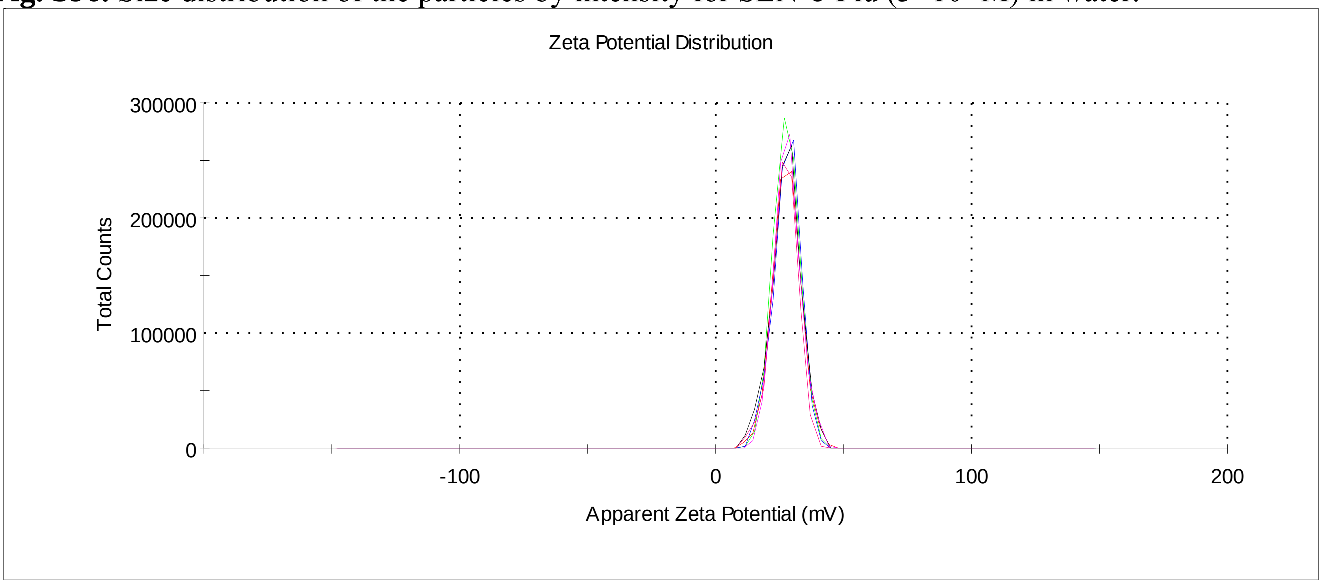

Fig. S97. Zeta potential distribution of the particles SLN-**6**-Flu (3×10^{-5}M) in water.

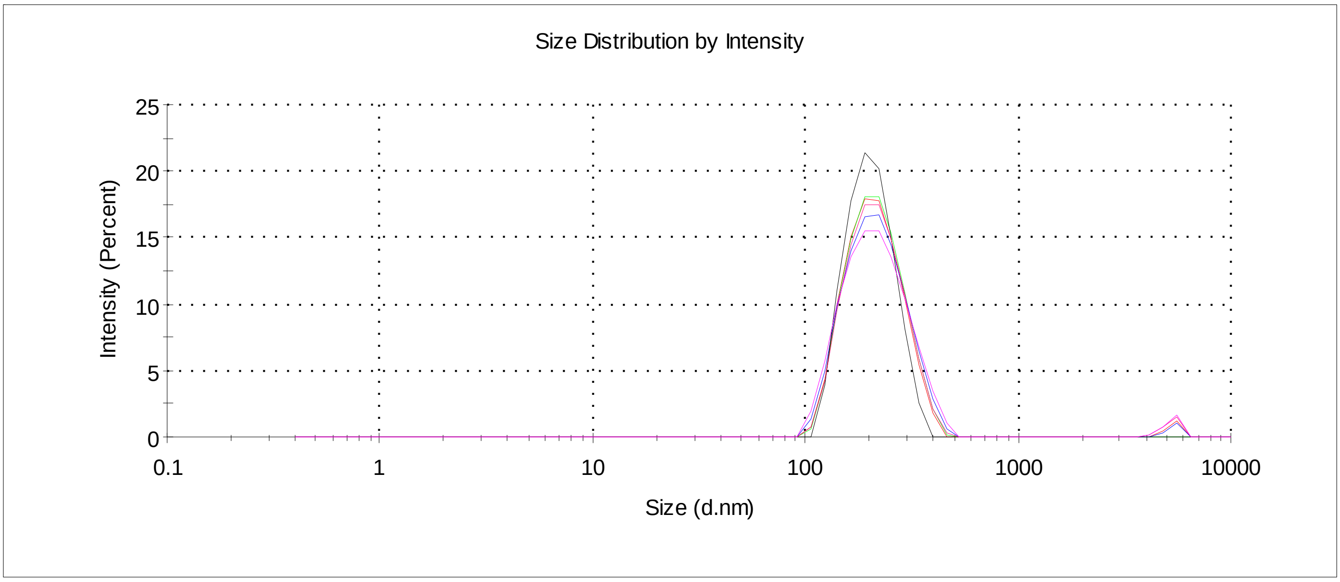

Fig. S98. Size distribution of the particles by intensity for SLN-**3**-RhB (3×10^{-5}M) in water.

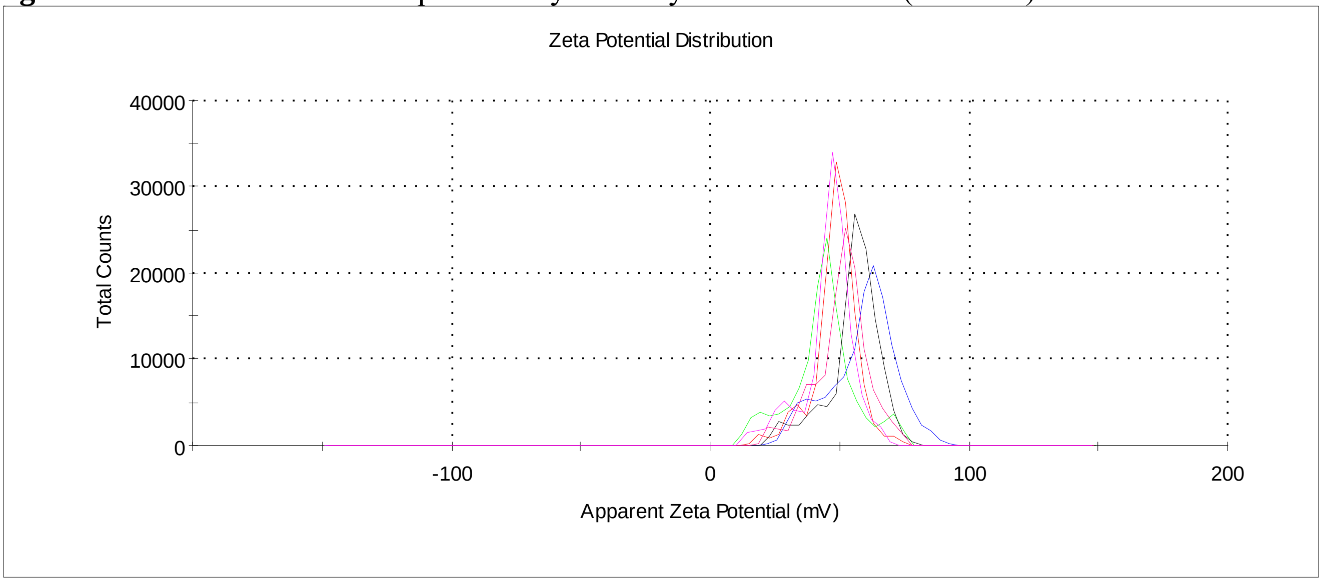

Fig. S99. Zeta potential distribution of the particles SLN-**3**-RhB (3×10^{-5}M) in water.

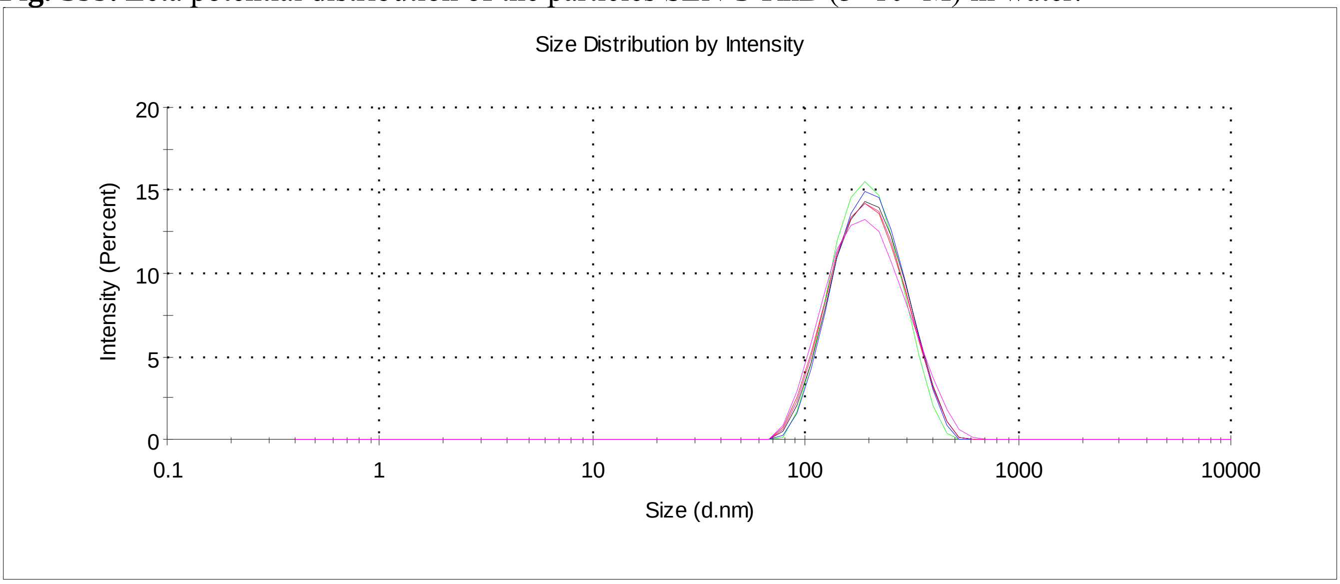

Fig. S100. Size distribution of the particles by intensity for SLN-**4**-RhB (3×10^{-5}M) in water.

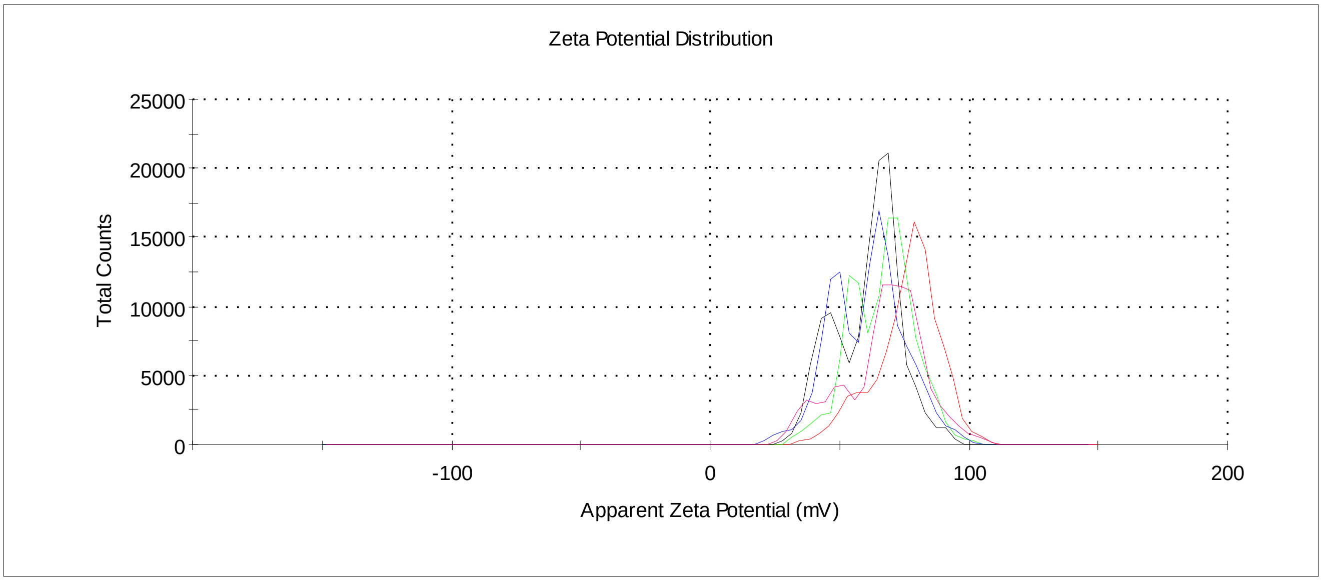

Fig. S101. Zeta potential distribution of the particles SLN-**4**-RhB (3×10^{-5}M) in water.

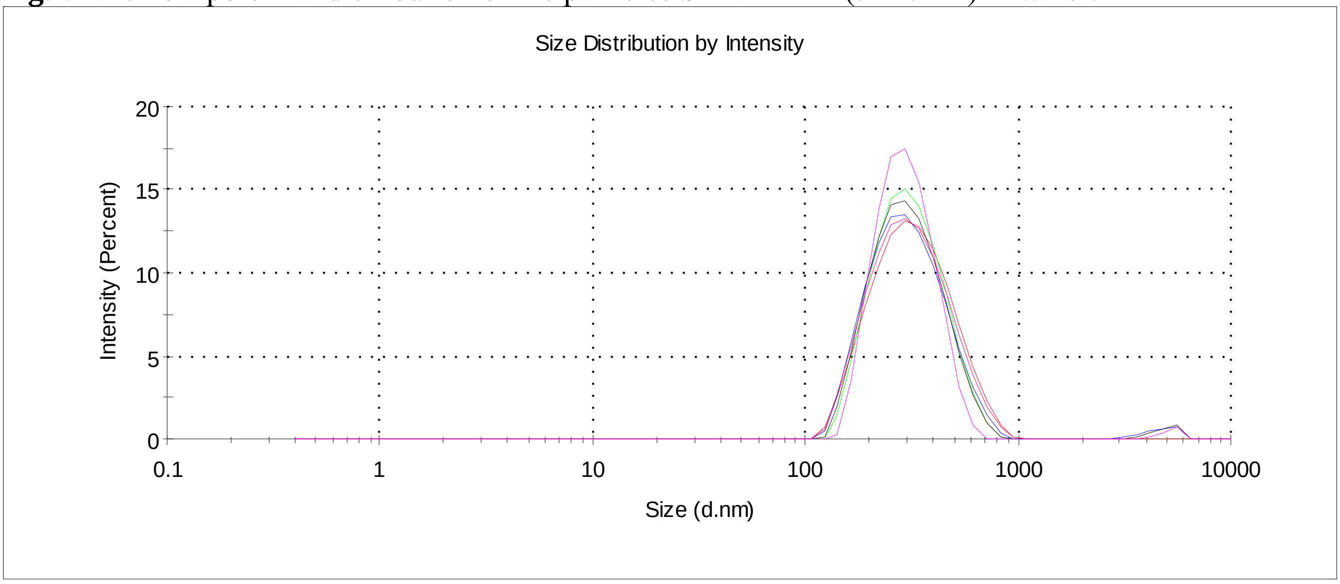

Fig. S102. Size distribution of the particles by intensity for SLN-**5**-RhB (3×10^{-5}M) in water.

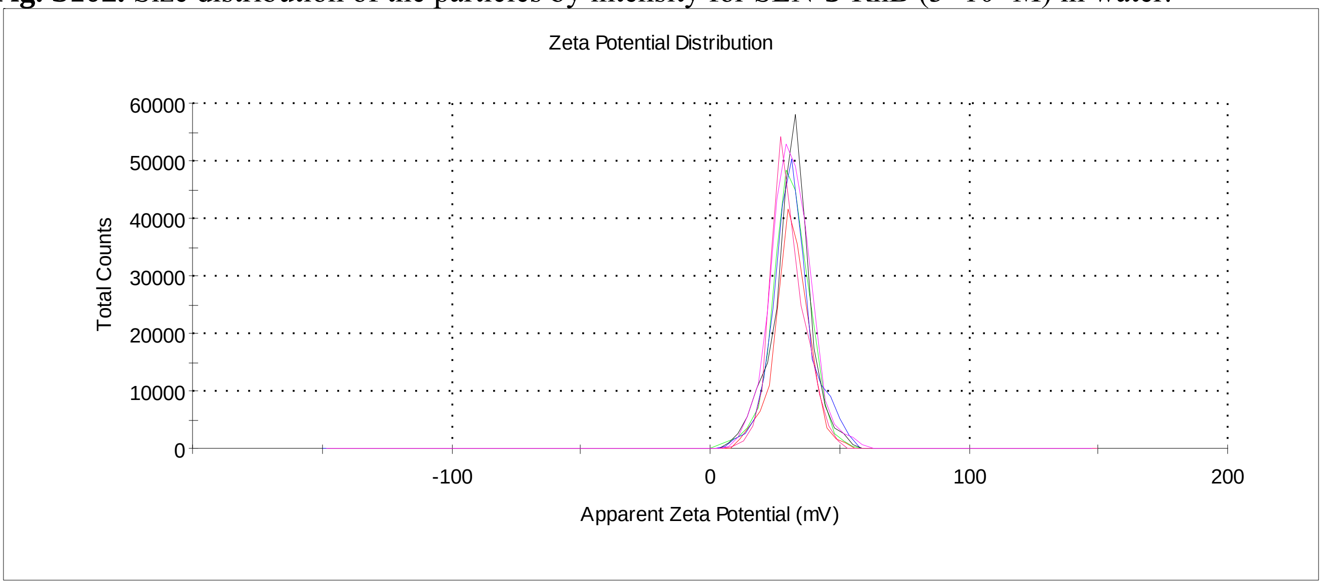

Fig. S103. Zeta potential distribution of the particles SLN-**5**-RhB (3×10^{-5}M) in water.

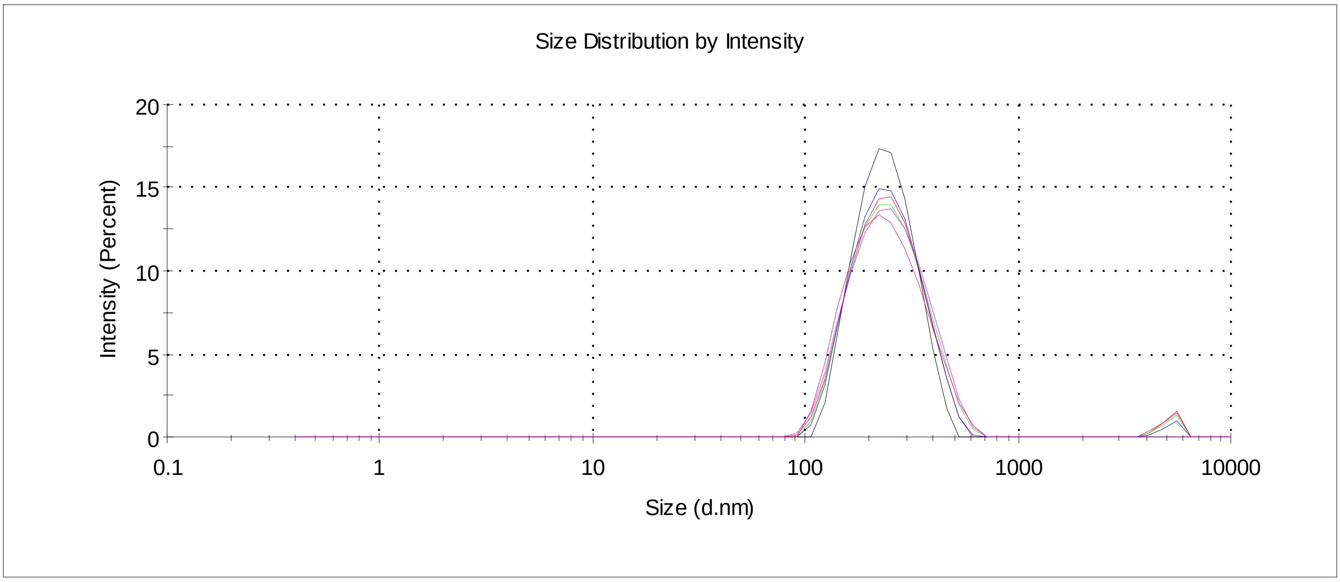

Fig. S104. Size distribution of the particles by intensity for SLN-**6**-RhB (3×10^{-5}M) in water.

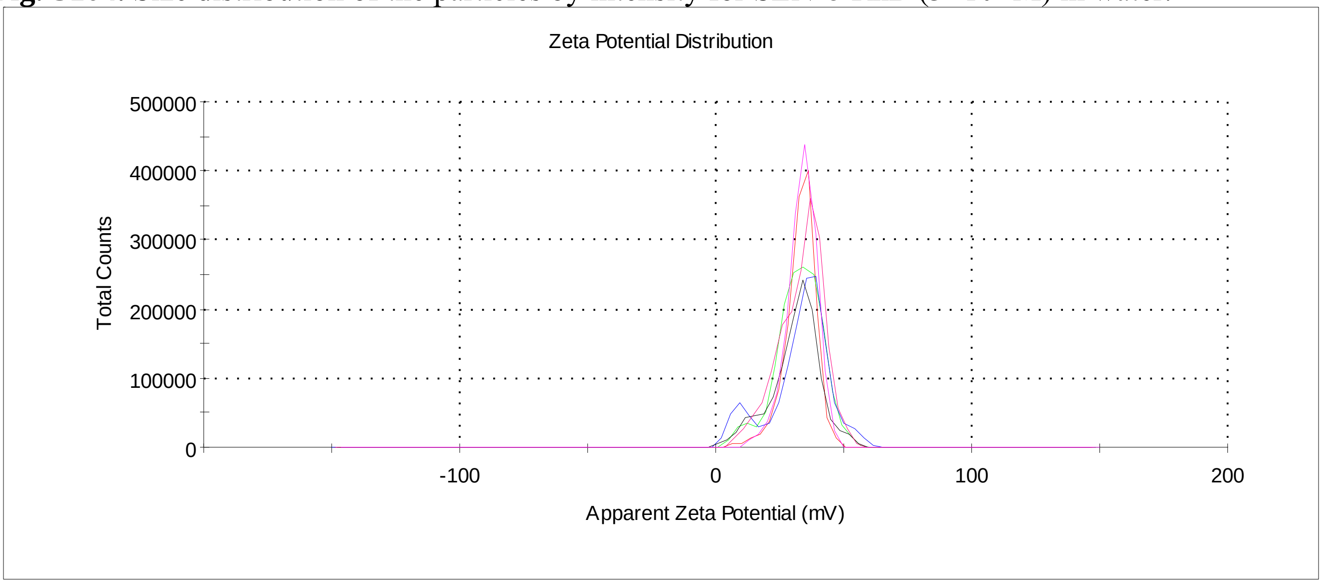

Fig. S105. Zeta potential distribution of the particles SLN-**6**-RhB (3×10^{-5}M) in water.

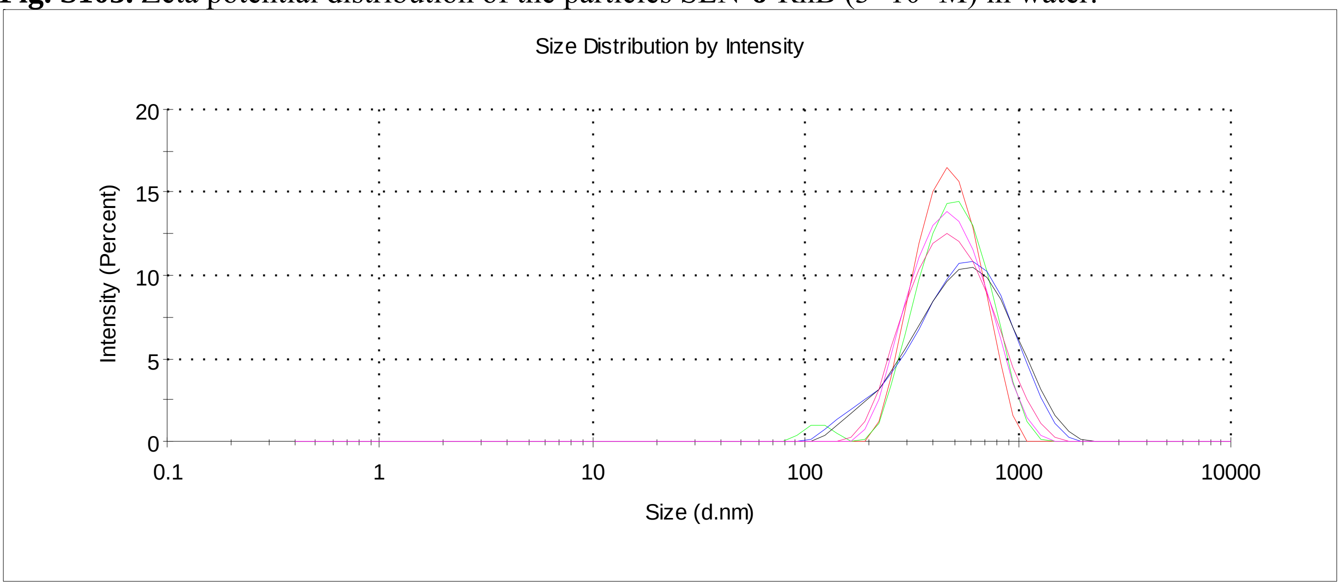

Fig. S106. Size distribution of the particles by intensity for SLN-**3**-Rh6G (3×10^{-5}M) in water.

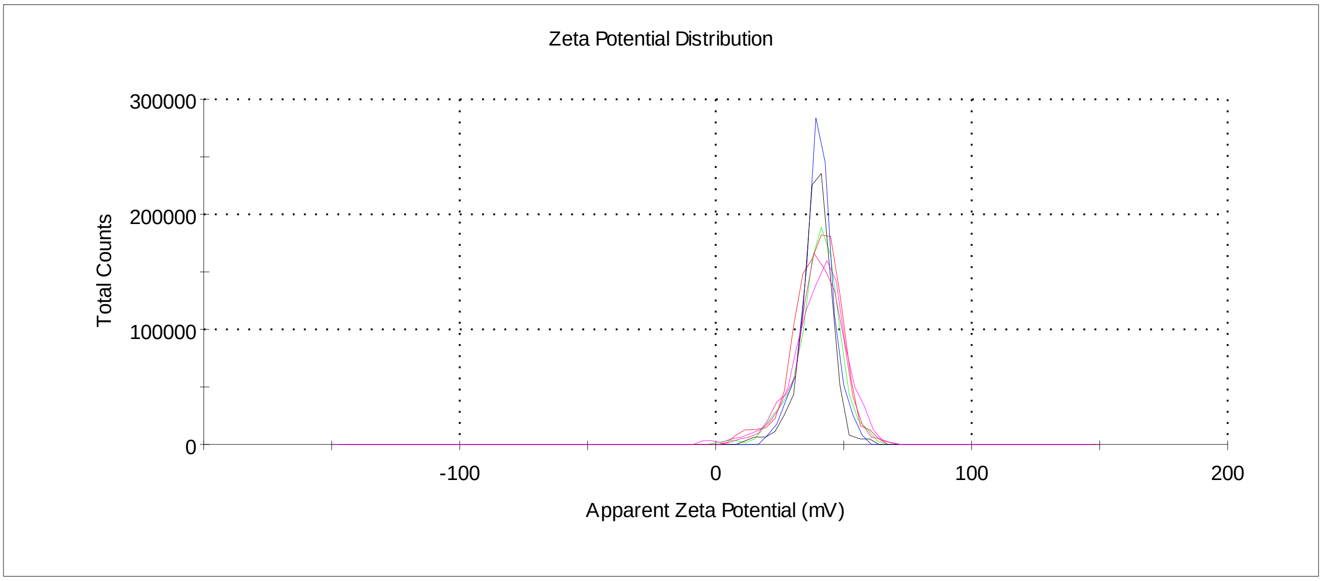

Fig. S107. Zeta potential distribution of the particles SLN-**3**-Rh6G (3×10^{-5}M) in water.

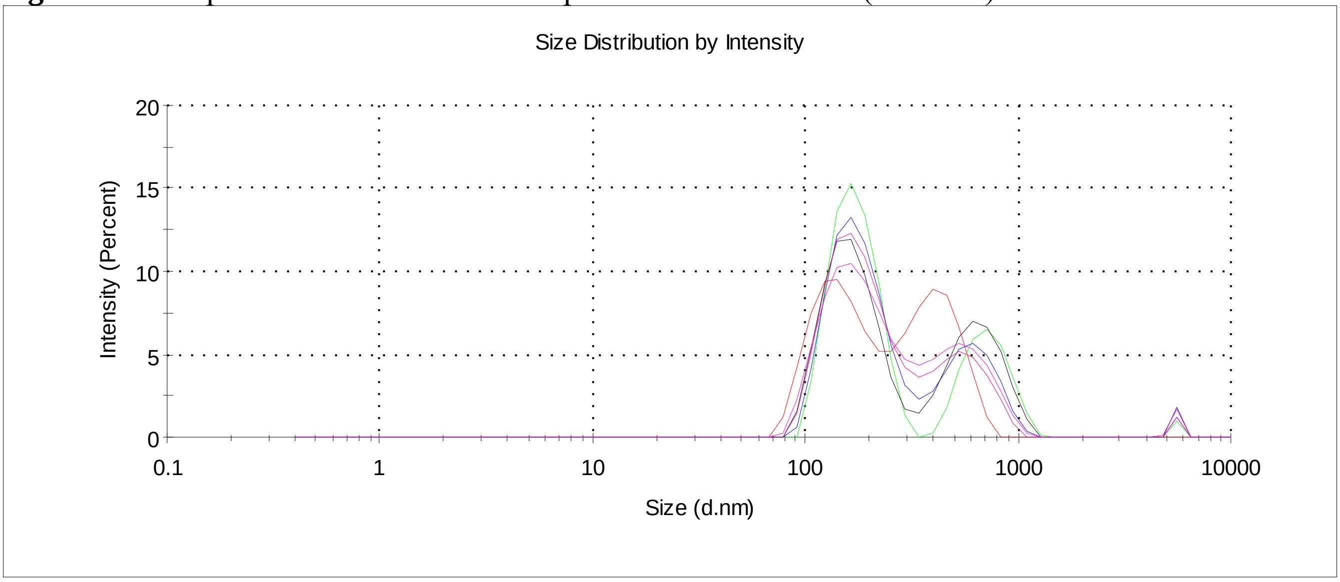

Fig. S108. Size distribution of the particles by intensity for SLN-**4**-Rh6G (3×10^{-5}M) in water.

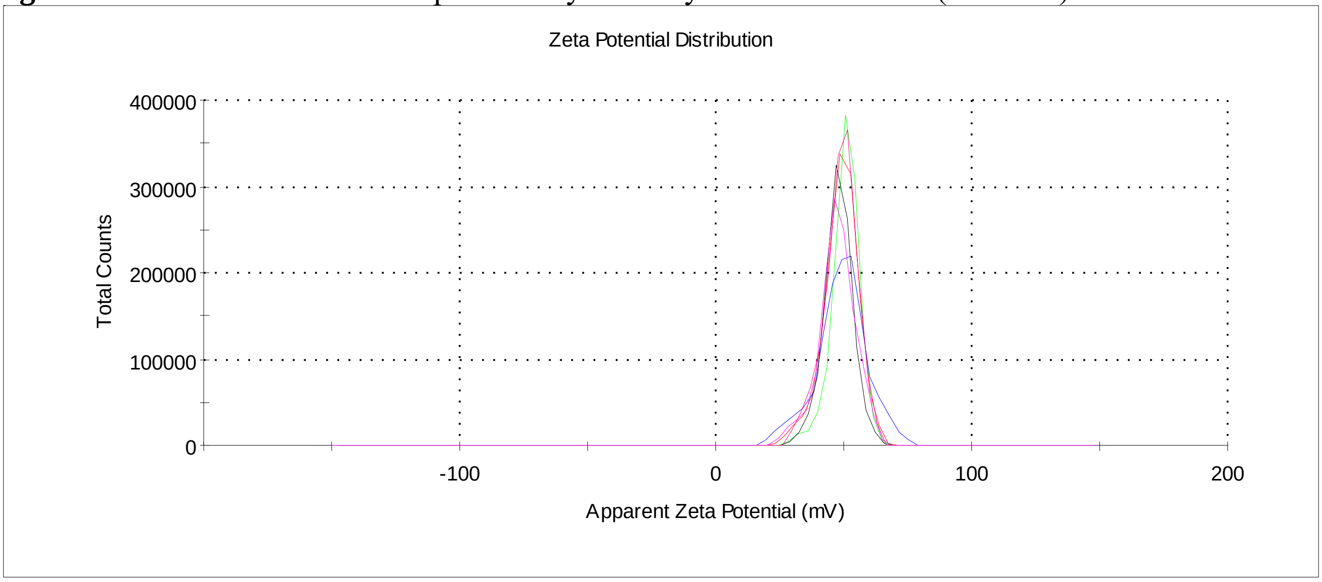

Fig. S109. Zeta potential distribution of the particles SLN-**4**-Rh6G (3×10^{-5}M) in water.

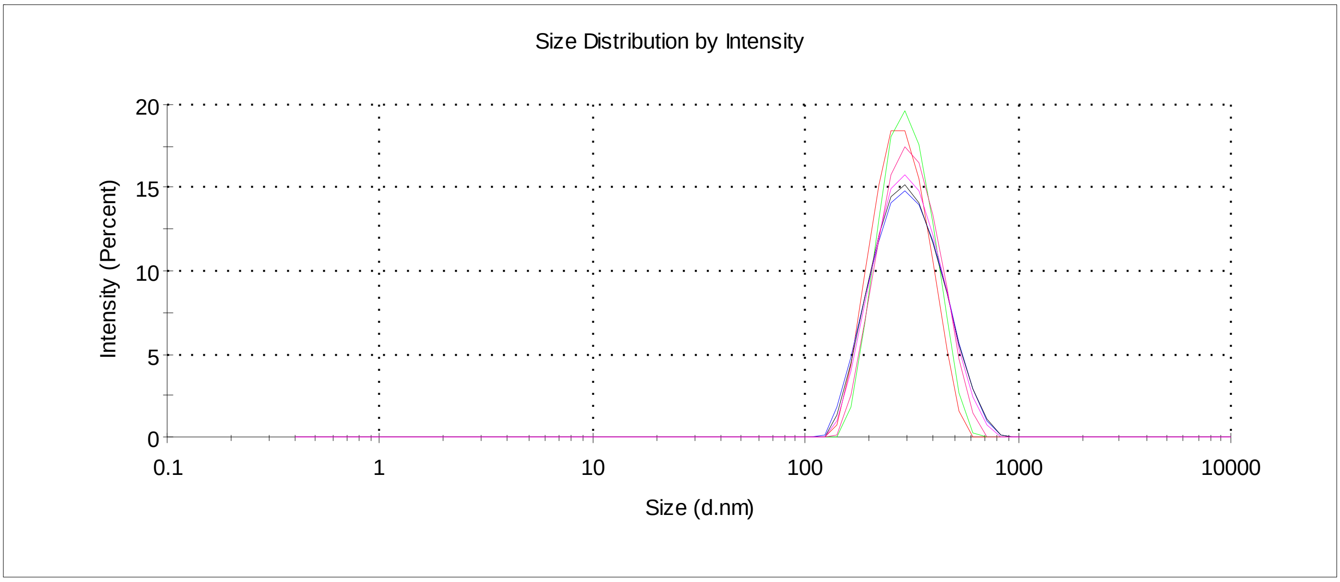

Fig. S110. Size distribution of the particles by intensity for SLN-**5**-Rh6G (3×10^{-5}M) in water.

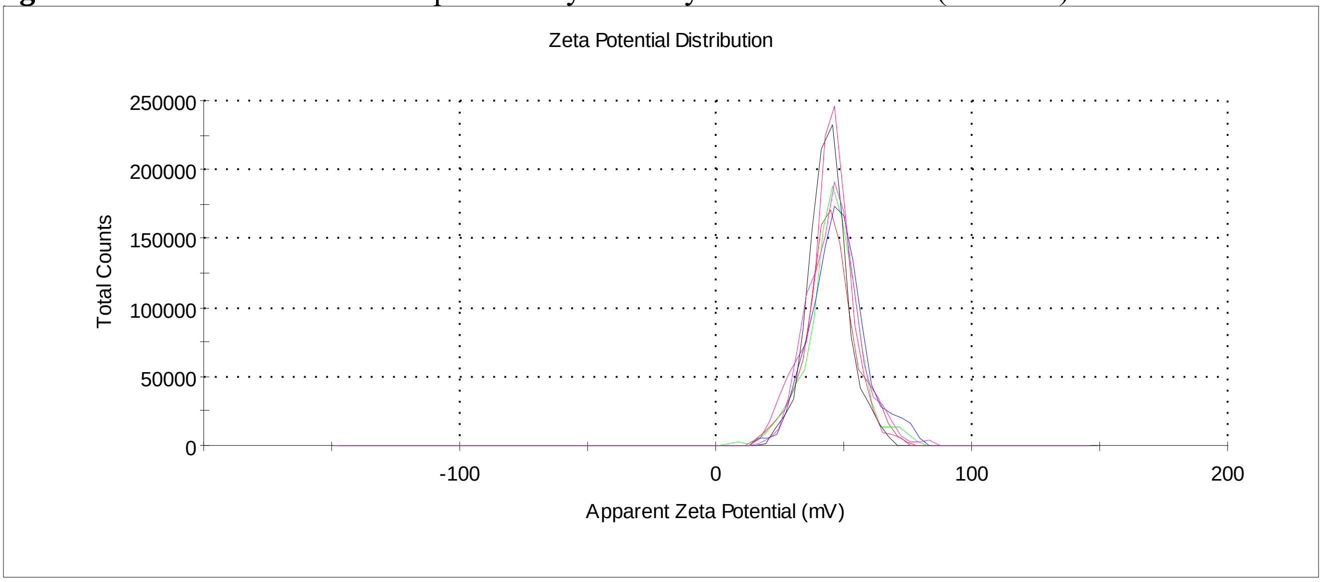

Fig. S111. Zeta potential distribution of the particles SLN-**5**-Rh6G (3×10^{-5}M) in water.

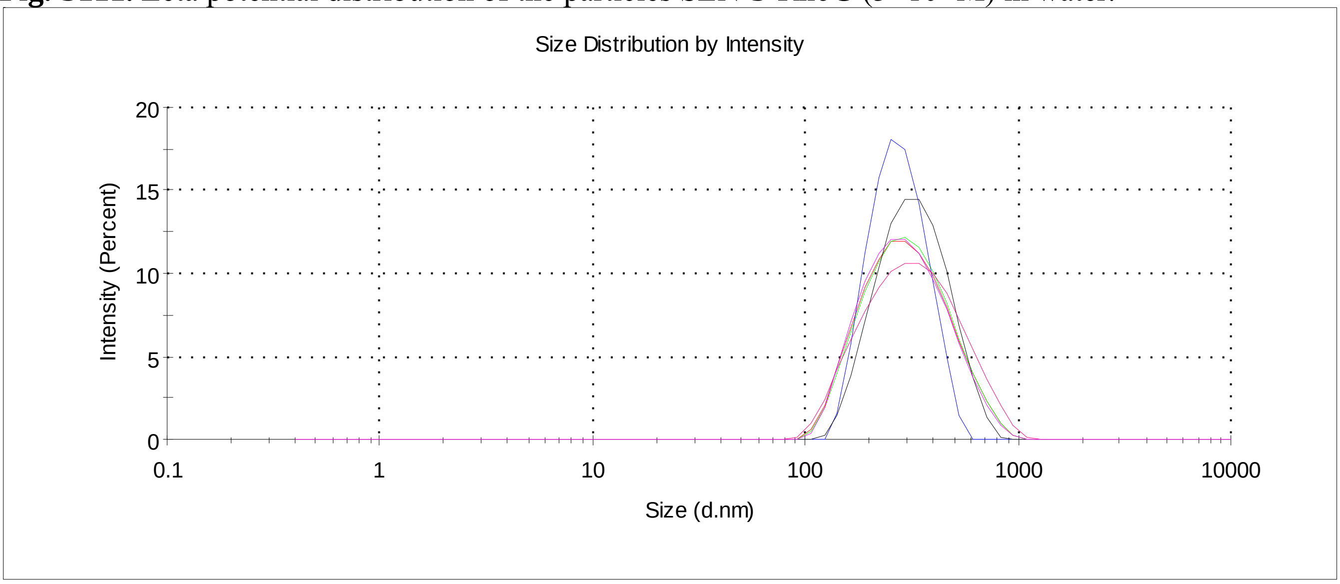

Fig. S112. Size distribution of the particles by intensity for SLN-**6**-Rh6G (3×10^{-5}M) in water.

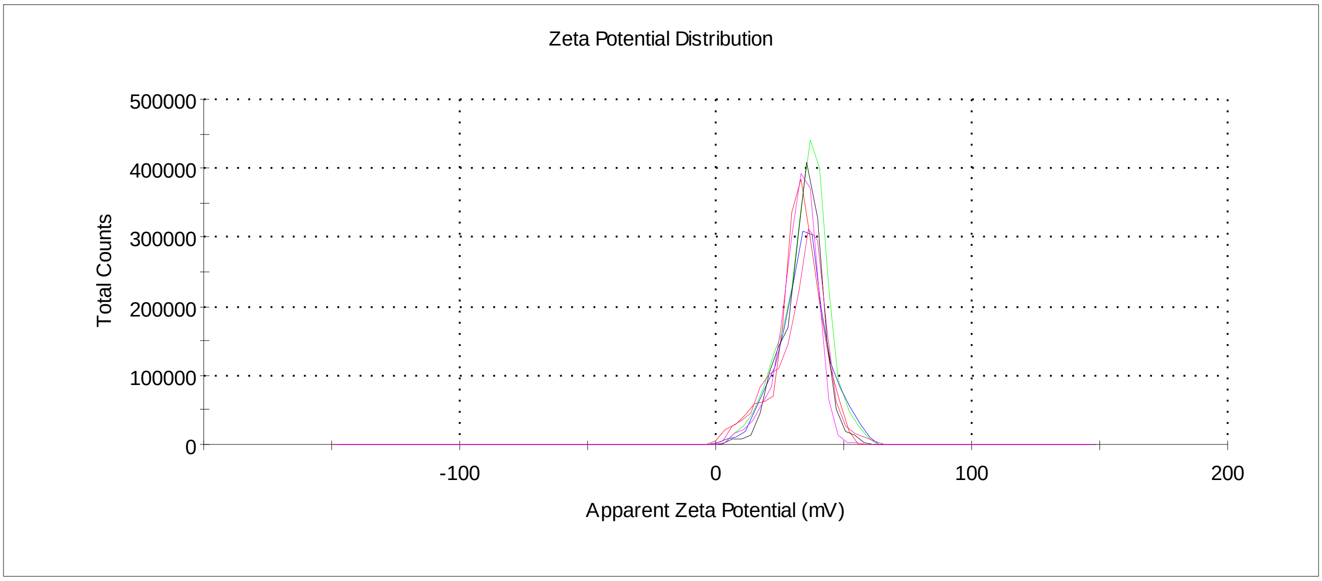

Fig. S113. Zeta potential distribution of the particles SLN-**6**-Rh6G (3×10^{-5}M) in water.

5. Confocal microscopy

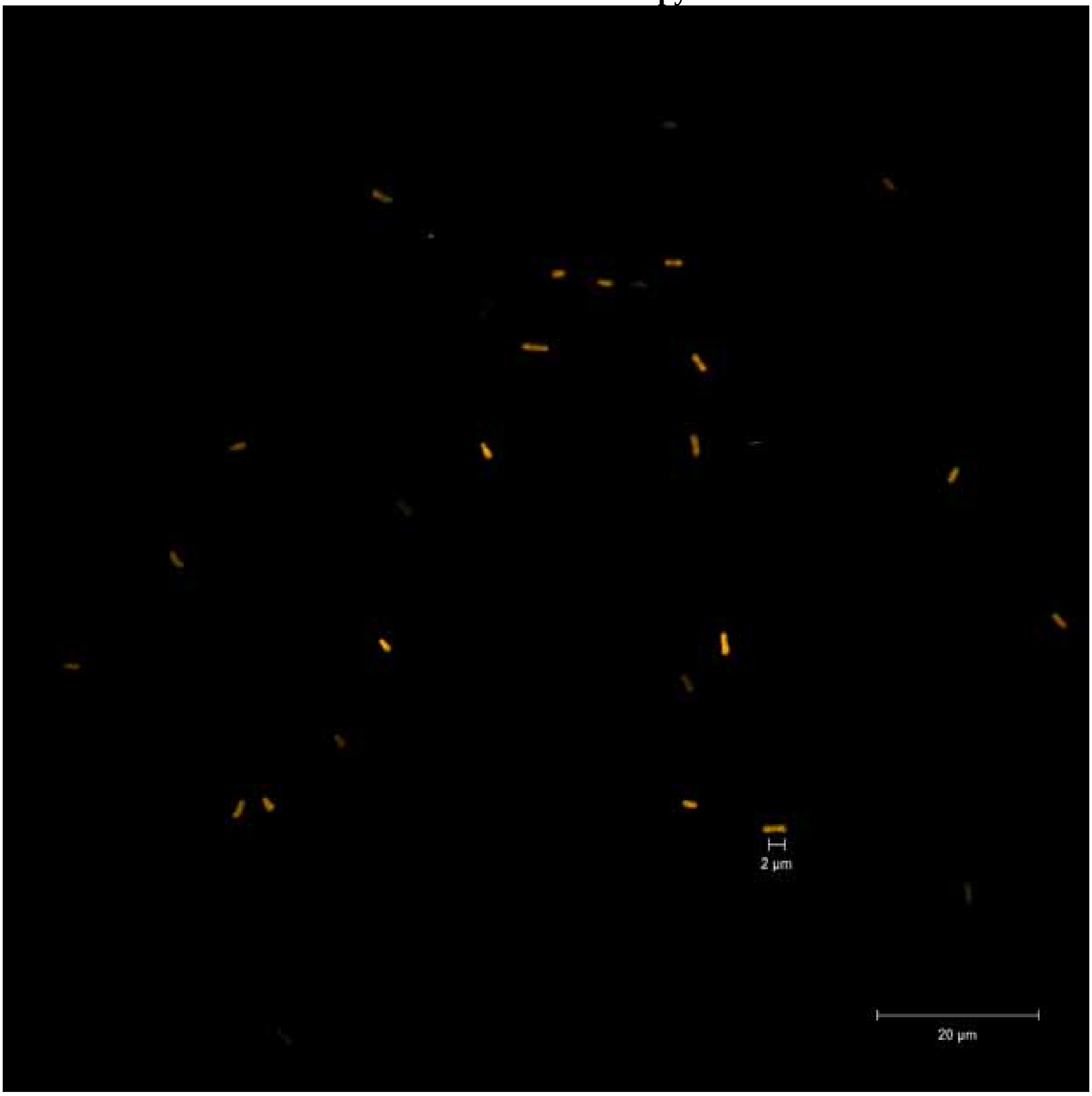

Fig. S114. Confocal microscopy image for SLN-**5**-RhB.

6. UV spectra

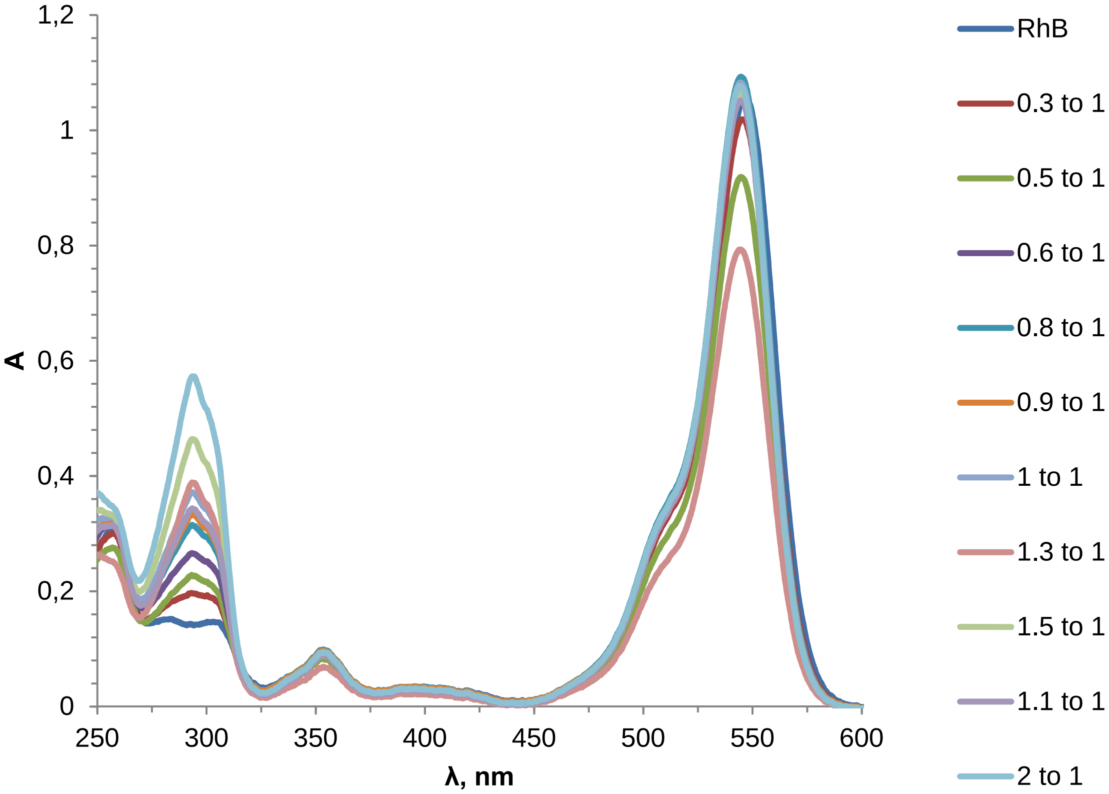

Fig. S115. UV titration spectra for the system **3**/RhB.

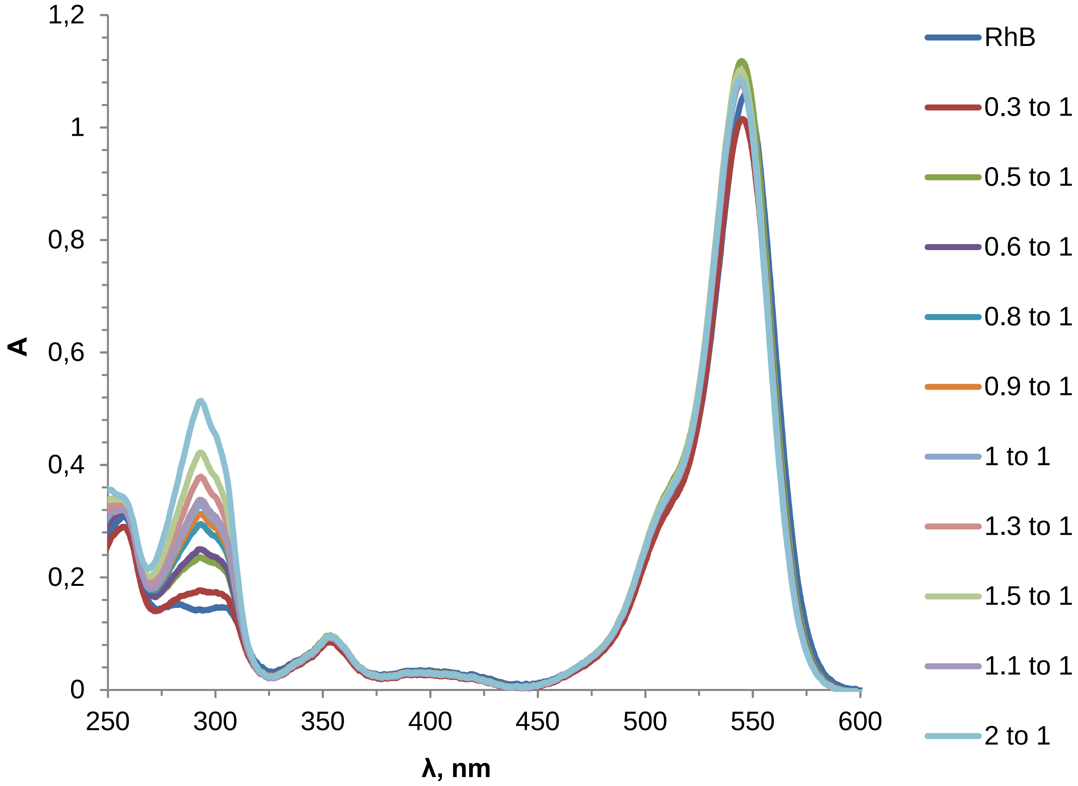

Fig. S116. UV titration spectra for the system **4**/RhB.

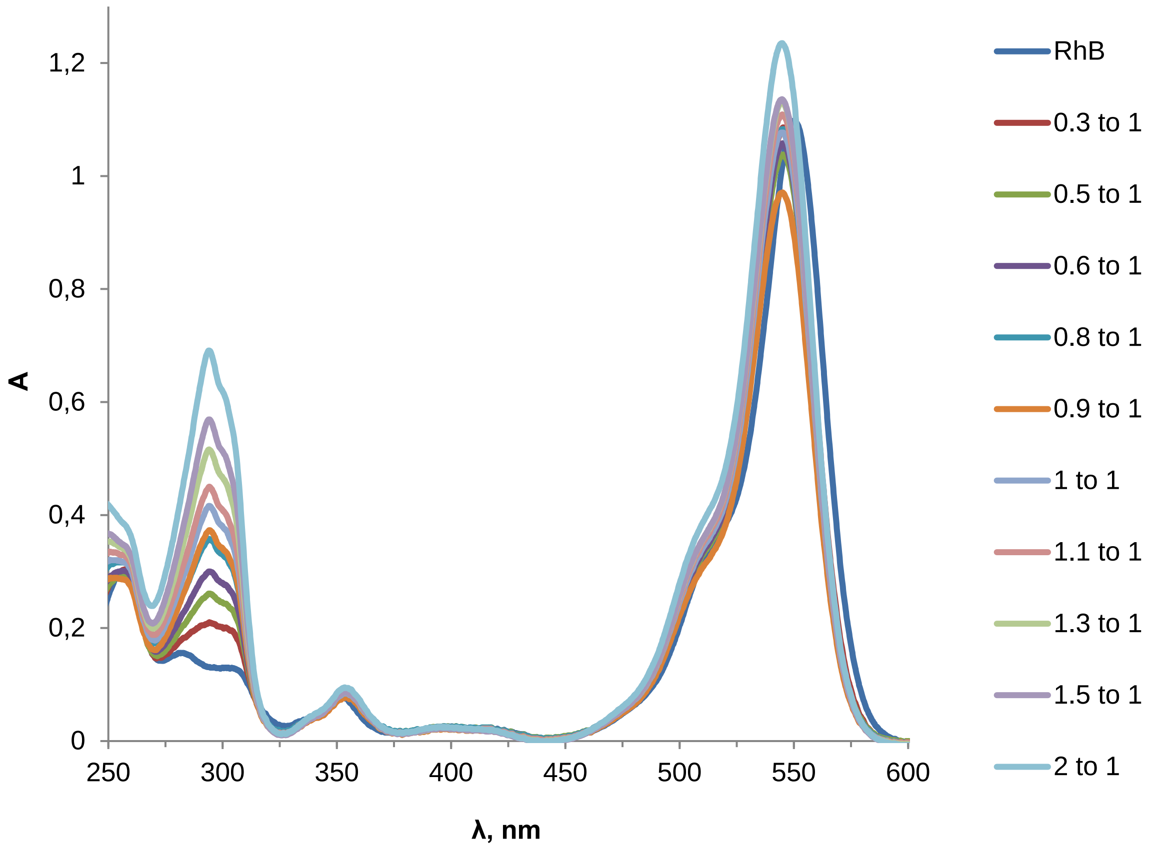

Fig. S117. UV titration spectra for the system **5**/RhB.

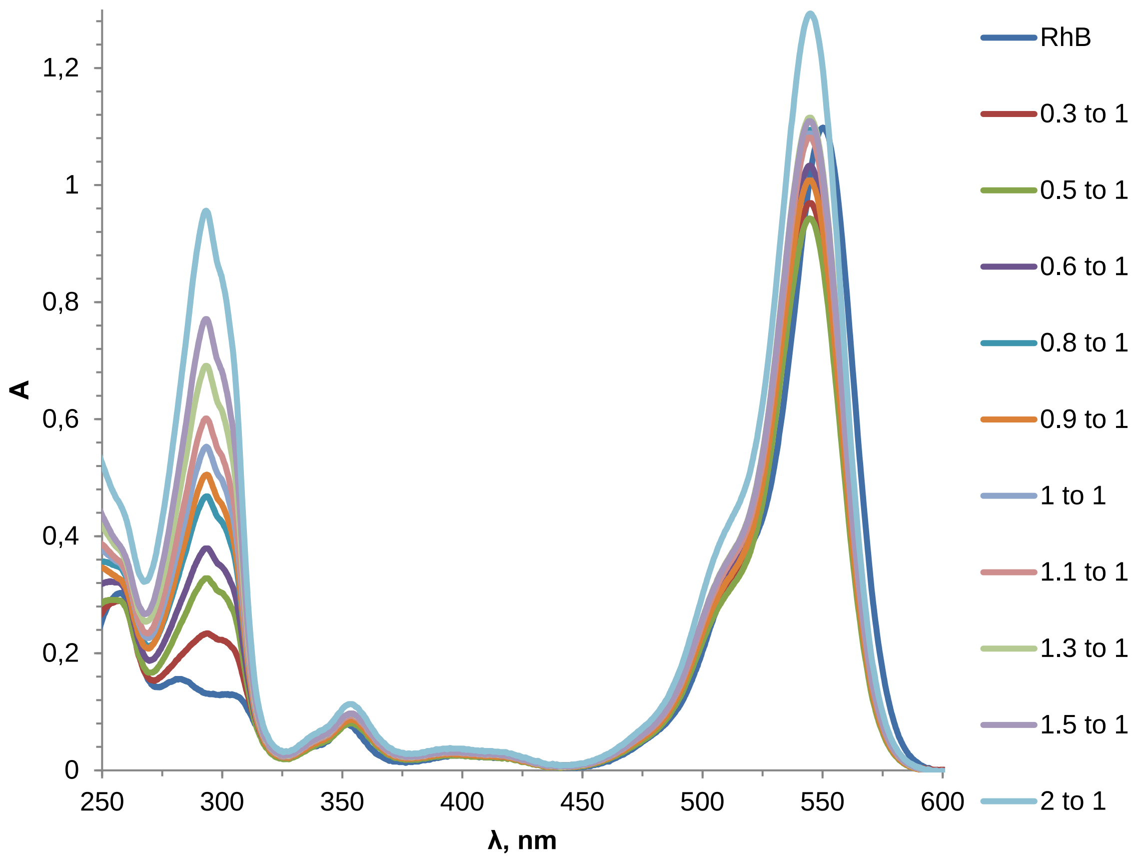

Fig. S118. UV titration spectra for the system **6**/RhB.

7. Determination of the stability constant and stoichiometry of the complex by the UV titration and isomolar series method

UV-visible spectra were recorded on the Shimadzu UV-3600 spectrophotometer using a 1 cm quartz cuvette at 25 °C. The 3.0×10^{-5} M solution of the pillar[5]arene **3-6** (300, 500, 600, 800, 900, 1000, 1100, 1300, 1500 and 2000 µl) in water was added to 30 µl of the solution of guest (Flu/RhB/Rh6G) (1.0×10^{-3} M) in water and diluted to final volume of 3 ml with water. The UV spectra of the solutions were then recorded. The stability constant and stoichiometry of complexes were calculated. Three independent experiments were carried out for each series. Student's t-test was applied in statistical data processing.

7. Cytotoxic activity

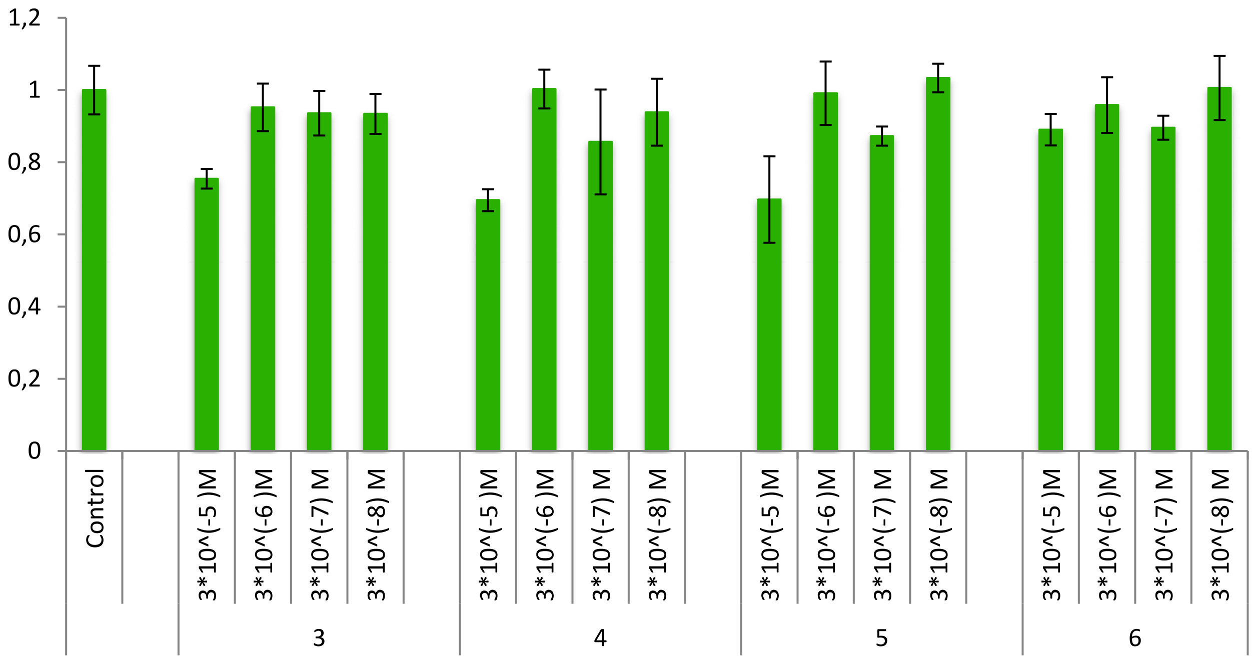

Fig. S119. Cytotoxic activity of SLNs-[**3-6**]-Flu to A549 cells.

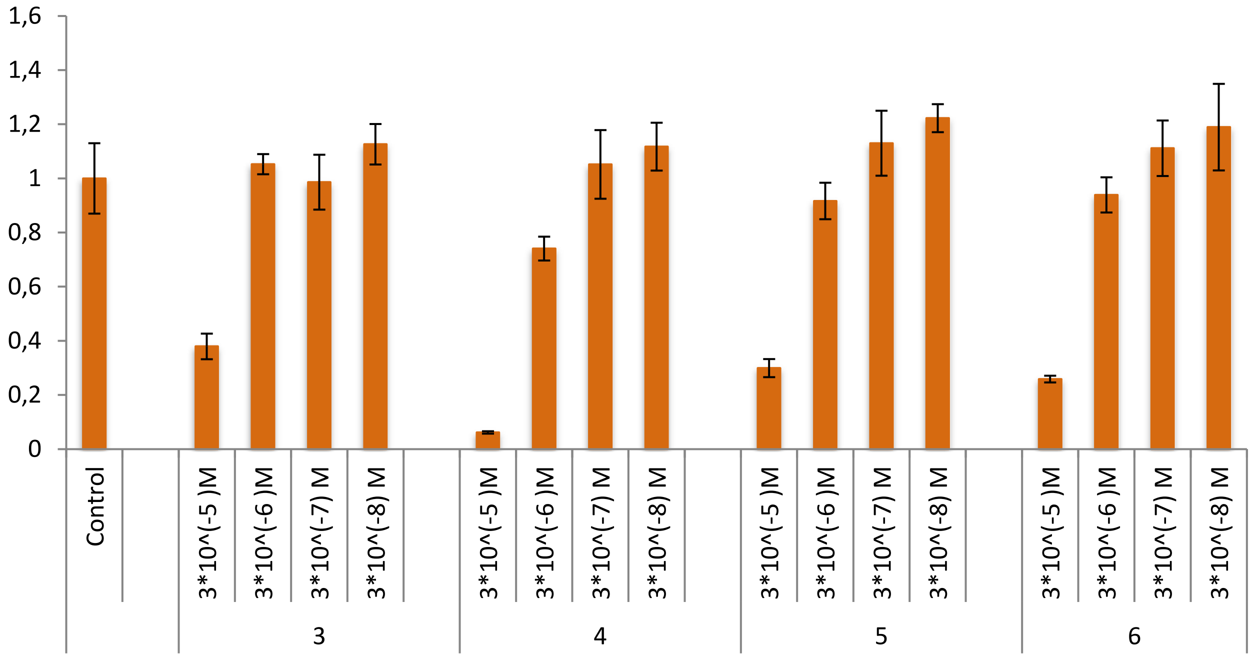

Fig. S120. Cytotoxic activity of SLNs-[**3-6**]-Rh6G to A549 cells.

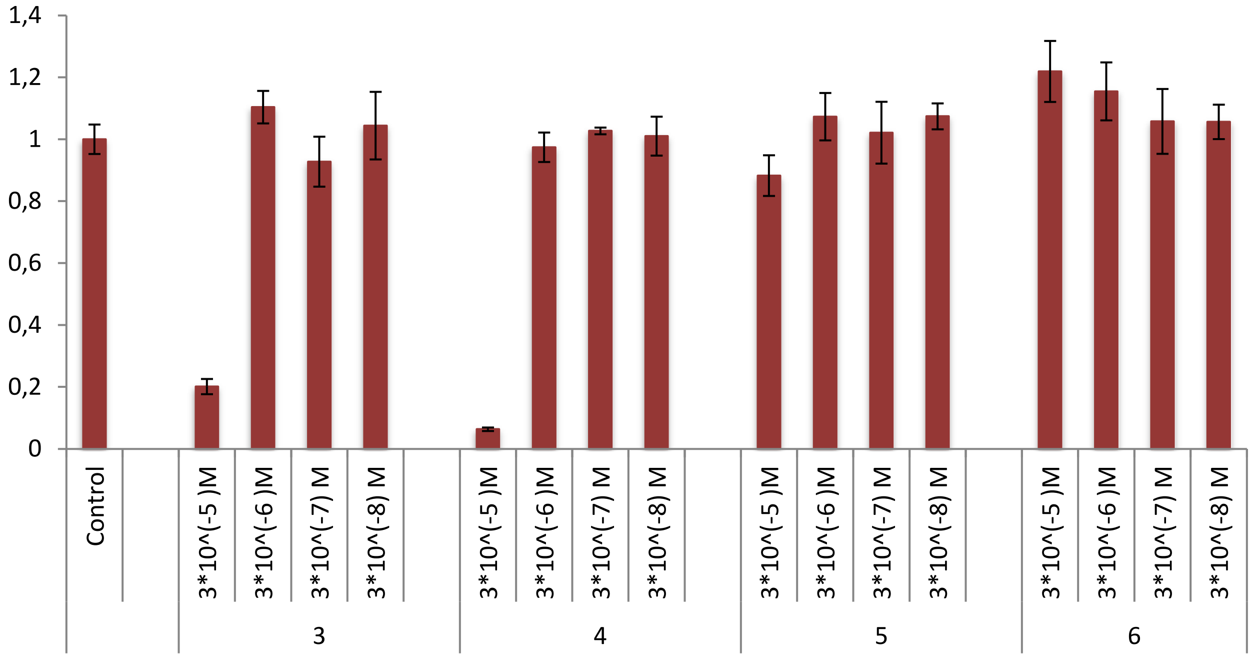

Fig. S121. Cytotoxic activity of SLNs-[**3-6**]-RhB to A549 cells.